

INFORMATION TO USERS

This manuscript has been reproduced from the microfilm master. UMI films the text directly from the original or copy submitted. Thus, some thesis and dissertation copies are in typewriter face, while others may be from any type of computer printer.

The quality of this reproduction is dependent upon the quality of the copy submitted. Broken or indistinct print, colored or poor quality illustrations and photographs, print bleedthrough, substandard margins, and improper alignment can adversely affect reproduction.

In the unlikely event that the author did not send UMI a complete manuscript and there are missing pages, these will be noted. Also, if unauthorized copyright material had to be removed, a note will indicate the deletion.

Oversize materials (e.g., maps, drawings, charts) are reproduced by sectioning the original, beginning at the upper left-hand corner and continuing from left to right in equal sections with small overlaps.

Photographs included in the original manuscript have been reproduced xerographically in this copy. Higher quality 6" x 9" black and white photographic prints are available for any photographs or illustrations appearing in this copy for an additional charge. Contact UMI directly to order.

**ProQuest Information and Learning
300 North Zeeb Road, Ann Arbor, MI 48106-1346 USA
800-521-0600**

UMI[®]



FINITE ELEMENT DYNAMIC
ANALYSIS OF DRILLSTRING

BY

HUSSEIN A. ALNASER

A Thesis Presented to the
DEANSHIP OF GRADUATE STUDIES

KING FAHD UNIVERSITY OF PETROLEUM & MINERALS

DHAHRAN, SAUDI ARABIA

In Partial Fulfillment of the
Requirements for the Degree of

MASTER OF SCIENCE

In

MECHANICAL ENGINEERING

Rabi' 1, 1423

May, 2002

UMI Number: 1409810

UMI[®]

UMI Microform 1409810

Copyright 2002 by ProQuest Information and Learning Company.
All rights reserved. This microform edition is protected against
unauthorized copying under Title 17, United States Code.

ProQuest Information and Learning Company
300 North Zeeb Road
P.O. Box 1346
Ann Arbor, MI 48106-1346

**KING FAHD UNIVERSITY OF PETROLEUM & MINERALS
DHAHRAN 31261, SAUDI ARABIA**

DEANSHIP OF GRADUATE STUDIES

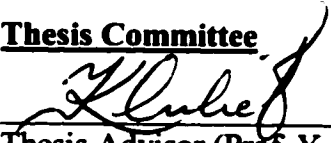
This thesis, written by

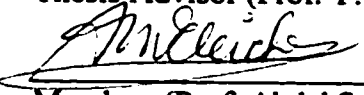
HUSSEIN ALI ALNASER

Under the direction of his thesis advisor, and approved by his thesis committee, has been presented to and accepted by the Dean of Graduate Studies, in partial fulfillment of the requirements for the degree of

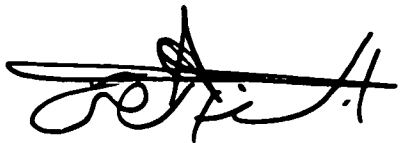
MASTER OF SCIENCE IN MECHANICAL ENGINEERING

Thesis Committee

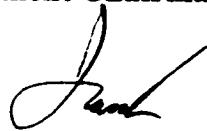

Thesis Advisor (Prof. Y. A. Khulief)


Member (Prof. Abdel Salam Eleiche)


Member (Dr. M. A. Mohiuddin)



**Dr. Abdulghani Al-Farayedhi
Department Chairman**



**Prof. Osama A. Jannadi
Dean of Graduate Studies**



Date: 3/7/2002

ACKNOWLEDGEMENT

In the name of Allah, most gracious, most merciful

First and the foremost, all praise to Allah, the almighty who gave me the opportunity, courage and patience to carryout this work.

I would like to express my sincere appreciation to my academic advisor and thesis committee chairman, Dr. Yehia A. Khulief, who has been a constant source of help and encouragement during this research, working with him was indeed a learning experience. I also greatly appreciate the invaluable cooperation and support extended by my thesis committee members: Dr. Abdel Salam Eleiche and Dr. M. Mohiuddin.

Sincere thanks are due to department chairman Dr. Abdulghani Al-Farayedhi for his immeasurable cooperation.

I am grateful to King Fahd University of Petroleum and Minerals for supporting my M. S. studies and this research work.

I wish to express my gratitude to my parents, wife and children, and my relatives, who motivated and guided me throughout my career.

Finally, I thank all my colleagues who helped me in this work.

TABLE OF CONTENTS

	page
Title page	i
Final approval	ii
Acknowledgement	iii
Table of Contents	iv
List of Tables	vii
List of Figures	ix
Nomenclature	xii
Abstract (English)	xiv
Abstract (Arabic)	xv
Chapter One: Introduction	1
1.1 Drilling methods	1
1.2 Drilling system components	1
1.3 Drillstring vibration	3
1.4 Literature review	5
1.5 Current status	11
1.6 Objective and approach	13
Chapter Two: The drillstring dynamic model	15
2.1 Elemental coordinate system	15
2.2 Kinetic energy of drillstring	17
2.3 Strain energy of drillstring	23

	Page
2.3.1 Strain energy due to bending.....	23
2.3.2 Strain energy due to torsion.....	24
2.3.3 Strain energy due to axial deformation.....	24
2.3.4 Strain energy due to axial stiffening.....	25
2.3.5 Elemental equation of motion.....	26
 Chapter Three: Finite Element Formulation.....	 28
3.1 Finite element model.....	28
3.2 Stiffness matrices.....	30
3.3 Axial stiffening due to gravitational field.....	34
3.4 Inertia properties.....	43
 Chapter Four: Equations of Motion of the Drillstring.....	 49
4.1 The Assembled equations of motion.....	49
4.2 The Eigenvalue solution.....	52
4.2.1 Solution scheme.....	53
4.3 Modal transformation.....	53
 Chapter Five: Numerical Simulation.....	 57
5.1 Modal analysis.....	57
5.2 Modeling accuracy.....	97
5.3 Transient response analysis.....	103
5.3.1 Response to initial displacement.....	103
5.3.2 Response to initial velocity.....	108
5.3.3 Response to impulsive force.....	118

Conclusions	128
Recommendations for future work	130
APPENDIX	131
REFERENCES	135

LIST OF TABLES

Table	Page
3.1 Explicit expression for the shaft element shape functions.....	32
3.2 Elastic stiffness matrix of rotating drillstring.....	33
3.3 Axial stiffness matrix of rotating drillstring.....	33
3.4 Torsional stiffness matrix of rotating drillstring.....	33
3.5 Drillpipe axial stiffening matrix of rotating drillstring.....	37
3.6 Drillcollar axial stiffening matrix of rotating drillstring.....	41
3.7 Translational mass matrix of rotating drillstring.....	45
3.8 Rotary inertia mass matrix of rotating drillstring.....	46
3.9 Torsional mass matrix of rotating drillstring.....	46
3.10 Torsional/lateral coupling mass matrix of rotating drillstring.....	47
3.11 Gyroscopic matrix of rotating drillstring.....	48
5.1 Drillstring configuration data.....	58
5.2 FEM discretization data.....	59
5.3 Bending natural frequency for rotating drillstring..... (Neutral point at bottom)	68
5.4 Torsional and axial natural frequency..... (Neutral point at bottom)	68
5.5 Bending natural frequency for rotating drillstring..... (Neutral point at 100m from bottom)	69
5.6 Torsional and axial natural frequency..... (Neutral point at 100m from bottom)	69
5.7 Bending natural frequency for rotating drillstring..... (Neutral point at 200m from bottom)	70

	Page
5.8 Torsional and axial natural frequency..... (Neutral point at 200m from bottom)	70
5.9 Bending natural frequency for rotating drillstring..... (Neutral point at 400m from bottom)	71
5.10 Torsional and axial natural frequency..... (Neutral point at 400m from bottom)	71
5.11 Bending natural frequency for rotating drillstring..... (Drillcollar length is 200m and drillpipe length is 300m)	89
5.12 Torsional and axial natural frequency..... (Drillcollar length is 200m and drillpipe length is 300m)	89
5.13 Bending natural frequency for rotating drillstring..... (Drillcollar length is 200m and drillpipe length is 300m)	90
5.14 Torsional and axial natural frequency..... (Drillcollar length is 200m and drillpipe length is 300m)	90
5.15 Bending natural frequency for rotating drillstring..... (Drillcollar length is 200m and drillpipe length is 600m)	91
5.16 Torsional and axial natural frequency..... (Drillcollar length is 200m and drillpipe length is 600m)	91
5.17 Bending natural frequency for rotating drillstring..... (Drillcollar length is 200m and drillpipe length is 600m)	92
5.18 Torsional and axial natural frequency..... (Drillcollar length is 200m and drillpipe length is 600m)	92
5.19 Bending natural frequency for rotating drillstring..... (Drillcollar length is 300m and drillpipe length is 900m)	93
5.20 Torsional and axial natural frequency..... (Drillcollar length is 300m and drillpipe length is 900m)	93
5.21 Bending natural frequency for rotating drillstring..... (Drillcollar length is 300m and drillpipe length is 900m)	94
5.22 Torsional and axial natural frequency..... (Drillcollar length is 300m and drillpipe length is 900m)	94
5.23 Bending natural frequency for rotating drillstring..... (Drillcollar length is 400m and drillpipe length is 800m)	95

	Page
5.24 Torsional and axial natural frequency..... (Drillcollar length is 400m and drillpipe length is 800m)	95
5.25 Bending natural frequency for rotating drillstring..... (Drillcollar length is 400m and drillpipe length is 800m)	96
5.26 Torsional and axial natural frequency..... (Drillcollar length is 400m and drillpipe length is 800m)	96
5.27 Nodal lateral initial displacement of drillstring.....	104

LIST OF FIGURES

Figure	Page
1.1 Rotary drilling equipment.....	2
2.1 Drillstring layout.....	16
2.2 Generalized coordinates.....	18
2.3 Rotation angles.....	19
3.1 Order of degrees of freedom.....	29
3.2 Buckling of drillpipe above drillcollar.....	36
3.3 Drillpipe under tension.....	38
3.4 Drillcollar under compression.....	40
3.5 Drillstring axial force distribution.....	42
4.1 Computer program flow chart.....	50
5.1 Bending frequency for neutral point located at bottom.....	62
5.2 Bending frequency for neutral point located at 100m above bottom.....	63
5.3 Bending frequency for neutral point located at 200m above bottom.....	64
5.4 Bending frequency for neutral point located at 400m above bottom.....	65
5.5 Bending frequencies for different location of neutral point.....	66
5.6 Torsional and axial frequencies for different location of neutral point.....	67
5.7 Bending frequency for drillcollar 200m and drillpipe 300m.....	74
5.8 Bending frequency for drillcollar 200m and drillpipe 300m.....	75
5.9 Bending frequency for drillcollar 200m and drillpipe 600m.....	76
5.10 Bending frequency for drillcollar 200m and drillpipe 600m.....	77
5.11 Bending frequency for different length of drillpipe Vs. Magnitude.....	78

	Page
5.12 Torsional frequencies for different length of drillpipe Vs. Magnitude.....	79
5.13 Axial frequencies for different length of drillpipe Vs. Magnitude.....	80
5.14 Bending frequency for 200m drillcollar, 600m drillpipe.....	81
5.15 Bending frequency for drillcollar 300m and drillpipe 900m.....	82
5.16 Bending frequency for drillcollar 300m and drillpipe 900m.....	83
5.17 Bending frequency for drillcollar 400m and drillpipe 800m.....	84
5.18 Bending frequency for drillcollar 400m and drillpipe 800m.....	85
5.19 Bending frequency for different length of drillpipe/drillcollar Vs. Magnitude.....	86
5.20 Torsional frequencies for different length of drillpipe/drillcollar Vs. Magnitude.....	87
5.21 Axial frequencies for different length of drillpipe/drillcollar Vs. Magnitude.....	88
5.22 No. of elements Vs. frequency for non-rotating drillstring.....	98
5.23 No. of elements Vs. backward bending frequency.....	99
5.24 No. of elements Vs. forward bending frequency.....	100
5.25 Speed Vs. backward bending frequency.....	101
5.26 Speed Vs. forward bending frequency.....	102
5.27 Transient response of node #3 due to initial displacement	105
5.28 Transient response of node #9 due to initial displacement.....	106
5.29 Transient response of node #15 due to initial displacement.....	107
5.30 Transient response of node #3 due to initial displacement	109
5.31 Transient response of node #9 due to initial displacement	110
5.32 Transient response of node #15 due to initial displacement	111

	Page
5.33 Transient response of node #3 due to initial velocity	112
5.34 Transient response of node #9 due to initial velocity	113
5.35 Transient response of node #15 due to initial velocity	114
5.36 Transient response of node #3 due to initial velocity	115
5.37 Transient response of node #9 due to initial velocity	116
5.38 Transient response of node #15 due to initial velocity	117
5.39 Transient response of node #3 due to impulsive force.....	119
5.40 Transient response of node #9 due to impulsive force	120
5.41 Transient response of node #15 due to impulsive force	121
5.42 Transient response of node #3 due to impulsive force.....	122
5.43 Transient response of node #9 due to impulsive force	123
5.44 Transient response of node #15 due to impulsive force	124
5.45 Axial transient response of node #3 due to impulsive force.....	125
5.46 Axial transient response of node #9 due to impulsive force	126
5.47 Axial transient response of node #15 due to impulsive force	127

NOMENCLATURE

$[C]$:	Damping matrix
E	:	Modulus of elasticity
$\{e\}$:	Deformation vector
f	:	Frequency parameter
G	:	Shear modulus
$[G]$:	Gyroscopic matrix
I_D	:	Diametral mass moment of inertia
I_P	:	Polar mass moment of inertia
$[K]$:	Global stiffness matrix
$[K_a]$:	Axial stiffness matrix
$[K_{ax}]$:	Axial stiffening matrix
$[K_e]$:	Elastic stiffness matrix
$[K_\phi]$:	Torsional stiffness matrix
L	:	Lagrangian function
L_c	:	Drillcollar length
L_p	:	Drillpipe length
$[M]$:	Global mass matrix
$[M_r]$:	Rotary inertia mass matrix
$[M_t]$:	Translational mass matrix
$[M_\phi]$:	Torsional mass matrix
$[M_c]$:	Coupled torsional/transverse mass matrix
N_v	:	Translational shape function

N_θ	:	Rotational shape function
N_φ	:	Torsional shape function
T	:	Kinetic energy of the drillstring element
U	:	Total strain energy of the drillstring element
U_1	:	Strain energy due to bending deformation
U_2	:	Strain energy due to torsional deformation
U_3	:	Strain energy due to axial deformation
U_4	:	Added strain energy due to axial stiffening
I	:	Second moment of inertia
$[I]$:	Identity matrix
ω	:	Angular velocity
γ	:	Drillpipe/drillcollar length ratio

THESIS ABSTRACT

FULL NAME OF STUDENT : Hussein A. Alnaser

TITLE OF STUDY : Finite Element Dynamic Analysis of Drillstring

MAJOR FIELD : Mechanical Engineering

DATE OF DEGREE : May, 2002

The bending, torsional and axial vibration of a rotating drillstring based on Euler-Bernoulli theory is presented by means of the finite element technique. The drillstring shaft with circular cross-section is discretized into a number of finite shaft elements with twelve degrees of freedom each. The equation of motion of the rotating drillstring shaft is derived using Lagrange approach. Explicit expressions of the finite element mass, stiffness, axial stiffening, and gyroscopic matrices are derived by using consistent mass formulation. The developed shaft finite element is integrated into a computational scheme to calculate the natural frequencies of the drillstring system. Modal transformations are invoked to obtain a reduced order modal form of the dynamic equations. The computational scheme proceeds further to integrate the equations of motion and solve for the dynamic response of the drillstring due to different excitations.

ملخص الرسالة

الاسم : حسين علي الناصر

عنوان الرسالة : التحليل الديناميكي لآلات الحفر بواسطة طريقة العناصر المتناهيه في الصغر

التخصص : هندسة ميكانيكية

تاريخ التخرج : مايو 2002 م

الأهترزات الأنحنانيه و الدورانيه و الطولييه لمحور توصيل آلات الحفر بالأعتماد علي نظرية أيولر جرنولي للعبه بواسطه طريقة العناصر المتناهيه في الصغر يدرس في هذه الرساله. محور التوصيل للآت الحفر الذي يتم دراسته هنا ذا مقطع جانبي دائري يتم تقسيمه إلي عناصر متناهيه الصغر لكل منها اثني عشر إتجاه في حريه الحركه. معادله الحركه لمحور التوصيل يتم إشتقاقها بواسطه معادله لاجرانج. المصفوفات الحاويه للتعابير الرمزيه الممثله للكتله و مقاومه الأنحناء و مقاومه الأنحناء نتيجه للوزن و الدوران يتم إشتقاقها هنا بواسطه طريقة توزيع الكتله المتكافئ. عناصر المحور المتناهيه في الصغر يتم دمجها في نظام لحساب الأهترزات الطبيعيه لأنظمة الحمل الدورانيه لحساب الترددات الطبيعيه لمحور توصيل آلات الحفر يتم أختزال معادلات الحركه لأقل عدد ممكن, ثم يتم حل المعادلات بطريقه التكامل للحصول علي الأنحراف الحاصل لمحور توصيل آلات الحفر نتيجه لإثارات مختلفه.

Chapter I

INTRODUCTION

Drilling is one of the most important operations in petroleum and mining industry, starting from exploration and continuing through every phase of production until completion of production activities. Drilling is performed for several processes such as geological exploration for mineral deposits, making holes for placement of explosives for blasting, for research purposes, drilling for petroleum and so forth. One of the uses for drilling is in oil industry and it is a complex technique, which is influenced by many factors. These factors include bit type and geometry, applied thrust and rotational speed, flushing media and flushing rate and borehole properties. Among those the first three factors are controllable parameters where as the last factor is beyond control.

1.1 Drilling methods:

Drilling methods can be classified according to several criteria. These include size of borehole, method of mounting and type of power used. Mechanical drilling process is the most successful method for practical applications and it can be performed basically in two ways, either by percussive action or rotary action, shown in figure 1.1 [1].

1.2 Drilling system components

The three main functional components of any drilling system are drill collar, drill pipe and the bit. To these may be added a fourth component, the circulation fluid, which cleans the borehole and cools the bit during the drilling operation.

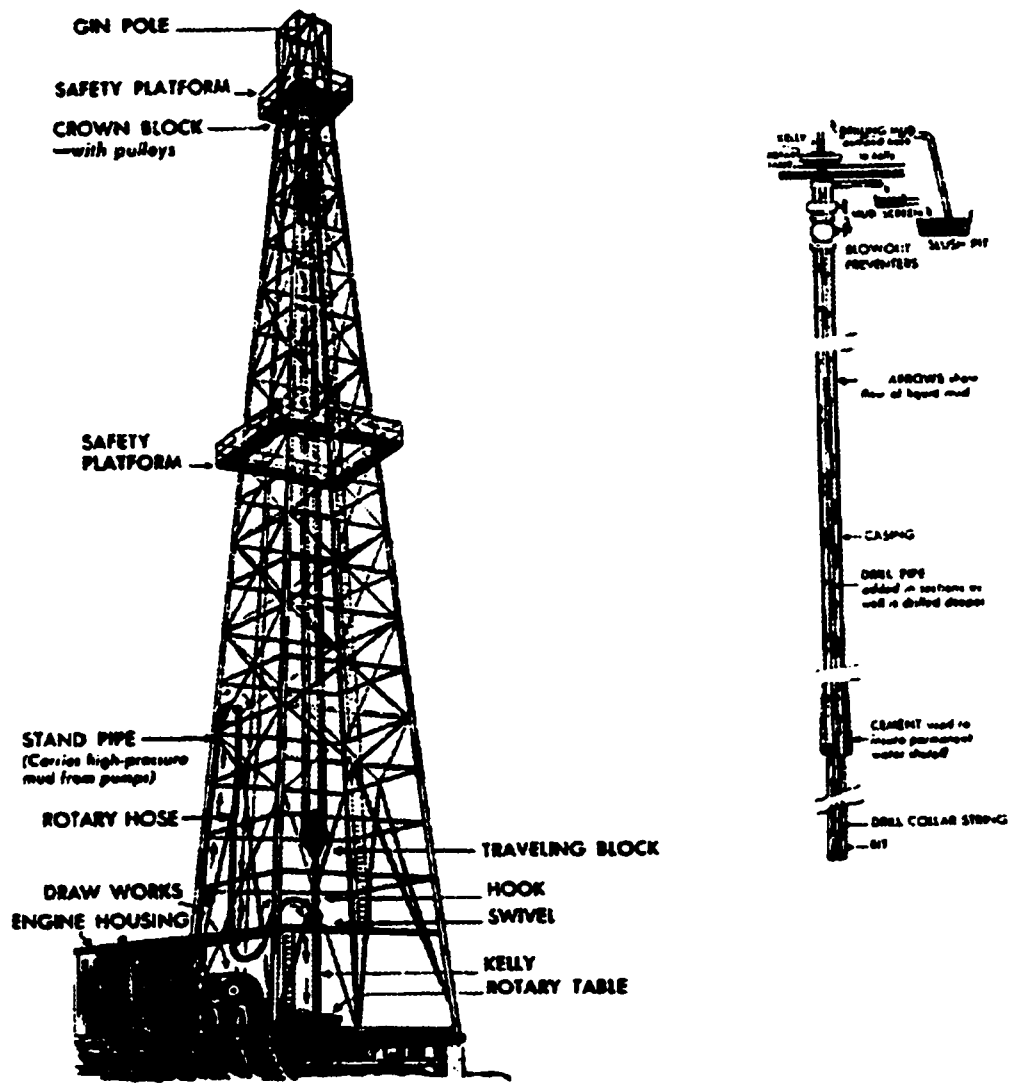


Figure 1.1: Rotary drilling equipment

The drillpipe is the prime movers and its main function is to convert energy from its original drive (electrical or combustion engine drive) into mechanical energy to actuate the system and to support the weight of the lower components of the drillstring. The drillpipe constitute the longest section of the drillstring and most of its length is under tension. Drillcollars, on the other hand, transmit the energy from the prime mover or source to the bit and are mostly under compression in order to supply the weight on bit (WOB). The bit is the applier of energy in the system, attacking the borehole formation mechanically to achieve penetration. The lower part of a drillstring is called bottom hole assembly (BHA) and is usually composed of drillcollars, stabilizers, and the bit. Along each section, the drillstring has nearly constant geometric and physical properties.

Two separate operations in drilling are involved to achieve penetration of the bit into the borehole formation. These are fracturing the borehole formation at the bit interface with ground and removal of the broken fragments formed during drilling. The effectiveness of drilling, in other words the rate of penetration of the bit, is certainly dependent on drilling method selected and how the drillstring is behaving. During the fracturing process drillstring vibrate and that would affect the drillstring performance. Vibration of drillstring has been the subject of extensive study, since it plays a critical role in drilling efficiency and cost.

1.3 Drillstring vibration

Drillpipe and bottom hole assemblies (BHA) experience a wide range of vibration during drilling operation. Excessive vibration level can lead to BHA component failure. Even moderate vibration levels, when sustained for extended periods of time can decrease the

useful life of BHA components. Eventually, the effect of vibration damage leads to the increase of the drilling cost due to loss of equipment or even loss of borehole.

The nature of drillstring vibration study is quite complicated because axial, torsional and lateral vibrations are all present at the same time. Axial or longitudinal vibration is associated with bit and Kelly bounce, which might damage the bit and BHA. Torsional vibration causes the rotation of the bit to become irregular, thus leading to drilling problems and deterioration of drill strength due to continuous loading and unloading, which may cause damage to the bit and pipe connections. Bending, transverse or lateral, vibrations are associated with drillstring buckling when the drillstring rotates with a center of rotation that is not coincident with the center of the borehole, which might cause hole enlargement. In general, the bit/formation interaction, stick-slip motion and drillstring/borehole interactions are the main cause of vibration in drillstrings. Vibration in drillstring involves other phenomena such as parametric resonance, whirling and contact with the borehole wall. The excessive vibrations caused by such phenomena were observed to cause wear, borehole enlargements, damage to the borehole wall and premature fatigue failure of downhole components.

When drillstring vibrates sometimes it create excitations that are at the rotational frequency or multiples of the rotational frequency. This phenomenon creates forces and stresses that oscillate at frequencies of the excitation mechanisms, which generate resonance condition with growing stresses. The speed at which resonance occur is called critical speed and it should be avoided during the drilling operation. Resonance or natural frequency of the drillstring system can be estimated with high accuracy if drillstring geometry and drilling

parameters are known. Accurate finite element models of drillstring can be used to predict drillstring resonances [2].

1.4 Literature Review

The analysis of the static deformation due to weight on bit of drillstring in two-dimensional curved boreholes was studied by Fischer [3]. Drillstring was modeled as elastic beam-column that has a constant geometric and material property over each element. The force and moment equilibrium relation along with the relation between bending moment and curvature of drillstring were used to derive the non-linear equations of motion, which were replaced by finite-difference equations. The drillstring deflection was obtained by solving the equations of motion using the standard matrix iterative procedure. Drillstring forces and deflections in three dimensions were analyzed by Walker et al. [4]. They assumed that the drilling assembly behaves as elastic bodies and the bit is centered in borehole. A simplified mathematical model using the ordinary approximate theory, a generalization of the Bernoulli-Euler theory, to relate the moments to the curvature was used to obtain the equations of motion for BHA. Mathematical modeling of drillstring as a straight beam using finite element technique was performed by Millheim [5], wherein they used a general-purpose finite element commercial system to study the drillstring deflection and bit forces. Variational principle or principle of minimum potential energy function was used to obtain nodal displacement. Two computational procedures to predict response characteristics were used; the first one used a straight beam element with six degrees of freedom at each node, and the second procedure employed a curved-beam element. In their formulation, the drillpipe was not considered, and they used the lumped mass approach at the nodal points of the drillcollar. Chandra [6] used the beam-column theory to analyze the static deflection of a

drillstring subjected to its self-weight and weight on bit. The drillstring was analyzed for two dimensions and three dimensions; however, it was restricted to static analysis of non-rotating drillstring, assuming no bending moment at the bit and no torsional effect. Euler buckling equation was used to determine the range of the buckling load, which is a function of modulus of elasticity, moment of inertia and length of drillstring.

Vandiver et al. [7] studied the transverse vibrations caused by whirling of a rotating unbalanced drillstring. The bending vibration relation was derived from the moment/curvature relationship, in which it includes the effect of rotating rate and whirling on bending stresses. Two principal sources of bottom hole assembly bending vibration were discussed: drillcollar whirling and linear coupling between axial forces on the bit and bending vibration of an initially curved drillstring. Drillcollar whirling is the centrifugally induced bowing of the drillcollar that result from rotation. Two types of drillcollar whirling were discussed forward whirl in which the same side of the collar is in continuous contact with the side of the hole causing flat worn in one place of drillstring. The other type discussed was the backward whirl where an expression was extracted from the relative tangential slip velocity between the drillcollar and the borehole wall assuming constant contact between drillcollar and borehole wall. The developed relation for the tangential velocity between the drill collar outside diameter and the borehole wall from which one can deduce the whirl type. In addition to whirling, they observed from field measurements that transverse vibrations are coupled with axial vibrations. Five different cases were discussed regarding forward and backward whirl and concluded that whirling of BHA in the borehole can occur during normal drilling operation. A predictive model for vibration was not presented. The theory of rotor dynamics was used by Jansen [8] to describe the dynamics of stabilized drillcollars, wherein the axial and torsional vibrations were not considered in the model. The equation of

motion for lateral deflection was developed for mass-spring system with two degrees of freedom by assuming a constant rotary speed and neglecting the influence of gravity on drillcollars. Virtual work approach was used to obtain the equivalent mass and stiffness parameters of the system.

In his experimental work Ford Brett [9] with one type of bits, polycrystalline diamond compact (PDC), found that torsional vibration was high in harder rocks, at higher applied WOB and at low rotary speed. It was found that drillstring vibrations normally occurred only when the bit was on bottom drilling ahead and it rotated smoothly while off bottom. In some cases, torsional vibration was eliminated by lifting up the bit off bottom and allowing the vibration to die, and then go back to the bottom at either a higher rotary speed or with less WOB. These resolutions might decrease the torsional vibration, however, higher rotary speed can increase the tendency toward other forms of vibration. A laboratory model was developed to describe the nonlinear self-excited torsional vibration of drillstring, with two coupled differential equations. The first equation describing the behavior of the drillstring as a lumped mass-spring system and the second equation describes the surface drive system. Thomas [10] attributed some of the drillstring torsional vibration to stick-slip operation. In the stick-slip operation the bit stops for a finite time interval and then slips at high angular velocity up to two or three times drillstring rotation. Hasley [11] presented a mathematical method for the computation of torsional resonance frequencies in drillstring using the generalized torsional displacement equation. The torsional equation of motion was solved by Fourier techniques to obtain torsional resonance frequencies. They indicated through experimental data that frequencies of the torsional resonance are not affected by the rotation rate of weight-on-bit. The limitation in these models is that it deals only with torsional vibration. Close [12] presented four experimental case studies of vibration levels in

drillstring attained during commercial drilling operation. They concluded that lateral vibration levels were larger than longitudinal vibration levels, significant lateral vibration can occur when reaming to bottom and when drilling a casing shoe. Clayer [13] studied the effect of surface and downhole boundary conditions on torsional and axial vibration of drillstring. Their conclusions were for torsional vibration damping at the bit is necessary to obtain good correlation between measured and simulated dynamic properties. In the axial response case, the bottom boundary conditions are complicated function of time and drilling parameters. The effective stiffness and damping of the rock appear to depend strongly on the weight on bit and on many other parameters, such as RPM, mud flow rate and bit type. Axisa [14] presented the physical phenomena concerning non-conservative coupling effects between the rotating shaft and the external fluid. They modeled the drillstring as a beam element having two nodes at the ends. The stabilizers were considered as bearing elements and the drill hole as radial gap element. The mud in the annulus between the drillstring and the well borehole was modeled with mass, damping-gyroscopic and stiffness matrices, while the mud inside the drillstring was modeled with a mass matrix only. Lumped parameter approach were used to obtain mass and stiffness matrices. The effects of gravity and buoyancy were taken into account in developing the equations of motion. The equations of motion were solved iteratively after neglecting the axial and torsional vibrations.

Further investigations by Dunayevsky et. al. [15] established the conditions under which the drillstring becomes laterally unstable as a result of axially induced vibrations. In their study, they assumed the drillstring to be in permanent contact with the borehole wall along its entire length, which will eliminate any impact between the drillstring and borehole wall. In addition, drillstring rotary motion was ignored; as a result, torsional and gyroscopic forces disappeared from the equations of motion. Parametric resonance theory was used to

develop the drillstring vibration model in which it was assumed that axial and lateral vibration modes to be coupled only through the parametric resonance mechanism which is valid for small-curvature boreholes. The governing equations for drillstring motion were derived in terms of the axial displacement and precession angle, in which, the finite element equations were obtained by using the variational technique. Solution of the equations of motion were not carried out, instead, the condition at which these equations had exponentially growing solutions that would correspond to the onset of rapidly growing lateral vibrations were established. Drillstring vibration severity with changing drilling parameters was evaluated using the finite_element analysis approach. Although Yigit and Christoforou [16] studied the transverse vibrations induced by axial loading and impact with the wellbore wall, it was restricted to non-rotating drillstrings, therefore, torsional vibration was not considered. They assumed all deformation to occur in a single plane with an intermittent contact between the drillstring and the wellbore wall, wherein the impact force obtained from the Hertzian contact law. The assumed mode method was used to derive the equations of motion for BHA. In the formulation of the equations several assumptions were made such as the upper portion of drillcollar is undergoing only axial vibration while the lower portion is under combined axial and lateral vibration, moreover, torsional vibration was neglected. The previous model was extended to include the effect of rotation on drillstring dynamics [17]. The effects of gyroscopic moments, contact with borehole wall, axial excitation due to bit/formation interactions and hydrodynamic damping were included. The drillcollars were modeled as Rayleigh beams with simply supported boundary conditions at the stabilizer locations. In the previous model as well as in this model the drillstring was assumed to be a solid cylinder of uniform cross section. Neglecting torsional vibration, equations of motion were obtained by using the assumed modes method and applying the Lagrangian approach, which were solved numerically for a number of parameter values.

Berlioz et al. [18] focused on laboratory tests concerned with the principal lateral instabilities. An experimental test rig was built to study the phenomena involved in the lateral drilling vibration. In their experimental work the effects of fluid, rotation speed, stabilizers, axial force and torque on natural frequencies and parametric instabilities were investigated. It was concluded that constant torque and compression forces decrease lateral frequency, on the other hand, tension force increases lateral frequencies. Drillcollars imbalance effect on vibration was addressed by Dykstra et al. [19]. Drillcollars imbalance generates high level of lateral vibration due to centrifugal forces when drillstring components are rotated. Neglecting axial and torsional deformations equations of motion were obtained by virtual work method for single degree of freedom system. Field observations showed that drillcollars were unbalanced initially causing bore misalignment, initial curvature, and gradual wears during service.

A linear stability approach was used by Abbassian et. al. [20] to describe the nature of torsional and lateral bit dynamics and identify the underlying relationship between various parameters such as rotating speed, WOB, string stiffness, bit and top drive characteristics required for a stable bit motion. Three models were discussed: torsional model, lateral model and coupled torsional-lateral model. Equations of motion were obtained for the three models by assuming a permanent contact between the bit and wellbore side, and neglecting axial deformation. The stability analysis lead to establishing the conditions under which the constant-speed bit rotation may be stable. Heisig et. al. [21] analyzed the lateral dynamic behavior of inclined drillstring in continuous contact with wellbore. In the analytical model developed for the BHA, they used the principle of virtual work to obtain the equation of motion in which the WOB is considered. In both of the modeled developed in the analytical and finite element models, only the BHA section is considered and rotation of drillstring is

not introduced, therefore neglecting the gyroscopic effect. The bit stick-slip motion was analyzed by Challamel et. al. [22] using rock mechanics considerations coupled with field bottomhole data. They attributed the self-excited torsional vibration phenomenon to the rock cutting process, which is an interaction between the bit and the rock. Two different stability methods (direct method and linearized method) were used to show the effect of rock/bit interaction in the stability of the drillstring.

1.5 Current Status

Vibration of rotating drillstring cannot be completely eliminated, however, it can be reduced and one of the techniques to reduce vibration is by operating away from resonance conditions, because when the excitation mechanisms match these resonances, damaging vibration can be induced. Considerable work has been carried out on various aspects of drillstring dynamics. These were mainly concerned either with the drillstring deflection or with axial, lateral, or torsional excitation mechanisms. Earlier studies focused on static analysis of the drillstring system due to buckling under WOB and the self-weight of drillcollar section. Most of the recent studies, however, focused on the dynamic analysis of drillstrings. Several studies addressed the different types of vibrations in a nonrotating drillstring; namely the axial, flexural and torsional vibrations. Some investigators also addressed the effect of drillstring rotation. The increasing demand for gaining more insight into the dynamics of such a complex dynamic system has directed the investigators to search for more accurate dynamic modules. In addition, a parallel search for better understanding of the drillstring dynamics is sought through some experimental studies. Although, experimental investigations are crucial to grasp what happens in the actual field application, they are time consuming, costly to perform on a full-scale drillstring, and may be difficult to

perform in a laboratory test rig. Mathematical modeling of drillstring, on the other hand, is much less costly, less time consuming, and easier to simulate.

Although many investigations are reported for modeling and analysis of drillstring dynamics, a comprehensive understanding of all vibration phenomena involved is still lacking. In the previously cited investigation some were restricted to non-rotating drillstring, therefore, neglecting gyroscopic effects, and in some other investigations the axial force generated by WOB was not accounted for. The previous models for drillstrings were restricted for BHA analysis, which will add more limitations on the model by ignoring the dynamics of the drillpipe. In addition, most of the reported formulations were either based on simple lumped mass-spring-damper elements, or on simple beam theory using standard reliability relations. Few investigations presented dynamic modals utilizing the assumed modes technique.

The finite element method, which has been established as the most powerful numerical technique, was not fully utilized in drillstring dynamics. Very few investigators used the FEM in developing the drillstring dynamic model. However, such finite element modules were for non-rotating drillstrings, where gyroscopic effects, as well as the gravitational stiffening effect were ignored. Moreover, the reported analysis using FEM were limited to modal frequency analysis, or stability analysis, while the time-response calculations were not addressed.

1.6 Objective and Approach

The objective of this study is to establish an accurate mathematical model to dynamically analyze drillstrings using the consistent mass FEM approach, which includes drillstring rotation, gyroscopic effect and gravitational stiffening. The developed model is derived to include all drillstring components, and made versatile to accommodate various boundary conditions and external excitations that may exist in real life drilling. The developed model is implemented in a computational scheme that is capable of performing both modal and time-response analysis. The development of the dynamic model consists of the following tasks:

1. To formulate a drillstring equation of motion using the Lagrange's approach in conjunction with the finite element method. The model to be developed accounts for the bending, torsional and axial vibrations, as well as the effect of rotary inertia, gyroscopic moments and axial stiffening due to gravitational force field.
2. To develop a finite shaft element to model the shaft geometry using the consistent mass approach of the FEM method. The finite shaft element has two nodes: with each node having six degrees of freedom. These are two transverse displacements, one axial displacement, two bending rotations and one torsional rotation. The developed finite shaft element permits different geometries of the drillstring components, as well as elements of different lengths and cross-sectional properties. The explicit form of the mass, stiffness and gyroscopic matrices of drillstring finite element are to be derived and tabulated in explicit form to enhance the computational efficiency.

3. To develop a finite element program that generates the consistent element matrices where the effect of rotary inertia, gyroscopic moments and axial stiffening are accounted for at the element level. The equation of motion of drillstring, which includes drillpipe, drillcollar and stabilizers, to be assembled using the finite element coefficient matrices.
4. To perform modal analysis for different drillstring configurations and rotational speeds. To this end, the generalized eigenvalue problem is obtained and solved numerically for the modal characteristics of the drillstring. In this regard, the non-self-adjoint eigenvalue is considered, which results in complex eigenvalues and eigenvectors due to presence of the gyroscopic effects.
5. To perform dynamic response analysis of the drillstring by calculating the time histories of the drillstring elastic deformations due to different external excitations. In this context, two forms of the equation of motion are considered. One that represents the full-order model in terms of the physical nodal coordinates, and another in terms of a reduced set of modal coordinates. To obtain the later, modal transformations are established in terms of a truncated set of significant modes and equations of motion are written in the modal form. In either case, equations of motion are integrated forward in time to for the dynamic response of the rotating drillstring. Perform a comparison between full-order model and reduced-order model solutions to test the accuracy and efficiency of the reduced model.

Chapter II

THE DRILLSTRING DYNAMIC MODEL

Introduction

Two reference frames are employed to describe the motion of the drillstring system. These are the fixed reference frame, and the rotating reference frame.

In this formulation, it is assumed that the material of the drillstring is elastic, homogeneous and isotropic. The deflection of the drillstring is produced by the displacement of points of the center-line. The internal damping and flow-induced forces are neglected. Drillstring boundary conditions are as shown in figure 2.1, at the top of drillstring assumed to be fixed to the rotary table and at the stabilizers area a pin joint condition is assumed, which will restrict translation in the Y and Z directions.

2.1 Elemental coordinate system of the drillstring

The finite element method is used to model the drillstring [30]. Referring to figure 2.2 let $X Y Z$ be a Cartesian coordinate system with its origin fixed to the undeformed element. The $x y z$ is a Cartesian coordinate system after deformation of the element. The $x y z$ coordinate system is rotated with respect to the $X Y Z$ coordinate system through a set of angles as shown in figure 2.3. The general orientation of beam element cross-section can be described by first rotating it by an angle φ around the X axis, then an angle θ_1 around the new y axis (y_1), and then by an angle θ_2 around the final z axis (z_2). The instantaneous angular velocity vector ω of the $x y z$ frame can be expressed as

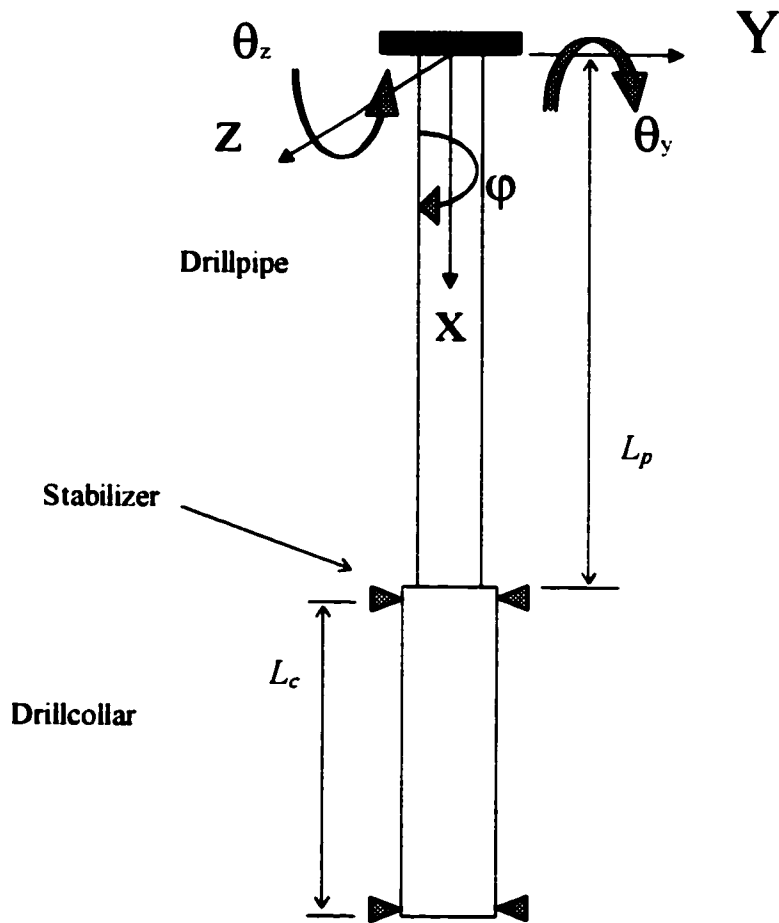


Figure 2.1: Drillstring layout

$$\omega = \dot{\varphi} I + \dot{\theta}_y j_1 + \dot{\theta}_z k_2 \quad (2.1)$$

where I , j_1 and k_2 are unit vectors along the X , y_1 and z_2 axes, respectively. Transforming equation (2.1) into $X Y Z$ coordinate system will yield

$$\begin{aligned} \omega = \dot{\varphi} I + \dot{\theta}_y [\cos(\varphi)J + \sin(\varphi)K] \\ + \dot{\theta}_z [-\sin(\theta_y)I - \sin(\varphi)\cos(\theta_y)J + \cos(\theta_y)\cos(\varphi)K] \end{aligned} \quad (2.2)$$

Assuming θ_y and θ_z to be small, which will simplify to

$$\cos(\theta_y) = \cos(\theta_z) = 1 \quad (2.3)$$

and

$$\sin(\theta_y) = \theta_y, \quad \sin(\theta_z) = \theta_z \quad (2.4)$$

Substituting the relations in equations (2.3)-(2.4) in the angular velocity equation (2.2), one gets

$$\begin{aligned} \omega = \dot{\varphi} I + \dot{\theta}_y [\cos(\varphi)J + \sin(\varphi)K] + \dot{\theta}_z [-\theta_y I - \sin(\varphi)J + \cos(\varphi)K] \\ = (\dot{\varphi} - \dot{\theta}_z \theta_y) I + (\dot{\theta}_y \cos(\varphi) - \dot{\theta}_z \sin(\varphi)) J + (\dot{\theta}_z \cos(\varphi) + \dot{\theta}_y \sin(\varphi)) K \end{aligned}$$

or

$$\omega = \begin{Bmatrix} \omega_x \\ \omega_y \\ \omega_z \end{Bmatrix} = \begin{Bmatrix} \dot{\varphi} - \dot{\theta}_z \theta_y \\ \dot{\theta}_y \cos(\varphi) - \dot{\theta}_z \sin(\varphi) \\ \dot{\theta}_z \cos(\varphi) + \dot{\theta}_y \sin(\varphi) \end{Bmatrix} \quad (2.5)$$

2.2 Kinetic energy of the drillstring

Referring to figure 2.2, let p be any point in the undeformed shaft element. The position of point p is defined by the vector r_p with respect to $X Y Z$. The global position of point p in figure 2.2 can be expressed as

$$r_p = R + r_o + u \quad (2.6)$$

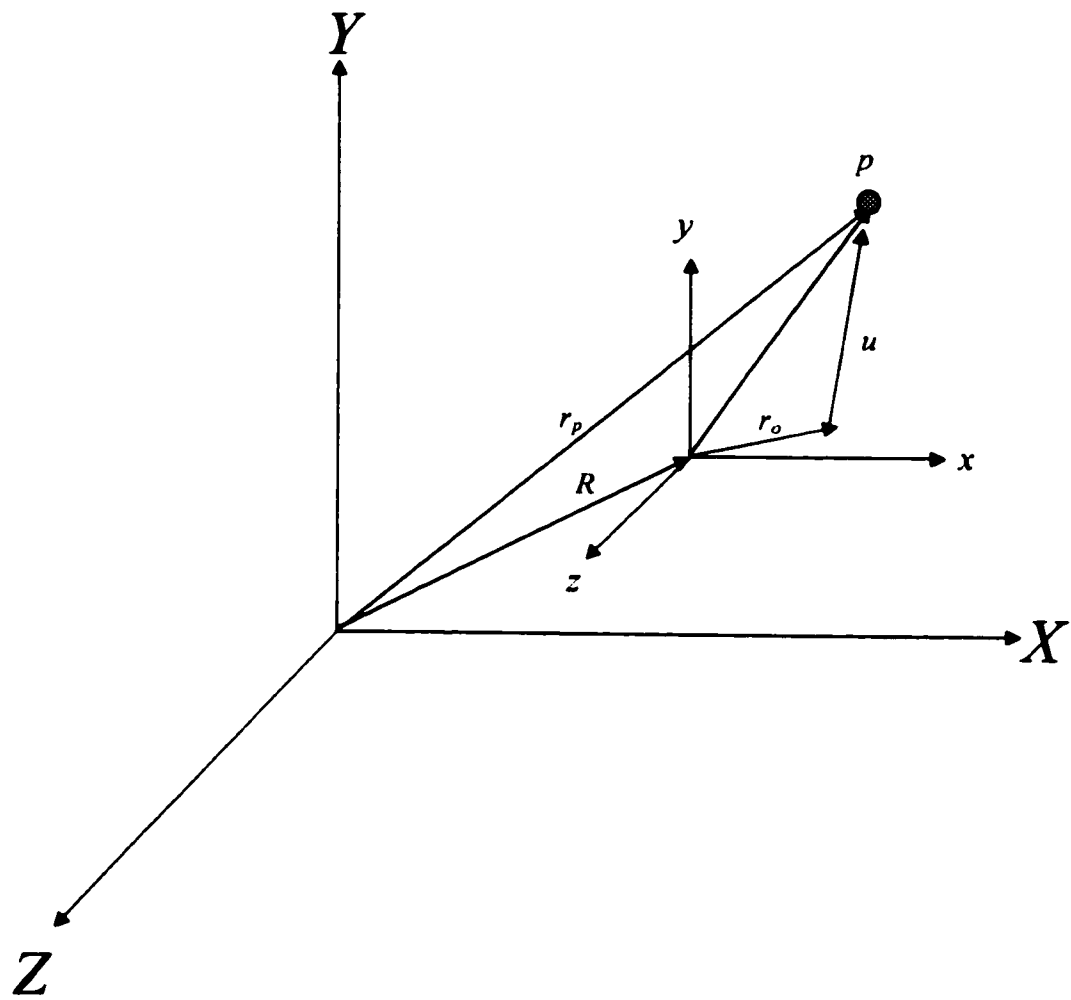


Figure 2.2: Generalized coordinates

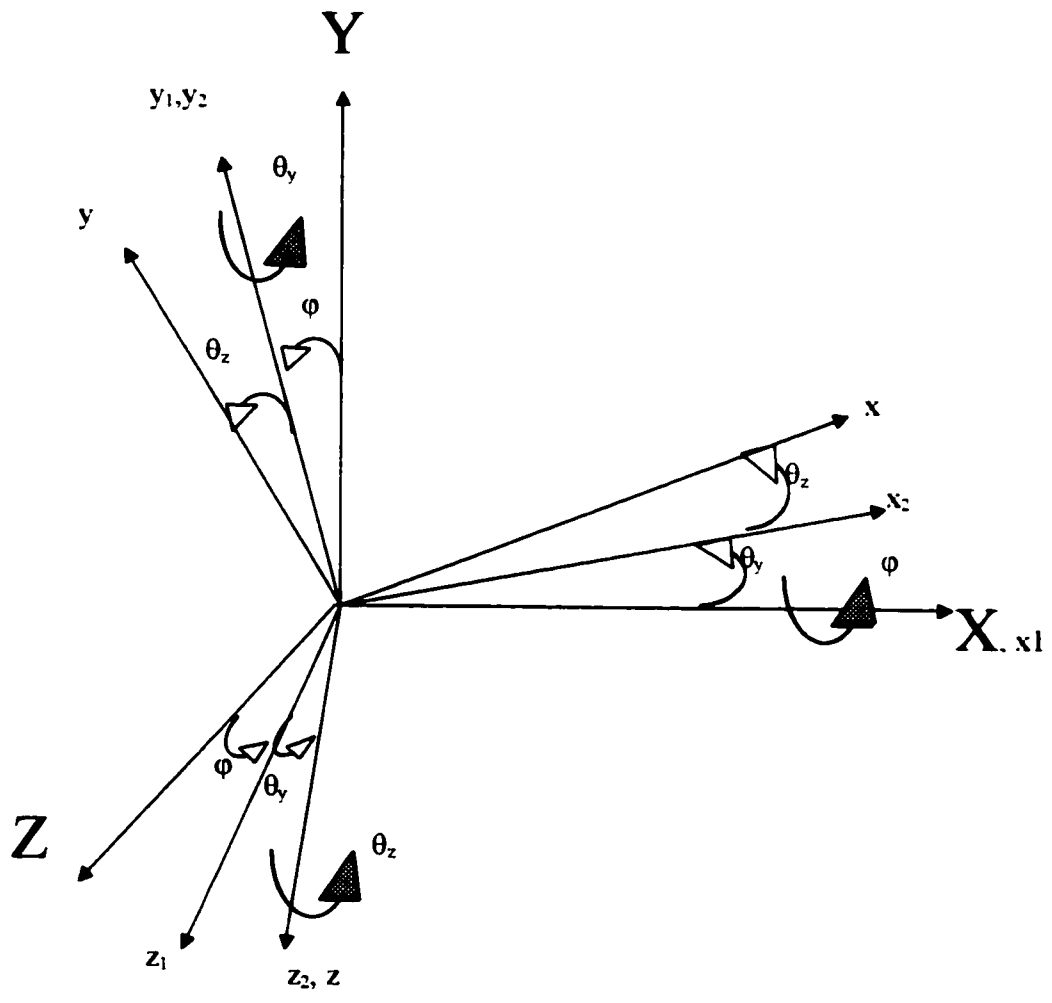


Figure 2.3: Rotation angles

where u represents the deformation vector of point p . Using the finite element analysis u can be written as

$$\{u\} = [N_v]\{e\} \quad (2.7)$$

The matrix $[N_v]$ is the translation shape function and $\{e\}$ is the vector containing nodal coordinates of the shaft element. The time derivative of equation (2.6) can be expressed in the form

$$\frac{dr_p}{dt} = \dot{r}_p + \omega \times r_p = \dot{r}_p + [\omega]\{r_p\} \quad (2.8)$$

where the skew-symmetric matrix $[\omega]$ is given by

$$[\omega] = \begin{bmatrix} 0 & -\omega_z & \omega_y \\ \omega_z & 0 & -\omega_x \\ -\omega_y & \omega_x & 0 \end{bmatrix}$$

Since there is no change in magnitude of R and r_o when the shaft element deforms, the rate of change of magnitude of the position r_p is given by

$$\{\dot{r}_p\} = \{\dot{u}\} = [N_v]\{\dot{e}\} \quad (2.9)$$

Substituting equation (2.9) in equation (2.8), we get

$$\frac{dr_p}{dt} = [N_v]\{\dot{e}\} + [\omega]\{r_p\} \quad (2.10)$$

The kinetic energy of the element is obtained by integrating the kinetic energy expression of the infinitesimal volume at point p over the volume V . This can be written as

$$T = \frac{1}{2} \int_V \mu \left\{ \frac{dr_p}{dt} \right\}^T \left\{ \frac{dr_p}{dt} \right\} dV \quad (2.11)$$

Where μ is the mass density of the shaft element. Now, substituting for $\frac{dr_p}{dt}$ from equation (2.8) in equation (2.11), we get

$$T = \frac{1}{2} \int_V \mu \left\{ \dot{e} \right\}^T [N_v]^T [N_v] \dot{e} + \dot{e} \right\}^T [N_v]^T [\omega] \{r_p\} + \{r_p\}^T [\omega]^T [N_v] \dot{e} + \{r_p\}^T [\omega]^T [\omega] \{r_p\} \} dV \quad (2.12)$$

The second and third terms in equation (2.12) are identically zero, because the moments of inertia are calculated with respect to the center of mass of the element. The first term represents the kinetic energy due to translation and the last term represents the kinetic energy due to rotational effects that include gyroscopic moments. The last term can be evaluated as follows

$$[\omega]^T [\omega] = \begin{bmatrix} \omega_z^2 + \omega_y^2 & -\omega_x \omega_y & -\omega_z \omega_x \\ -\omega_x \omega_y & \omega_z^2 + \omega_x^2 & -\omega_y \omega_z \\ -\omega_x \omega_z & -\omega_y \omega_z & \omega_y^2 + \omega_x^2 \end{bmatrix} \quad (2.13)$$

Therefore, the last term in equation (2.12) is rewritten as

$$\int_V \mu \{r_p\}^T [\omega]^T [\omega] \{r_p\} dV = \int_0^l \mu (I_x \omega_x^2 + I_y \omega_y^2 + I_z \omega_z^2) dx \quad (2.14)$$

Substituting equation (2.5) in equation (2.14), one obtains

$$\int_V \mu \{r_p\}^T [\omega]^T [\omega] \{r_p\} dV = \int_0^l \mu \left[I_x (\dot{\varphi} - \dot{\theta}_z \theta_y)^2 + I_y (\dot{\theta}_y \cos(\varphi) - \dot{\theta}_z \sin(\varphi))^2 + I_z (\dot{\theta}_z \cos(\varphi) + \dot{\theta}_y \sin(\varphi))^2 \right] dx \quad (2.15)$$

Defining

$$\mu I_z = \mu I_y = I_D, \quad \mu I_x = I_p \quad (2.16)$$

And expressing the variables and their derivatives as

$$\varphi = [N_\varphi] \{e\}, \quad \dot{\varphi} = [N_{\dot{\varphi}}] \{\dot{e}\} \quad (2.17)$$

$$\theta_y = [N_{\theta_y}] \{e\}, \quad \dot{\theta}_y = [N_{\dot{\theta}_y}] \{\dot{e}\} \quad (2.18)$$

$$\theta_z = [N_{\theta_z}] \{e\}, \quad \dot{\theta}_z = [N_{\dot{\theta}_z}] \{\dot{e}\} \quad (2.19)$$

Where the matrix $[N_\phi]$ is the torsional shape function and $[N_\theta]$, $[N_\alpha]$ are the bending rotational shape functions. Substituting the relations in equations (2.16)-(2.19) in equation (2.15), we get

$$\begin{aligned} \frac{1}{2} \int_V \mu \{\dot{r}_p\}^T \{\omega\}^T \{\omega\} \{r_p\} dV = \frac{1}{2} C \dot{\phi}^2 + \frac{1}{2} \{\dot{e}\}^T [M_\phi] \{\dot{e}\} - \\ \dot{\phi} \{\dot{e}\}^T [G] \{e\} - \{\dot{e}\}^T [M_c] \{\dot{e}\} + \frac{1}{2} \{\dot{e}\}^T [M_r] \{\dot{e}\} \end{aligned} \quad (2.20)$$

Where

$$\begin{aligned} C &= \int_0^l I_p dx \\ G &= \int_0^l I_p [N_\phi]^T [N_\alpha] dx \\ [M_\phi] &= \int_0^l I_p [N_\phi]^T [N_\phi] dx \\ [M_c] &= \int_0^l I_p \left([N_\phi]^T [N_\alpha] \{e\} [N_\theta] - [N_\phi]^T [N_\theta] \{e\} [N_\alpha] \right) dx \\ [M_r] &= \int_0^l I_D \begin{bmatrix} N_\theta \\ N_\alpha \end{bmatrix}^T \begin{bmatrix} N_\theta \\ N_\alpha \end{bmatrix} dx \end{aligned}$$

Therefore, the kinetic energy of the element can be written as

$$\begin{aligned} T = \frac{1}{2} \{\dot{e}\}^T [M_c] \{\dot{e}\} + \frac{1}{2} C \dot{\phi}^2 + \frac{1}{2} \{\dot{e}\}^T [M_\phi] \{\dot{e}\} - \\ \dot{\phi} \{\dot{e}\}^T [G] \{e\} - \{\dot{e}\}^T [M_c] \{\dot{e}\} + \frac{1}{2} \{\dot{e}\}^T [M_r] \{\dot{e}\} \end{aligned}$$

And if we add the similar terms together we get

$$T = \frac{1}{2} \{\dot{e}\}^T [M] \{\dot{e}\} + \frac{1}{2} C \dot{\phi}^2 - \dot{\phi} \{\dot{e}\}^T [G] \{e\} \quad (2.21)$$

Now, the augmented mass matrix $[M]$ can be defined as

$$[M] = [M_i] + [M_r] + [M_\phi] - 2[M_c] \quad (2.22)$$

Where $[M_c]$ represents the coupling between torsional and transverse vibration, which is time dependent.

2.3 Strain energy of the drillstring

There are three translations (u, v, w) : two of them (v, w) are due to bending. The rotations (θ_y, θ_z) are related to bending deformations by

$$\theta_y = \frac{\partial v(x, t)}{\partial x} \quad (2.23)$$

$$\theta_z = -\frac{\partial w(x, t)}{\partial x} \quad (2.24)$$

2.3.1 Strain Energy due to bending:

The strain energy expression due to bending U_1 is given by

$$U_1 = \frac{1}{2} \int_V \varepsilon \sigma dV \quad (2.25)$$

where

$$\sigma = E\varepsilon \quad (2.26)$$

and

$$\varepsilon = -y \frac{\partial^2 v}{\partial x^2} - z \frac{\partial^2 w}{\partial x^2} \quad (2.27)$$

Substituting the relation of equation (2.26) into equation (2.25), we get

$$U_1 = \frac{1}{2} \int_V E\varepsilon^2 dV \quad (2.28)$$

Similarly substituting the relation of equation (2.27) into equation (2.28), one can express the strain energy due to bending as

$$\begin{aligned}
U_1 &= \frac{E}{2} \int_0^l \int_A \left[-y \frac{\partial^2 v}{\partial x^2} - z \frac{\partial^2 w}{\partial x^2} \right] dA dx \\
&= \frac{E}{2} \int_0^l \int_A \left[y^2 \left(\frac{\partial^2 v}{\partial x^2} \right)^2 + z^2 \left(\frac{\partial^2 w}{\partial x^2} \right)^2 + 2yz \frac{\partial^2 v}{\partial x^2} \frac{\partial^2 w}{\partial x^2} \right] dA dx
\end{aligned} \tag{2.29}$$

It is noted that the last term in equation (2.29) is zero due to symmetry. Now, let us designate

$$I_z = \int_A y^2 dA, \quad \text{and} \quad I_y = \int_A z^2 dA \tag{2.30}$$

Substituting the relations in equation (2.30) into equation (2.29), we obtain

$$U_1 = \frac{E}{2} \int_0^l \left[I_z \left(\frac{\partial^2 v}{\partial x^2} \right)^2 + I_y \left(\frac{\partial^2 w}{\partial x^2} \right)^2 \right] dx \tag{2.31}$$

2.3.2 Strain energy due to torsion:

The strain energy expression U_2 due to torsion is given by

$$U_2 = \frac{1}{2} \int_0^l G I_p \left(\frac{\partial \phi}{\partial x} \right)^2 dx \tag{2.32}$$

Where G is the shear modulus and I_p is the polar moment of inertia.

2.3.3 Strain energy due to axial deformation:

The strain energy due to axial deformation U_3 is given by

$$U_3 = \frac{1}{2} \int_V \epsilon \sigma dV \tag{2.33}$$

Where

$$\sigma = E \epsilon, \quad \text{and} \quad \epsilon = \frac{du}{dx} \tag{2.34}$$

Substituting equation (2.34) into equation (2.33) will yield

$$U_3 = \frac{E}{2} \int_0^l \int_A \left(\frac{du}{dx} \right)^2 dA dx \quad (2.35)$$

Assuming constant cross sectional area, equation (2.35) reduces to the following equation:

$$U_3 = \frac{EA}{2} \int_0^l \left(\frac{du}{dx} \right)^2 dx \quad (2.36)$$

2.3.4 Strain energy due to axial stiffening:

The strain energy associated with the axial stiffening due to gravity can be expressed as

$$U_4 = \frac{1}{2} \int_0^l EA \frac{\partial u}{\partial x} \left(\left(\frac{\partial w}{\partial x} \right)^2 + \left(\frac{\partial v}{\partial x} \right)^2 \right) dx \quad (2.37)$$

In this case, the term $EA \frac{\partial u}{\partial x}$ represents the gravitation force. Designating the gravitational force by F , we can write equation (2.37) in the form

$$U_4 = \frac{1}{2} \int_0^l F \left(\left(\frac{\partial w}{\partial x} \right)^2 + \left(\frac{\partial v}{\partial x} \right)^2 \right) dx \quad (2.38)$$

Now, the total strain energy is obtained by adding the strain energies in equations (2.31), (2.32), (2.36), and (2.38), which can be written in the form

$$\begin{aligned} U &= U_1 + U_2 + U_3 + U_4 \\ U &= \frac{E}{2} \int_0^l \left(I_z \left(\frac{\partial v}{\partial x} \right)^2 + I_y \left(\frac{\partial w}{\partial x} \right)^2 + A \left(\frac{du}{dx} \right)^2 \right) dx + \frac{1}{2} \int_0^l GI_p \left(\frac{\partial \varphi}{\partial x} \right)^2 dx \\ &\quad + \frac{1}{2} \int_0^l F \left(\left(\frac{\partial w}{\partial x} \right)^2 + \left(\frac{\partial v}{\partial x} \right)^2 \right) dx \end{aligned} \quad (2.39)$$

Because of symmetry we can set

$$I_z = I_y = I(x) \quad (2.40)$$

Substituting from the relations in equations (2.23), (2.24), and (2.40) into equation (2.39), one obtains

$$U = \frac{E}{2} \int_0^l I(x) \left[\left(\frac{\partial \theta_y}{\partial x} \right)^2 + \left(\frac{\partial \theta_z}{\partial x} \right)^2 \right] dx + \frac{EA}{2} \int_0^l \left(\frac{du}{dx} \right)^2 dx + \frac{GI_p}{2} \int_0^l \left(\frac{\partial \varphi}{\partial x} \right)^2 dx + \frac{1}{2} \int_0^l F \left(\left(\frac{\partial w}{\partial x} \right)^2 + \left(\frac{\partial v}{\partial x} \right)^2 \right) dx \quad (2.41)$$

Equation (2.41) can be written in matrix form as

$$U = \frac{1}{2} \{e\}^T [K] \{e\} \quad (2.42)$$

Where $[K]$ is the augmented stiffness matrix given by

$$[K] = [K_b] + [K_a] + [K_\varphi] + [K_{ax}]$$

$[K_b]$: stiffness matrix due to bending deformation

$[K_a]$: stiffness matrix due to axial deformation

$[K_\varphi]$: stiffness matrix due to torsional deformation

$[K_{ax}]$: stiffness matrix due to the gravitational force field

2.3.5 Elemental equation of motion

The equation of motion of the element can be derived using Lagrange equation as

$$\frac{d}{dt} \left(\frac{\partial L}{\partial \dot{q}} \right) - \frac{\partial L}{\partial q} = Q \quad (2.43)$$

where

$L = T - U$: Lagrangian function

q : generalized coordinates

Q : vector of generalized forces

T : total kinetic energy

U : total strain energy

Substituting for L and q in equation (2.43) will yield the following equation of motion

$$[M]\{\dot{e}\} + \phi[G]\{\dot{e}\} + [K]\{e\} = \{Q\} \quad (2.44)$$

where

$[M]$: augmented mass matrix

$[G]$: gyroscopic matrix

$[K]$: augmented stiffness matrix

Equation (2.44) represents the dynamic equation of motion at the element level. The equation of motion of the whole drillstring is then derived by assembling the discretized element equations. In the next chapter, the elemental coefficient matrices $[M]$, $[G]$ and $[K]$ are established, and the standard finite element modeling assembly procedure is invoked to obtain the equations of motion of the drillstring.

Chapter III

FINITE ELEMENT FORMULATION

3.1 Finite Element Model

The finite element formulation is applied to solve the equation of motion developed in the previous chapter. The basic concept of the finite element approach is to subdivide a large complex structure into a finite number of simple elements, such as beam, plate, and shaft elements. In this case, a set of n second-order differential equations are obtained where n is the number of discretized degrees of freedom. A properly generated mesh of finite elements can define the drillstring configuration. In this formulation, the drillstring element has circular cross-section and consists of two nodes. Each node has six degrees of freedom, two transverse displacements, two bending rotations, one torsional rotation, and one axial displacement. The drillstring element deformation vector is defined as

$$\{e(t)\} = \{u_1, v_1, w_1, \theta_{y1}, \theta_{z1}, \phi_1, u_2, v_2, w_2, \theta_{y2}, \theta_{z2}, \phi_2\}^T \quad (3.1)$$

Utilizing the assumed displacement fields, the transverse and axial deformation of an element is represented in terms of shape functions as

$$\begin{aligned} \begin{Bmatrix} u(x,t) \\ v(x,t) \\ w(x,t) \end{Bmatrix} &= \begin{bmatrix} N_{u1} & 0 & 0 & 0 & 0 & 0 & N_{u2} & 0 & 0 & 0 & 0 & 0 \\ 0 & N_{v1} & 0 & 0 & N_{v2} & 0 & 0 & N_{v3} & 0 & 0 & N_{v4} & 0 \\ 0 & 0 & N_{v1} & N_{v2} & 0 & 0 & 0 & 0 & N_{v3} & -N_{v4} & 0 & 0 \end{bmatrix} \{e(t)\} \\ &= [N_v(x)]\{e(t)\} = \begin{bmatrix} N_u \\ N_v \\ N_w \end{bmatrix} \{e(t)\} \end{aligned} \quad (3.2)$$

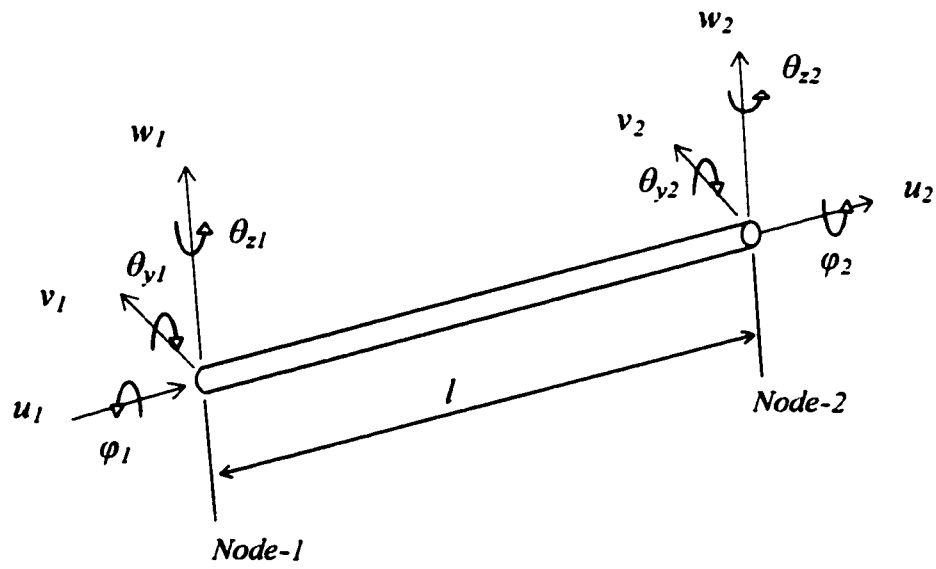


Figure 3.1: Order of degrees of freedom for drillstring element

The rotation of a typical cross section is expressed as

$$\begin{aligned} \begin{Bmatrix} \theta_y \\ \theta_z \end{Bmatrix} &= \begin{bmatrix} 0 & N_{\theta 1} & 0 & 0 & N_{\theta 2} & 0 & 0 & N_{\theta 3} & 0 & 0 & N_{\theta 4} & 0 \\ 0 & 0 & -N_{\theta 1} & N_{\theta 2} & 0 & 0 & 0 & 0 & -N_{\theta 3} & N_{\theta 4} & 0 & 0 \end{bmatrix} \{e(t)\} \\ &= [N_{\theta_x}(x)] \{e(t)\} = \begin{bmatrix} N_{\theta_y} \\ N_{\theta_z} \end{bmatrix} \{e(t)\} \end{aligned} \quad (3.3)$$

Similarly the torsional displacement of a typical cross section is written as

$$\begin{aligned} \varphi(x,t) &= [0 \ 0 \ 0 \ 0 \ 0 \ N_{\phi 1} \ 0 \ 0 \ 0 \ 0 \ 0 \ N_{\phi 2}] \\ &= [N_{\phi}] \{e(t)\} \end{aligned} \quad (3.4)$$

Where N_u , N_v , and N_w represent static displacement modes associated with unit displacement of one of the end point. The matrices N_{θ_y} , N_{θ_z} represent bending rotation shape functions, and N_{ϕ} represents the torsional shape function. The explicit expressions of the aforementioned shape functions are derived in reference [23] and given in table 3.1.

3.2 Stiffness Matrices

The strain energy expression of a rotating drillstring element of length l in matrix form is given by

$$U = \frac{1}{2} \{e\}^T [K] \{e\} \quad (3.5)$$

The matrix $[K]$ is the augmented stiffness matrix given by

$$[K] = [k_e] + [k_a] + [k_{\theta}] + [k_{\phi}] \quad (3.6)$$

where

$$[k_e] = \int_0^l [B_e]^T EI [B_e] dx \quad \equiv \quad \text{Elastic stiffness matrix} \quad (3.7)$$

$$[k_a] = \int_0^l [B_a]^T EA [B_a] dx \equiv \text{Axial stiffness matrix} \quad (3.8)$$

$$[k_\phi] = \int_0^l [B_\phi]^T GI_p [B_\phi] dx \equiv \text{Torsional stiffness matrix} \quad (3.9)$$

$$[k_{ax}] = \int_0^l F [B_{ax}]^T [B_{ax}] dx \equiv \text{Axial stiffening matrix} \quad (3.10)$$

While

$$[B_a] = \frac{\partial}{\partial x} [N_u] \quad (3.11)$$

$$[B_\phi] = \frac{\partial}{\partial x} [N_\phi] \quad (3.12)$$

$$[B_{ax}] = \frac{\partial}{\partial x} [N_v] \quad (3.13)$$

$$[B_{ax}] = \frac{\partial}{\partial x} [N_v] \quad (3.14)$$

Integrating equations (3.7)-(3.10), the stiffness matrices are obtained in explicit form with non-zero entries as presented in tables 3.2-3.4.

Table 3.1
Explicit expression of the shaft element shape functions

$N_{v1} = 1 - 3\left(\frac{x}{l}\right)^2 + 2\left(\frac{x}{l}\right)^3$	$N_{\theta1} = \frac{6}{l}\left(\left(\frac{x}{l}\right)^2 - \frac{x}{l}\right)$
$N_{v2} = l\left(\frac{x}{l} - 2\left(\frac{x}{l}\right)^2 + \left(\frac{x}{l}\right)^3\right)$	$N_{\theta2} = 1 - 4\left(\frac{x}{l}\right) + 3\left(\frac{x}{l}\right)^2$
$N_{v3} = 3\left(\frac{x}{l}\right)^2 - 2\left(\frac{x}{l}\right)^3$	$N_{\theta3} = \frac{6}{l}\left(\frac{x}{l} - \left(\frac{x}{l}\right)^2\right)$
$N_{v4} = l\left(-\left(\frac{x}{l}\right)^2 + \left(\frac{x}{l}\right)^3\right)$	$N_{\theta4} = 3\left(\frac{x}{l}\right)^2 - 2\frac{x}{l}$
$N_{u1} = 1 - \frac{x}{l}$	$N_{\phi1} = 1 - \frac{x}{l}$
$N_{u2} = \frac{x}{l}$	$N_{\phi2} = \frac{x}{l}$

Table 3.2

Elastic stiffness matrix of rotating drillstring element $[k_e] = EI[k_{ab}^e]$
 The non-zero entries of the upper triangular part of $[k_{ab}]$, $a, b = 1, 2, \dots, 12$

$$k_{22}^e = -k_{28}^e = k_{33}^e = -k_{29}^e = k_{88}^e = k_{99}^e = \frac{12}{l^3}$$

$$k_{25}^e = k_{211}^e = -k_{34}^e = -k_{310}^e = k_{39}^e = -k_{58}^e = -k_{811}^e = k_{910}^e = \frac{6}{l^2}$$

$$k_{44}^e = k_{55}^e = k_{1010}^e = k_{1111}^e = \frac{4}{l}$$

$$k_{410}^e = k_{511}^e = \frac{2}{l}$$

Table 3.3

Axial stiffness matrix of rotating drillstring element $[k_a] = EA[k_{ab}^a]$
 The non-zero entries of the upper triangular part of $[k_{ab}]$, $a, b = 1, 2, \dots, 12$

$$k_{11}^a = k_{77}^a = \frac{2}{l}$$

$$k_{17}^a = \frac{1}{l}$$

Table 3.4

Torsional stiffness matrix of rotating drillstring element $[k_\phi] = GI_p[k_{ab}^\phi]$
 The non-zero entries of the upper triangular part of $[k_{ab}]$, $a, b = 1, 2, \dots, 12$

$$k_{66}^\phi = -k_{612}^\phi = k_{1212}^\phi = \frac{1}{l}$$

3.3 Axial Stiffening due to Gravitational Field

Drillpipe section is a long section of the drillstring, which has a low resistance to any applied axial loads and tend to fail by buckling when subjected to a vertical compression load. Therefore, drillpipe is generally under tension load and the point separating drillpipe from drillcollar is called neutral point. The neutral point is defined as the point having zero axial force. Figure 3.2 shows the desired location of the neutral point [1].

The axial stiffening term $[k_{ax}]$ is given by equation (3.10) and is written again here to derive an expression for the force F :

$$[k_{ax}] = \int_0^{l_i} F[B_{ax}]^T [B_{ax}] dx \quad (3.15)$$

where

$$[B_{ax}] = \frac{\partial}{\partial x} [N_v] \quad (3.16)$$

The axial force F due to the weight associated with a differential element located at point p of the finite element i can be written as

$$dF = \rho gA dr_p \quad (3.17)$$

where

A : cross sectional area

g : acceleration of gravity

ρ : density

In this context, since one needs to refer to a specific element, let us denote l_i as the length of element i . For drillpipe under tension, referring to figure 3.3, the length r_p from the neutral point to point p can be written as

$$r_p = L_i + (l_i - x) \quad (3.18)$$

where

$$L_i = \sum_{j=i+1}^n l_j$$

Differentiating equation (3.18) with respect to x

$$dr_p = -dx \quad (3.19)$$

Substituting for dr_p in equation (3.17), the axial force F_i due to gravity on point p can be expressed as

$$dF_i = \rho g A (-dx) \quad (3.20)$$

Now, the tensile force acting on a section at point p due to the weight can be calculated by integrating equation (3.20) over the span between point p and the neutral point. The resulting tensile force is

$$F_i = - \left[\int_{L_p-L_i}^{L_p} \rho g A dx + \int_x^{l_i} \rho g A dx \right] \quad (3.21)$$

Where L_p is the length of the drillpipe segment under tension. Evaluating the integral in equation (3.21) while taking ρ , g , and A as constants will yield the following expression

$$F_i = -\rho g A [L_i + (l_i-x)] \quad (3.22)$$

The axial stiffening stresses resulting from the tensile force F_i are incorporated into the integration of $[k_{ax}]$ in equation (3.10), resulting in the stiffening matrix of the rotating drillstring element given in table 3.5.

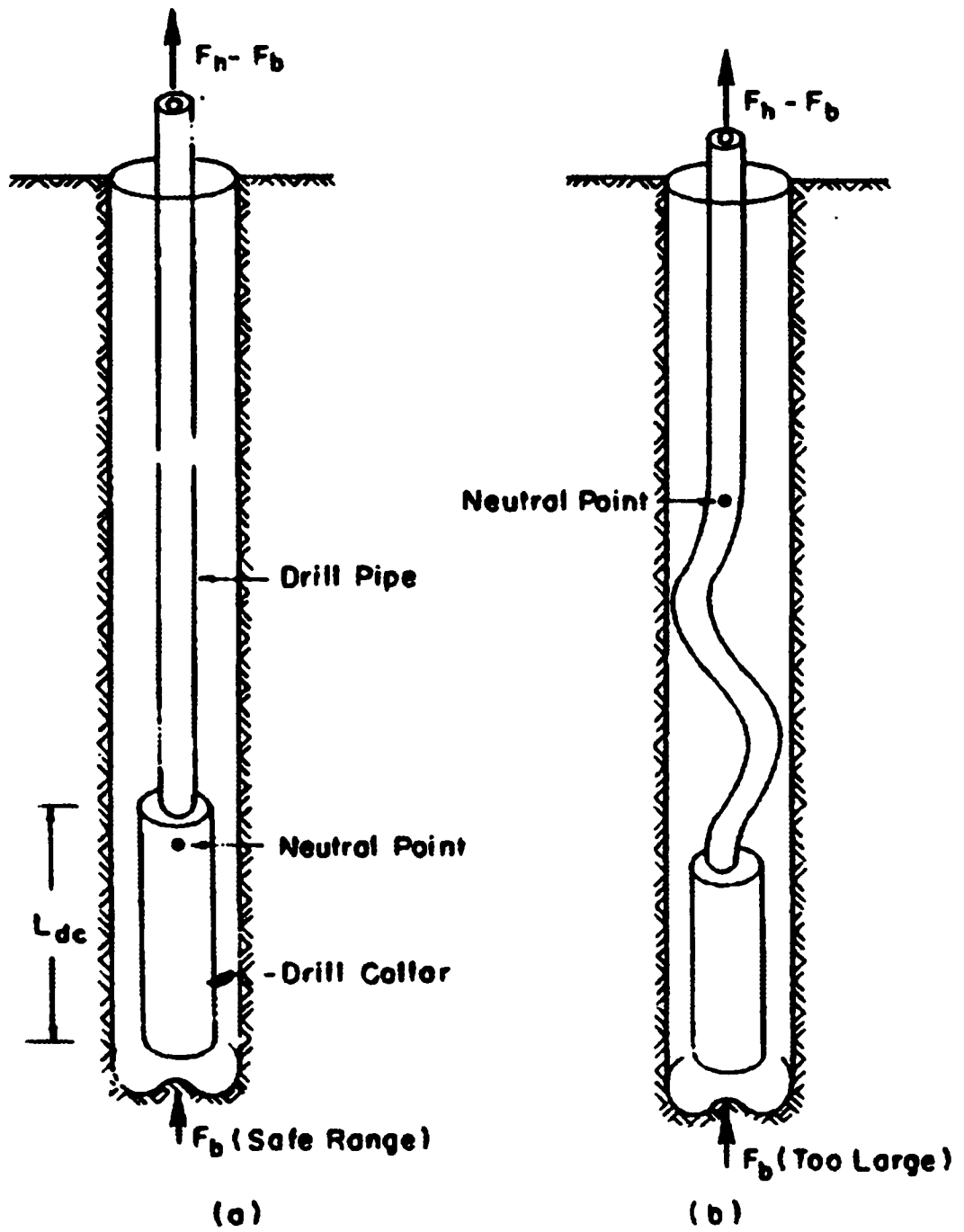


Figure 3.2: Buckling of drillpipe above drillcollar : (a) desired condition and (b) undesired buckled condition

Table 3.5

Axial stiffening matrix of rotating drillstring element $[k_{as}] = \rho g A [k_{ab}]$
 The non-zero entries of the upper triangular part of $[k_{ab}]$, $a, b = 1, 2, \dots, 12$
 for drillpipe (under tension)

$$k_{22}^{as} = k_{33}^{as} = -k_{28}^{as} = -k_{39}^{as} = k_{88}^{as} = k_{99}^{as} = \frac{3}{5} + \frac{6}{5} \frac{L_t}{l_i}$$

$$k_{25}^{as} = -k_{34}^{as} = k_{49}^{as} = -k_{58}^{as} = \frac{1}{10} L_t$$

$$k_{211}^{as} = -k_{310}^{as} = k_{910}^{as} = -k_{811}^{as} = \frac{1}{10} l_i + \frac{1}{10} L_t$$

$$k_{44}^{as} = k_{55}^{as} = \frac{1}{10} l_i^2 + \frac{2}{15} L_t l_i$$

$$k_{410}^{as} = k_{511}^{as} = -\frac{1}{60} l_i^2 - \frac{1}{30} L_t l_i$$

$$k_{1010}^{as} = k_{1111}^{as} = \frac{1}{30} l_i^2 + \frac{2}{15} L_t l_i$$

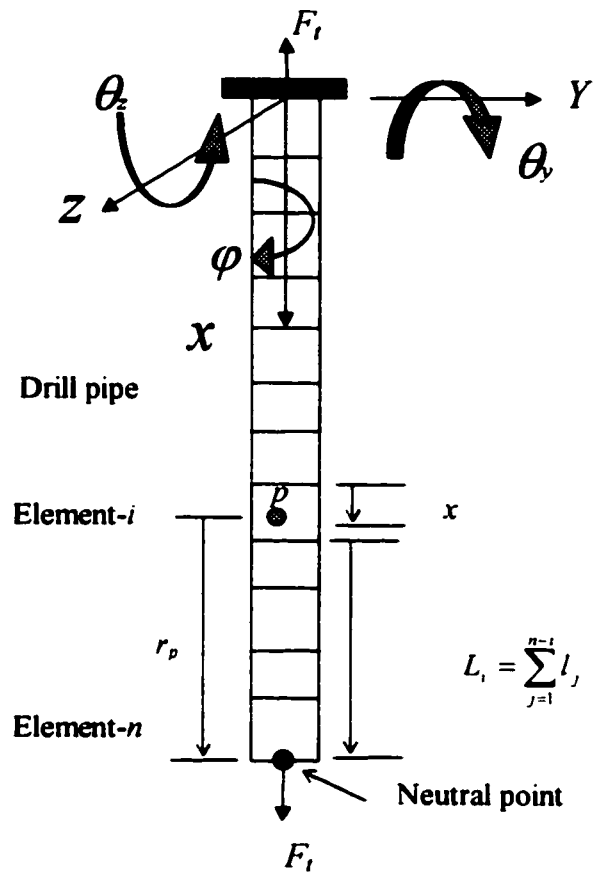


Figure 3.3: Drillpipe under tension

For drillcollar under compression, the length r_p from the neutral point to point p , as shown in figure 3.4, can be written as

$$r_p = L_i + x \quad (3.23)$$

where

$$L_i = \sum_{j=1}^{i-1} l_j$$

Differentiating equation (3.23) with respect to x , will yield

$$dr_p = dx \quad (3.24)$$

Substituting for dr_p in equation (3.17), the gravity force on point p is

$$dF_c = \rho g A dx \quad (3.25)$$

The compression force acting on a section at p due to the weight of the drillcollar segment about this point can be calculated by integrating equation (3.25) over the span between point p and the neutral point. The resulting compression force is

$$F_c = \int_0^{L_i} \rho g A dx + \int_{L_i}^{L_i+x} \rho g A dx \quad (3.26)$$

Evaluating the integral in equation (3.26) while taking ρ , g and A as constants will yield the following expression

$$F_c = \rho g A [L_c + x] \quad (3.27)$$

The axial stiffening stresses resulting from this compression force are incorporated into the integration of $[K_{ax}]$ in equation (3.10), resulting in the stiffening matrix of the rotating drillstring element given in table 3.6. Figure 3.5 shows the drillstring force distribution due to gravitational field.

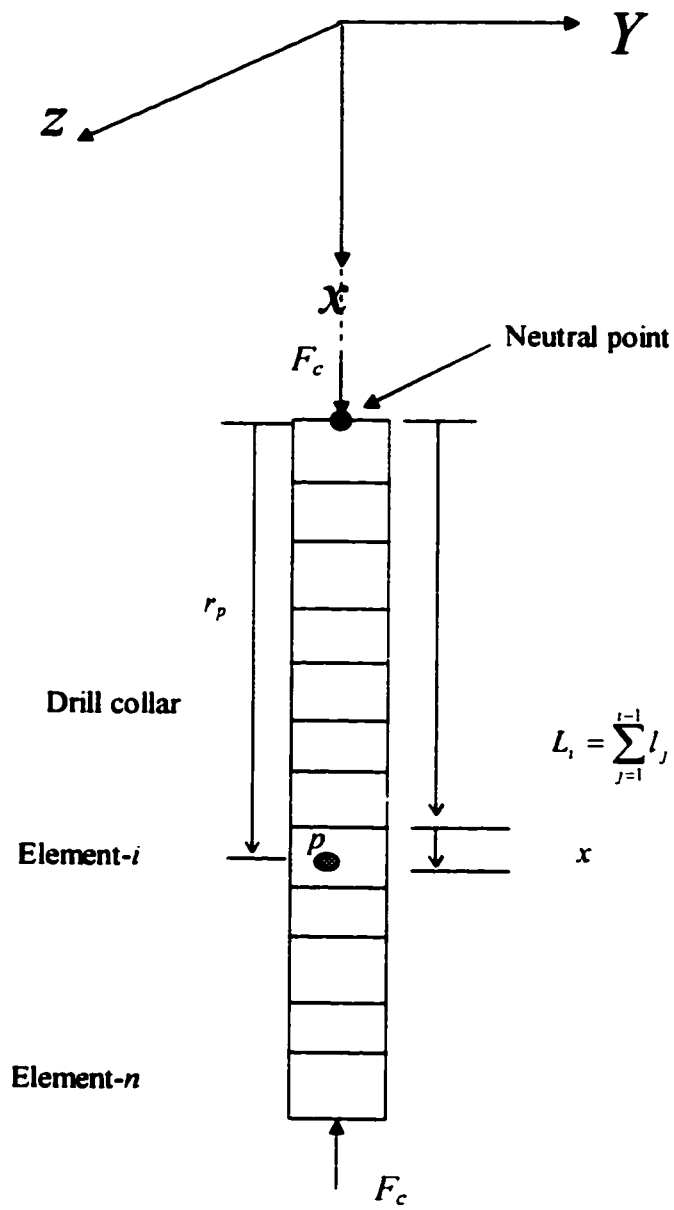


Figure 3.4: Drillcollar under compression

Table 3.6

Axial stiffening matrix of rotating drillstring element $[k_{as}] = \rho g A [k_{ab}^{as}]$
 The non-zero entries of the upper triangular part of $[k_{ab}]$, $a, b = 1, 2, \dots, 12$
 for drillcollar (under compression)

$$k_{22}^{as} = k_{33}^{as} = -k_{28}^{as} = -k_{39}^{as} = k_{88}^{as} = k_{99}^{as} = \frac{3}{5} + \frac{6}{5} \frac{L_c}{l_i}$$

$$k_{25}^{as} = -k_{34}^{as} = k_{49}^{as} = -k_{58}^{as} = \frac{1}{10} l_i + \frac{1}{10} L_c$$

$$k_{211}^{as} = -k_{310}^{as} = k_{910}^{as} = -k_{811}^{as} = \frac{1}{10} L_c$$

$$k_{44}^{as} = k_{55}^{as} = \frac{1}{30} l_i^2 + \frac{2}{15} L_c l_i$$

$$k_{310}^{as} = k_{511}^{as} = -\frac{1}{60} l_i^2 - \frac{1}{30} L_c l_i$$

$$k_{1010}^{as} = k_{1111}^{as} = \frac{1}{10} l_i^2 + \frac{2}{15} L_c l_i$$

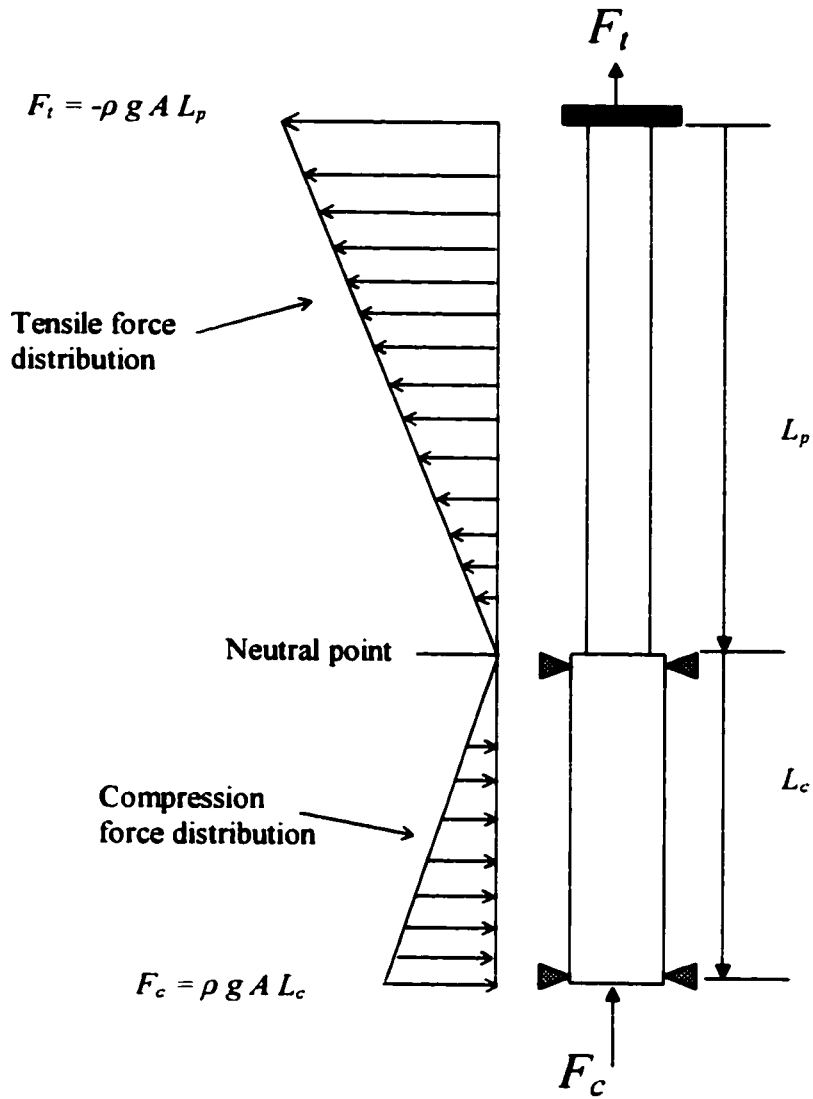


Figure 3.5: Drillstring axial force distribution

3.4 Inertia Properties

The kinetic energy of a rotating drillstring element of length l derived earlier (equation 2.8) is given by

$$T = \frac{1}{2} \{\dot{e}\}^T [M] \{\dot{e}\} + \frac{1}{2} C \dot{\phi}^2 - \dot{\phi} \{\dot{e}\}^T [G] \{\dot{e}\} \quad (3.28)$$

The matrix $[M]$ is the augmented mass matrix (equation 2.9) given by

$$[M] = [M_t] + [M_r] + [M_\theta] - 2[M_e] \quad (3.29)$$

Where

$$[M_t] = \int_0^l [N_v]^T \mu A [N_v] dx \quad (3.30)$$

$$[M_r] = \int_0^l [N_\theta]^T I_D [N_\theta] dx \quad (3.31)$$

$$[M_\theta] = \int_0^l [N_\phi]^T I_p [N_\phi] dx \quad (3.32)$$

$$[M_e] = \int_0^l I_p \left([N_\phi]^T [N_\alpha] \{e\} [N_\phi] - [N_\phi]^T [N_\phi] \{e\} [N_\alpha] \right) dx \quad (3.33)$$

Where $[M_t]$ is the translational mass matrix, $[M_r]$ is the rotary inertia mass matrix, $[M_\theta]$ is the torsional mass matrix, and $[M_e]$ is the coupled torsional-transverse mass matrix. The gyroscopic matrix $[G]$ and can be obtained by the following expression

$$[G] = [G_t] - [G_t]^T \quad (3.34)$$

For constant rotating speed

$$[G_t] = \int_0^l [N_\alpha]^T I_p [N_\phi] dx \quad (3.35)$$

and for constant I_p

$$[G_1] = I_p \int_0^l [N_{\alpha}]^T [N_{\phi}] dx \quad (3.36)$$

Integrating equations (3.30)-(3.33) and (3.36), the mass matrices are obtained with non-zero entries presented in tables 3.7-3.11.

Table 3.7

Translational mass matrix of rotating drillstring element $[M_t] = \mu A [M_{ab}^e]$
 The non-zero entries of the upper triangular part of $[M_{ab}]$, $a, b = 1, 2, \dots, 12$

$$M_{11}^e = M_{77}^e = \frac{1}{3}l$$

$$M_{17}^e = \frac{1}{6}l$$

$$M_{22}^e = M_{33}^e = M_{88}^e = M_{99}^e = \frac{13}{35}l$$

$$M_{25}^e = -M_{34}^e = -M_{811}^e = M_{910}^e = \frac{11}{210}l^2$$

$$M_{28}^e = M_{310}^e = \frac{9}{70}l$$

$$M_{44}^e = M_{55}^e = M_{99}^e = M_{1010}^e = \frac{l^3}{105}$$

$$-M_{211}^e = M_{310}^e = -M_{49}^e = M_{58}^e = \frac{13}{420}l^2$$

$$M_{410}^e = M_{511}^e = -\frac{l^3}{140}$$

Table 3.8

Rotary inertia mass matrix of rotating drillstring element $[M_r] = I_D [M'_{ab}]$
 The non-zero entries of the upper triangular part of $[M_{ab}]$, $a, b = 1, 2, \dots, 12$

$$M'_{22} = M'_{33} = -M'_{28} = -M'_{39} = M'_{88} = M'_{99} = \frac{6}{5l}$$

$$M'_{25} = M'_{211} = -M'_{310} = -M'_{811} = M'_{910} = -M'_{34} = M'_{410} = -M'_{59} = \frac{1}{10}$$

$$M'_{44} = M'_{55} = M'_{1010} = M'_{1111} = \frac{2}{15}l$$

$$M'_{410} = M'_{511} = -\frac{1}{30}l$$

Table 3.9

Torsional mass matrix of rotating drillstring element $[M_\sigma] = I_p [M''_{ab}]$
 The non-zero entries of the upper triangular part of $[M_{ab}]$, $a, b = 1, 2, \dots, 12$

$$M''_{66} = 2M''_{612} = M''_{1212} = \frac{1}{3}l$$

Table 3.10

Torsional and lateral coupling mass matrix of rotating drillstring element $[M_c] = I_p [M_{ab}^c]$
 The non-zero entries of $[M_{ab}]$, $a, b = 1, 2, \dots, 12$

$$M_{62}^c = -M_{68}^c = \varphi_1 \left[-\frac{6}{5l} w_1 + \frac{1}{10} \theta_{y1} + \frac{6}{5l} w_2 + \frac{1}{10} \theta_{y2} \right]$$

$$M_{63}^c = -M_{69}^c = \varphi_1 \left[\frac{6}{5l} v_1 + \frac{1}{10} \theta_{z1} - \frac{6}{5l} v_2 + \frac{1}{10} \theta_{z2} \right]$$

$$M_{64}^c = -\varphi_1 \left[\frac{1}{10} v_1 + \frac{2l}{15} \theta_{z1} - \frac{1}{10} v_2 - \frac{l}{30} \theta_{z2} \right]$$

$$M_{65}^c = \varphi_1 \left[\frac{1}{10} w_1 + \frac{2l}{15} \theta_{y1} - \frac{1}{10} w_2 - \frac{l}{30} \theta_{y2} \right]$$

$$M_{610}^c = -\varphi_1 \left[\frac{1}{10} v_1 - \frac{l}{30} \theta_{z1} - \frac{1}{10} v_2 + \frac{2l}{15} \theta_{z2} \right]$$

$$M_{611}^c = \varphi_1 \left[\frac{1}{10} w_1 - \frac{l}{30} \theta_{y1} - \frac{1}{10} w_2 + \frac{2l}{15} \theta_{y2} \right]$$

$$M_{122}^c = -M_{128}^c = \varphi_2 \left[-\frac{6}{5l} w_1 + \frac{1}{10} \theta_{y1} + \frac{6}{5l} w_2 + \frac{1}{10} \theta_{y2} \right]$$

$$M_{123}^c = -M_{129}^c = \varphi_2 \left[\frac{6}{5l} v_1 + \frac{1}{10} \theta_{z1} - \frac{6}{5l} v_2 + \frac{1}{10} \theta_{z2} \right]$$

$$M_{124}^c = -\varphi_2 \left[\frac{1}{10} v_1 + \frac{2l}{15} \theta_{z1} - \frac{1}{10} v_2 - \frac{l}{30} \theta_{z2} \right]$$

$$M_{125}^c = \varphi_2 \left[\frac{1}{10} w_1 + \frac{2l}{15} \theta_{y1} - \frac{1}{10} w_2 - \frac{l}{30} \theta_{y2} \right]$$

$$M_{1210}^c = -\varphi_2 \left[\frac{1}{10} v_1 - \frac{l}{30} \theta_{z1} - \frac{1}{10} v_2 + \frac{2l}{15} \theta_{z2} \right]$$

$$M_{1211}^c = \varphi_2 \left[\frac{1}{10} w_1 - \frac{l}{30} \theta_{y1} - \frac{1}{10} w_2 + \frac{2l}{15} \theta_{y2} \right]$$

Table 3.11

Gyroscopic matrix of rotating drillstring element $[G] = I_p [G_{ab}]$
The non-zero entries of the upper triangular part of $[G_{ab}]$, $a, b = 1, 2, \dots, 12$

$$G_{23} = G_{29} = G_{38} = G_{89} = -\frac{6}{5l}$$

$$G_{24} = G_{210} = G_{35} = G_{311} = G_{48} = G_{59} = -G_{810} = -G_{911} = \frac{1}{10}$$

$$G_{45} = G_{1011} = -\frac{2}{15}l$$

$$G_{411} = -G_{510} = -\frac{1}{30}l$$

Chapter IV

EQUATIONS OF MOTION OF THE DRILLSTRING

4.1 The Assembled Equations of Motion

The equations of motion for an element is derived in chapter II, equation (2.44), is written again here, which is indexed to element i as

$$[M_i]\{\ddot{e}_i\} + \phi[G_i]\{\dot{e}_i\} + [K_i]\{e_i\} = \{Q_i\} \quad (4.1)$$

Where $[M_i]$, $[K_i]$, and $[G_i]$ are the elemental mass, stiffness, and gyroscopic matrices. The consistent mass FEM approach is used to calculate the elements of these matrices, which are tabulated in chapter III for an arbitrary element of the drillstring. Using the standard finite element assembly procedure, the equations of motion of the whole drillstring can be written as

$$[M]\{\ddot{q}\} + \phi[G]\{\dot{q}\} + [K]\{q\} = \{Q\} \quad (4.2)$$

where $\{q\}$ is the vector of nodal coordinates of the whole drillstring. The matrices $[M]$, $[G]$ and $[K]$ are the assembled mass, gyroscopic and stiffness matrices, respectively. The vector $\{Q\}$ represents the applied force vector acting on the drillstring.

A finite element program that evaluates the elemental mass and stiffness matrices and assembles them into global matrices is developed. Referring to the computer flow chart figure 4.1, the dynamic analysis computer program is developed to automatically generate and assemble the system matrices and solve the eigenvalue problem for the system modal characteristics. The drillstring assemblies treated by this program can be of any complexity in

COMPUTER PROGRAM

FLOW CHART

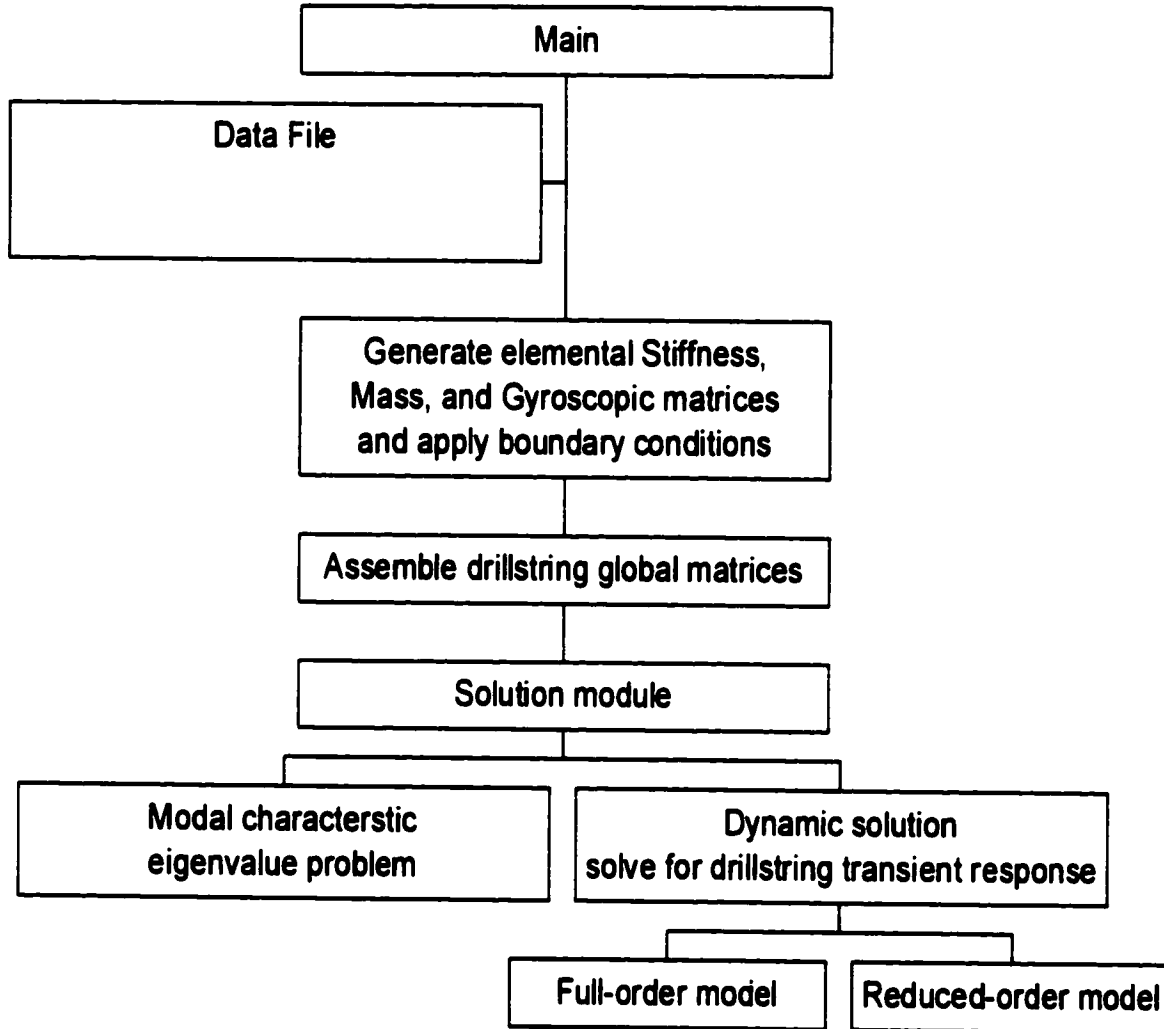


Figure 4.1: Computer program flow chart

terms of number of elements, element length, length ratio of drillpipe/drillcollar or neutral point location. The developed computer program is written in MATLAB[®] code and is described by the following four modules:

I. Main Program

The main program first calls the data file where the data of the concerned problem is stored. The data file contains the material properties, problem geometry, boundary conditions, element connectivity data, and element properties.

II. Finite Element Module

This module establishes the elemental mass, stiffness and gyroscopic matrices based on the data given. Apply the boundary conditions at elemental level, for all elements. The global matrices are then assembled for the whole drillstring system.

III. Modal Characteristics Module

In this module the modal characteristics of the drillstring system are obtained by solving the eigenvalue problem. The eigenvectors or modes shape, which are obtained in this module represent the basis for modal transformations.

IV. Dynamic Analysis Module

The dynamic analysis module solves for the drillstring transient response based on initial displacement conditions and/or any forcing function chosen by the user. The equations of motion are constructed using either

- Full-order model using physical (nodal) coordinates
- Reduced-order model using a truncated set of modal coordinates that includes the significant modes.

4.2 The Eigenvalue Solution

In order to define the eigenvalue problem, the force vector is dropped from equation (4.2). Thus the differential equations of motion governing the free vibrations of the rotating drillstring can be written in the general form as

$$[M]\{\ddot{q}\} + \dot{\phi}[G]\{\dot{q}\} + [K]\{q\} = \{0\} \quad (4.3)$$

Where $[M]$ is the global assembled mass matrix of the system, $[G]$ is the gyroscopic matrix of the system, $[K]$ is the global assembled stiffness matrix of the system, and $\{e\}$ is the deformation vector. The mass matrix $[M]$ is symmetric and consists of the following constituent matrices

$$[M] = [M_t] + [M_r] + [M_\phi] - 2[M_c] \quad (4.4)$$

Where $[M_t]$ is the translational mass matrix, $[M_r]$ is the rotary inertia mass matrix, $[M_\phi]$ is the torsional mass matrix, and $[M_c]$ represents the inertia coupling between torsional and transverse vibrations. The time-dependent coupling matrix $[M_c]$ does not contribute to the modal characteristics of the drillstring, and therefore is neglected in the eigenvalue solution. The stiffness matrix $[K]$ is also symmetric while the gyroscopic matrix $[G]$ is skew symmetric.

The solution of the general equation of motion for free vibration, equation (4.3), is obtained by representing it in the following state space form:

$$\begin{bmatrix} [0] & -[M] \\ [M] & [G] \end{bmatrix} \begin{Bmatrix} \{\ddot{q}\} \\ \{\dot{q}\} \end{Bmatrix} + \begin{bmatrix} [M] & [0] \\ [0] & [K] \end{bmatrix} \begin{Bmatrix} \{\dot{q}\} \\ \{q\} \end{Bmatrix} = \{0\} \quad (4.5)$$

4.2.1 Solution Scheme

To find the natural frequencies of the drillstring system, the equation of motion can be viewed in two ways. In the first approach, the natural frequencies are extracted from equation (4.5), which is the free vibrational equation derived with respect to the fixed reference frame and rewritten in state variable form. The solution of the eigenvalue problem described by equation (4.5) can be obtained by using any eigenvalue solver. Forward and backward frequencies are obtained from the same eigenvalue.

In the second approach, the system equation of motion is transformed to the rotating frame. In this case, only bending frequencies can be found as the transformation to the rotating frame loses track of the torsional and axial motion. Due to this reason the first method will be used to obtain not only the bending frequencies, but also the torsional and axial natural frequencies of a rotating drillstring.

4.3 Modal Transformation

The equations of motion are either solved by direct method for a full-order model solution, in which it will take a long time for a huge system, or use reduction scheme. The modal reduction method is used to reduce the number of equations to be solved for dynamic response. Eliminating the insignificant modes, which are, in general, higher modes that do not contain an appreciable amount of the system's kinetic energy sets a pre-determined reduction. However, the retained modes must include the first few lower ones in terms of which the dynamic characteristics of the system must be preserved. The advantage of this method is the reduction in computer calculation time with accurate dynamic response results. In general, the results obtained by this method are very close to those obtained by solving the full-order model.

In this context, two modal reduction schemes are established in the literature [34,36,37]. The first employs planar modes, which are obtained by solving the self-adjoint eigenvalue problem, while the second invokes the complex modes of the non-self-adjoint eigenvalue. The self-adjoint problem is obtained by ignoring the gyroscopic and damping terms in the equations of motion. On the other hand, the complex or non-planar modes represent the accurate deformations of the drillstring, whereas they account for the effect of gyroscopic forces. Accordingly, we will adapt the scheme of complex modal transformations to obtain a reduced set of the equations of motion.

Now, the state space form of equation (4.5) can be written in the compact matrix form as

$$[A]\{\dot{y}\} + [B]\{y\} = \{Q\} \quad (4.6)$$

where

$$[A] = \begin{bmatrix} [0] & -[M] \\ [M] & [G] \end{bmatrix}$$

$$[B] = \begin{bmatrix} [M] & [0] \\ [0] & [K] \end{bmatrix}$$

$$\{y\} = \begin{Bmatrix} \{e\} \\ \{e\} \end{Bmatrix}$$

$$\{Q\} = \begin{Bmatrix} \{0\} \\ \{F\} \end{Bmatrix}$$

Where the matrix $[B]$ is symmetric while matrix $[A]$ is skew-symmetric. Notice that the dimensions of $[M]$, $[K]$ and $[G]$ are $(6n \times 6n)$ where n is the number of nodes, and therefore the dimensions of $[A]$ and $[B]$ are $(12n \times 12n)$. The forcing vector $\{F\}$ represent the force applied at each node of the drillstring system. The two homogeneous adjoint equations can be written as

$$[A]\{\dot{y}\} + [B]\{y\} = \{0\} \quad (4.7)$$

And

$$[A]^T \{\dot{y}\} + [B]^T \{y\} = \{0\} \quad (4.8)$$

Assuming a solution of the form

$$\{y\} = \{\bar{y}\} \exp(i\omega t) \quad (4.9)$$

Where $\{\bar{y}\}$ is the vector of displacement amplitudes, ω is the vibration frequency and $i = \sqrt{-1}$. Substituting equation (4.9) in equations (4.7) and (4.8), one can write

$$(\lambda_i [A] + [B])\{R\} = \{0\} \quad (4.10)$$

And

$$(\lambda_i [A]^T + [B]^T)\{L\} = \{0\} \quad (4.11)$$

Where $\lambda_i = \pm i\omega_i$ denotes the i th eigenvalue associated with right-hand and left-hand eigenvectors $\{R\}$ and $\{L\}$, respectively. For symmetric $[A]$ and $[B]$, the eigenvectors $\{R\}$ and $\{L\}$ are equal, otherwise they are distinct.

Let $[R]$ and $[L]$ denote the complex modal matrices for the differential operators of equations (4.7) and (4.8), respectively. Introducing the transformation

$$\{y\} = [R] \{u\} \quad (4.12)$$

Where $\{u\}$ is the vector of modal coordinates. Because only the significant modes are retained pre-multiplying both sides of equation (4.6) by $[L]^T$ and substituting for $\{y\}$ from equation (4.12), the truncated modal form of the equations of motion can be written as

$$[L]^T [A] [R] \{\dot{u}\} + [L]^T [B] [R] \{u\} = [L]^T \{Q\} \quad (4.13)$$

Where $[R]$ and $[L]$ contain only those complex eigenvectors that represent the n lowest mode shapes of equation (4.10) and (4.11) obtained by solving the eigenvalue problem. Equation (4.13) can be written as

$$[A_r]\{\dot{u}\} + [B_r]\{u\} = \{Q_r\} \quad (4.14)$$

Where $[A_r]$ and $[B_r]$ represent the reduced $[A]$ and $[B]$ matrices and $\{Q_r\}$ represent the reduced force vector. Equation (4.14) represents the reduced-order model using complex modal reduction.

Chapter V

NUMERICAL SIMULATIONS

5.1 Modal Analysis

In this case study, a drillstring of the specifications adopted in reference [16] and given in table 5.1 is considered. The numerical simulations are designed to cover a range of situations including uniform, rotating and non-rotating drillstring.

The results are obtained using the consistent mass FEM formulation with 25 nodes connected by 24 equal finite shaft elements. A total of 140 degrees of freedom is attained after applying the boundary conditions for the drillstring system. Each node consists of 6 degrees of freedom; that is two translations, two bending rotations, one axial and one torsional. The discretization data for the drillstring elements is listed in table 5.2. The following discussion is primarily meant for drillstring in vertical borehole where no initial curvature or normal load is involved.

The natural frequencies of the drillstring system are extracted from the equation in the state space form, which is the free vibrational equation derived with respect to the fixed frame and written in state variable form. Every lateral mode of the rotating drillstring shaft gives rise to two distinct modes; direct or forward mode and retrograde or backward mode. The frequency of the backward mode decreases when drillstring rotation is increased while the forward mode frequency increases. Such a distinction between forward and backward modes disappears for a non-rotating drillstring.

Table 5.1
Drillstring configuration data

<u>Drillpipe specification</u>	
Drillpipe length (L_p)	1000m
Drillpipe outer diameter (D_o)	0.127m
Drillpipe inside diameter (D_i)	0.095m
<u>Drillcollar specification</u>	
Drillcollar length (L_c)	200m
Drillcollar outer diameter (D_o)	0.2286m
Drillcollar inside diameter (D_i)	0.0762m
<u>Material specification</u>	
Drillstring density (ρ)	7850 kg/m ³
Modulus of elasticity (E)	210 X 10 ⁹ N/m ²
Shear modulus (G)	7.6923 X 10 ¹⁰ N/m ²

Table 5.2
FEM discretization data

Node No.	Node location (m)	Inner radius(m)	Outer radius(m)
1	0	0.095	0.127
2	50	0.095	0.127
3	100	0.095	0.127
4	150	0.095	0.127
5	200	0.095	0.127
6	250	0.095	0.127
7	300	0.095	0.127
8	350	0.095	0.127
9	400	0.095	0.127
10	450	0.095	0.127
11	500	0.095	0.127
12	550	0.095	0.127
13	600	0.095	0.127
14	650	0.095	0.127
15	700	0.095	0.127
16	750	0.095	0.127
17	800	0.095	0.127
18	850	0.095	0.127
19	900	0.095	0.127
20	950	0.095	0.127
21	1000	0.0762	0.2286
22	1050	0.0762	0.2286
23	1100	0.0762	0.2286
24	1150	0.0762	0.2286
25	1200	0.0762	0.2286

The natural frequencies of drillstring could not be extracted from existing literature due to lack of some information. Consequently, to check our approach and the developed computer program results, an alternate means of solving the problem is needed. A model is generated for a drillstring using ANSYS[®] in order to extract the natural frequencies. The comparison of the results tabulated for torsional and axial natural frequencies shown in tables 5.4-5.26 (only even number tables) display a very good agreement with the results obtained by our model. Results for bending natural frequencies could not be obtained due to complexity of the drillstring force distribution. The effect of the gravitational force field, which includes both tension and compression, on such long flexible structure is significant. Such an effect is not considered by standard ANSYS[®] finite elements. A Further check by ANSYS[®] of the developed approach for simple boundary conditions is presented in the Appendix.

Now, the developed FEM scheme will be utilized in calculating the modal characteristics of the drillstring detailed in table 5.1. Three cases were studied and reported in this section; one is to study the effect of neutral point location on drillstring natural frequencies, another one to study the effect of drillpipe length on the natural frequencies, and the third one is to study the effect of drillpipe/drillcollar length ratio on the natural frequencies. In all reported frequencies, the axial stiffening effect due to the weight of the section under compression and the section under tension is included. The effect of drillstring rotation speed is also studied in the range from 0 rpm up to 1000 rpm (104.7 rad/sec).

a) Effect of neutral point location:

The first simulation, the effect of different position of neutral point is studied. The neutral point is the interface point at which there is a force change from tension to

compression to provide the needed weight on bit (WOB) for drilling. In order to study its effect on the bending, torsional and axial natural frequencies, the neutral point was located at four different locations; the bottom of drillstring (bit), at 100m above the bit, at 200m above the bit, and at 400m above the bit. The first ten forward (F) and backward (B) bending, torsional and axial natural frequencies of drillstring are tabulated in Tables 5.3-5.10. For a drillstring with two stabilizers, one at bottom and the other at 200m from bottom, neutral point is located at bottom, implies that the drillstring is under tension, the results were shown in table 5.3 for bending natural frequencies and the first three F and B modes were plotted in figure 5.1 which shows the effect of speed on bending modes. Relocating neutral point to 100m above the bit, implies that the lower 100m of the drillcollar section is under compression, the drillstring becomes less stiff as shown in figure 5.2 for the first three modes and tabulated for the rest of the ten modes in table 5.5. Further raising the neutral point to 200m and 400m above the bit, shown in figures 5.3 and 5.4 for the first three modes and tabulated in tables 5.7 and 5.9, the drillstring becomes even less stiff. As the neutral point is raised up further the drillstring becomes less and less stiff. This is visible in the bending frequencies for drillstring results plotted in figure 5.5 for the first ten modes of different location of neutral point.

Torsional and axial natural frequencies were not affected by the rotation speed. Moreover, the neutral point location also did not affect the torsional and axial natural frequencies as shown in figure 5.6 and tabulated in tables 5.4, 5.6, 5.8 and 5.10 for different location of neutral point.

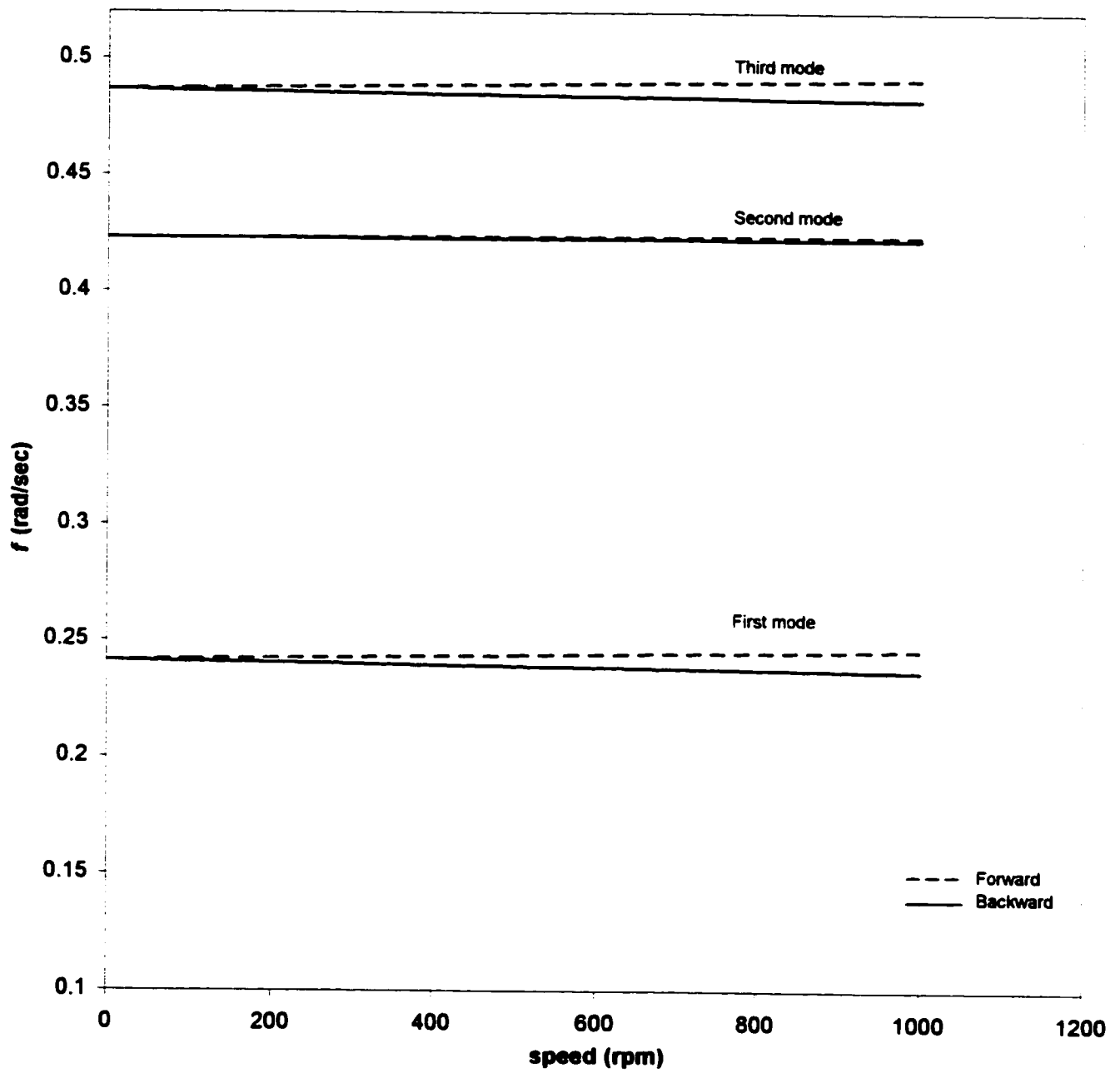


Figure 5.1: Bending frequency for neutral point located at the bottom

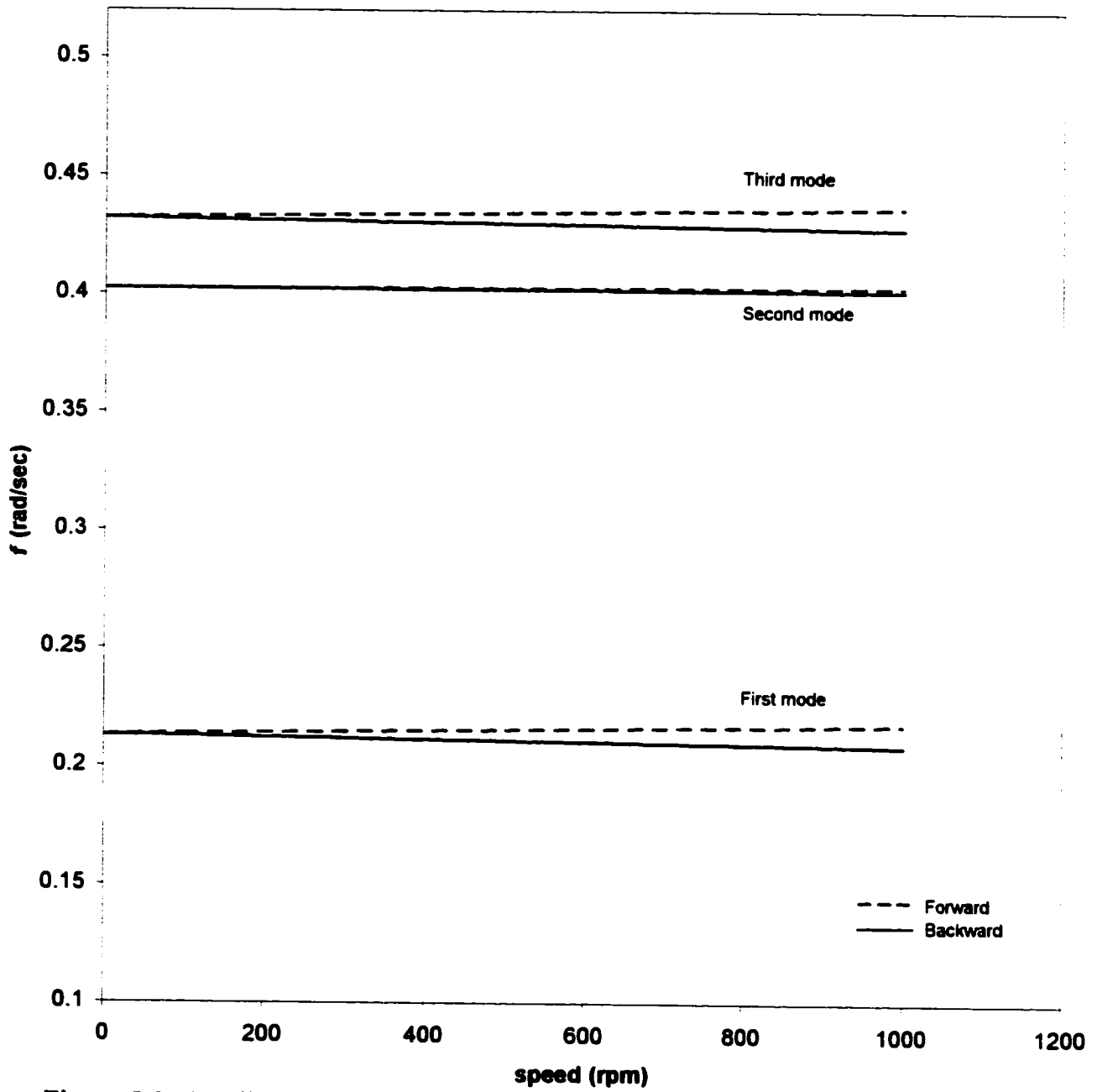


Figure 5.2: Bending frequency for neutral point located at 100m above the bottom

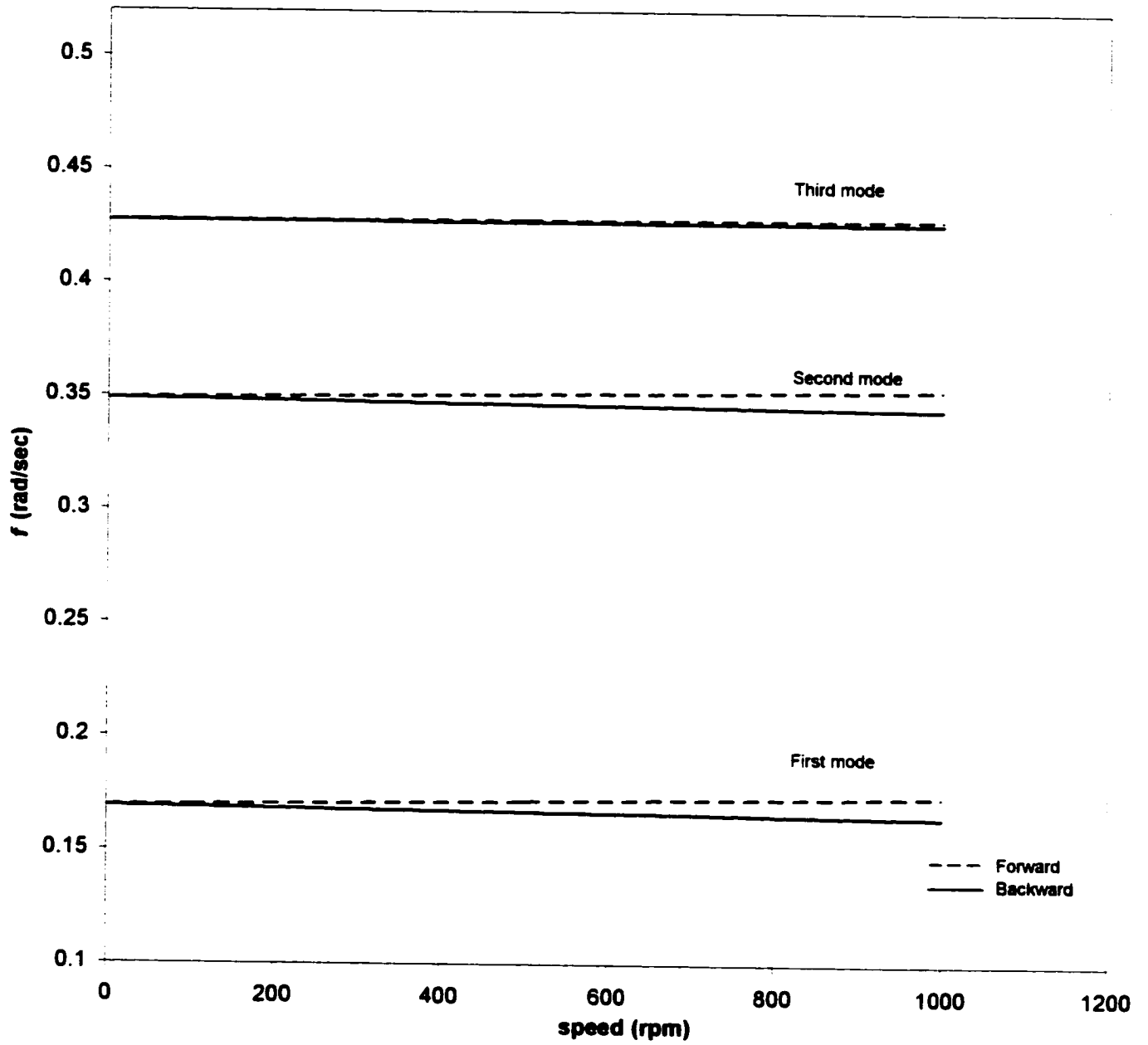


Figure 5.3: Bending frequency for neutral point located at 200m above the bottom

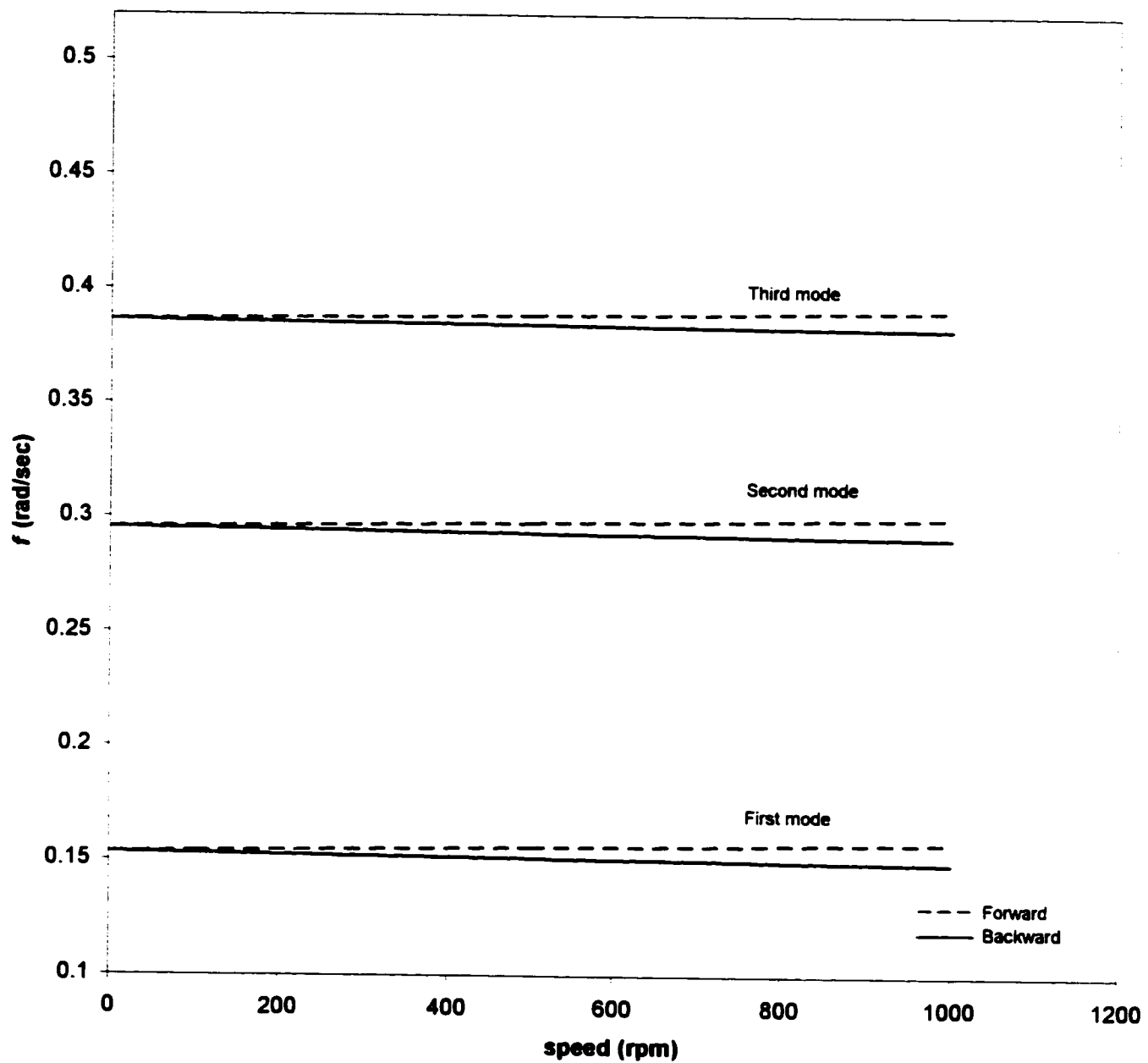


Figure 5.4: Bending frequency for neutral point located at 400m above the bottom

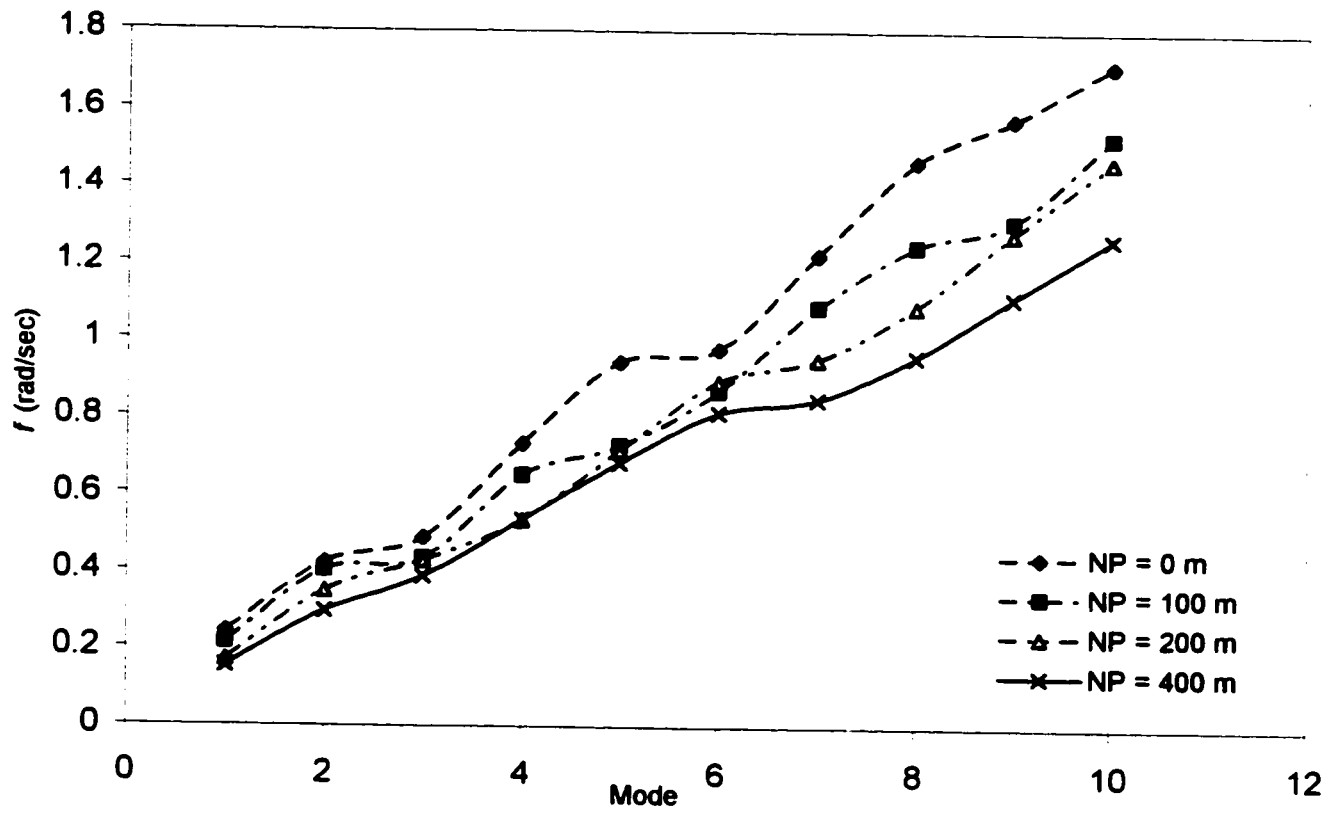


Figure 5.5: Frequencies of the first ten bending modes for different location of neutral point (NP)

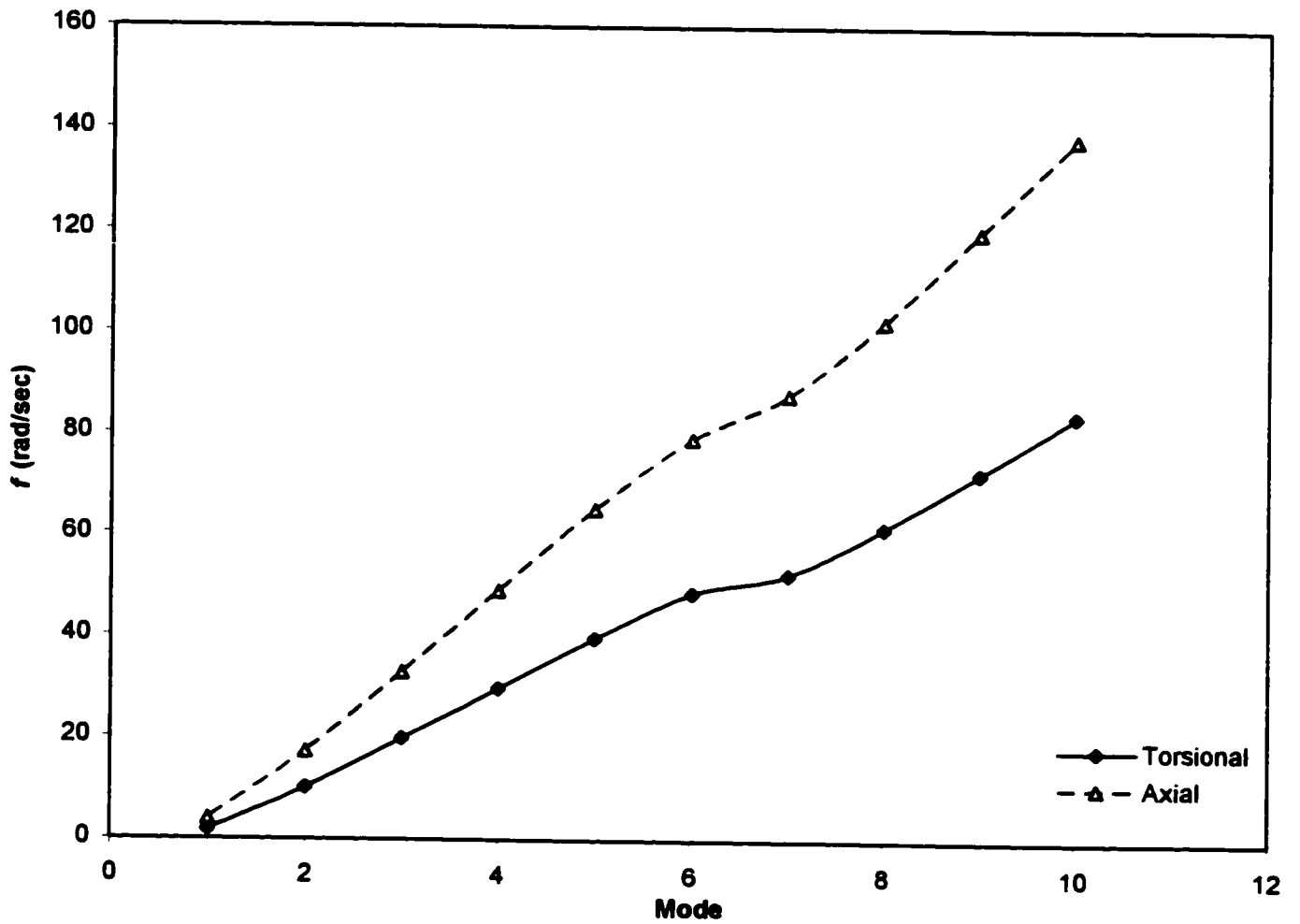


Figure 5.6: Frequencies of the first ten torsional and axial modes for different location of neutral point (NP)

Table 5.3

Bending Natural frequencies for rotating drillstring, neutral point at bottom

Drillcollar length is 200m, Drillpipe length is 1000m, two stabilizers one at bottom and one is 200m from bottom.

rad/sec	f_1	f_2	f_3	f_4	f_5	f_6	f_7	f_8	f_9	f_{10}
0 RPM	0.2415	0.423	0.4867	0.731	0.9422	0.977	1.2207	1.4651	1.5747	1.7134
30 RPM	B 0.2414	0.423	0.4865	0.7308	0.9421	0.9768	1.2205	1.465	1.5747	1.7133
	F 0.2417	0.423	0.4868	0.7311	0.9422	0.9771	1.2208	1.4653	1.5747	1.7135
60 RPM	B 0.2413	0.423	0.4864	0.7307	0.9421	0.9767	1.2204	1.4649	1.5747	1.7132
	F 0.2418	0.423	0.4869	0.7312	0.9422	0.9772	1.2209	1.4654	1.5747	1.7135
100 RPM	B 0.2411	0.4229	0.4862	0.7305	0.9421	0.9766	1.2203	1.4648	1.5746	1.713
	F 0.242	0.423	0.4871	0.7314	0.9422	0.9774	1.221	1.4655	1.5748	1.7137
500 RPM	B 0.2393	0.4227	0.4844	0.7288	0.9419	0.975	1.2188	1.4634	1.5744	1.7118
	F 0.2438	0.4233	0.4889	0.7331	0.9424	0.9789	1.2225	1.4669	1.575	1.7149
1000RPM	B 0.237	0.4224	0.4822	0.7267	0.9416	0.9731	1.2169	1.4617	1.5741	1.7102
	F 0.2461	0.4236	0.4911	0.7352	0.9427	0.9809	1.2244	1.4686	1.5753	1.7165

Table 5.4

Torsional & Axial natural frequencies for rotating drillstring

rad/sec	f_1	f_2	f_3	f_4	f_5	f_6	f_7	f_8	f_9	f_{10}
Torsional	1.705	10.1197	19.8168	29.7083	39.699	48.6099	52.2853	61.5118	72.4139	83.8122
	*1.7048	*10.1184	*19.814	*29.7038	*39.693	*48.603	*52.2774	*61.5023	*72.4011	*83.7988
Axial	4.0076	17.2617	32.8832	48.9437	65.028	79.0416	87.6804	102.2349	119.8074	138.3143
	*4.0077	*17.2618	*32.8831	*48.9435	*65.031	*79.0425	*87.6819	*102.2337	*119.8078	*138.3118

* ANSYS Result, B:backward, F:forward

Table 5.5

Bending Natural frequencies for rotating drillstring, neutral point at 100m above bottom.

Drillcollar length is 200m, Drillpipe length is 1000m, two stabilizers one at bottom and one is 200m from bottom.

rad/sec	f_1	f_2	f_3	f_4	f_5	f_6	f_7	f_8	f_9	f_{10}
0 RPM	0.2133	0.4023	0.4322	0.6492	0.7255	0.8682	1.086	1.2434	1.3086	1.5271
30 RPM	B 0.2132	0.4023	0.4321	0.6491	0.7255	0.868	1.0859	1.2434	1.3085	1.527
	F 0.2135	0.4023	0.4323	0.6493	0.7255	0.8683	1.0862	1.2434	1.3087	1.5272
60 RPM	B 0.2131	0.4023	0.4319	0.6489	0.7254	0.8679	1.0858	1.2434	1.3084	1.5269
	F 0.2136	0.4024	0.4324	0.6494	0.7255	0.8684	1.0863	1.2434	1.3088	1.5273
100 RPM	B 0.2129	0.4023	0.4317	0.6488	0.7254	0.8678	1.0857	1.2434	1.3083	1.5268
	F 0.2138	0.4024	0.4326	0.6496	0.7255	0.8686	1.0864	1.2435	1.3089	1.5274
500 RPM	B 0.2111	0.402	0.43	0.6471	0.7253	0.8662	1.0842	1.2432	1.3069	1.5255
	F 0.2156	0.4026	0.4344	0.6513	0.7257	0.8702	1.0879	1.2436	1.3103	1.5287
1000RPM	B 0.2088	0.4017	0.4278	0.645	0.725	0.8642	1.0823	1.2431	1.3053	1.524
	F 0.2179	0.403	0.4366	0.6534	0.7259	0.8722	1.0898	1.2438	1.3119	1.5302

Table 5.6

Torsional & Axial natural frequencies for rotating drillstring

rad/sec	f_1	f_2	f_3	f_4	f_5	f_6	f_7	f_8	f_9	f_{10}
Torsional	1.705	10.1197	19.8168	29.7083	39.699	48.6099	52.2853	61.5118	72.4139	83.8122
	*1.7048	*10.1184	*19.814	*29.7038	*39.693	*48.603	*52.2774	*61.5023	*72.4011	*83.7988
Axial	4.0076	17.2617	32.8832	48.9437	65.028	79.0416	87.6804	102.2349	119.8074	138.3143
	*4.0077	*17.2618	*32.8831	*48.9435	*65.031	*79.0425	*87.6819	*102.2337	*119.8078	*138.3118

* ANSYS Result, B:backward, F:forward

Table 5.7

Bending Natural frequencies for rotating drillstring, neutral point at 200m above bottom.

Drillcollar length is 200m, Drillpipe length is 1000m, two stabilizers one at bottom and one at 200m from bottom

rad/sec	f_1	f_2	f_3	f_4	f_5	f_6	f_7	f_8	f_9	f_{10}	
0 RPM	0.1694	0.3488	0.4272	0.5327	0.7134	0.8927	0.951	1.0879	1.2761	1.4663	
30 RPM	B	0.1692	0.3487	0.4272	0.5325	0.7133	0.8926	0.951	1.0878	1.276	1.4662
	F	0.1695	0.349	0.4273	0.5328	0.7135	0.8928	0.951	1.088	1.2762	1.4664
60 RPM	B	0.1691	0.3486	0.4272	0.5324	0.7132	0.8925	0.9509	1.0877	1.2759	1.4661
	F	0.1696	0.3491	0.4273	0.5329	0.7136	0.8929	0.951	1.0881	1.2763	1.4665
100 RPM	B	0.1689	0.3484	0.4272	0.5322	0.713	0.8924	0.9509	1.0876	1.2758	1.466
	F	0.1698	0.3493	0.4273	0.5331	0.7138	0.893	0.9511	1.0883	1.2764	1.4666
500 RPM	B	0.1671	0.3467	0.4269	0.5306	0.7115	0.8911	0.9505	1.0863	1.2746	1.4648
	F	0.1717	0.351	0.4276	0.5347	0.7153	0.8943	0.9515	1.0896	1.2776	1.4678
1000RPM	B	0.1649	0.3446	0.4265	0.5286	0.7096	0.8895	0.9501	1.0847	1.273	1.4634
	F	0.174	0.3532	0.428	0.5368	0.7173	0.8959	0.9519	1.0912	1.2791	1.4692

Table 5.8

Torsional & Axial natural frequencies for rotating drillstring

rad/sec	f_1	f_2	f_3	f_4	f_5	f_6	f_7	f_8	f_9	f_{10}
Torsional	1.705	10.1197	19.8168	29.7083	39.699	48.6099	52.2853	61.5118	72.4139	83.8122
	*1.7048	*10.1184	*19.814	*29.7038	*39.693	*48.603	*52.2774	*61.5023	*72.4011	*83.7988
Axial	4.0076	17.2617	32.8832	48.9437	65.028	79.0416	87.6804	102.2349	119.8074	138.3143
	*4.0077	*17.2618	*32.8831	*48.9435	*65.031	*79.0425	*87.6819	*102.2337	*119.8078	*138.3118

* ANSYS Result, B:backward, F:forward

Table 5.9

Bending Natural frequencies for rotating drillstring, neutral point at 400m above bottom.

Drillcollar length is 200m, Drillpipe length is 1000m, two stabilizers one at bottom and one at 200m from bottom

rad/sec	f_1	f_2	f_3	f_4	f_5	f_6	f_7	f_8	f_9	f_{10}	
0 RPM	0.1534	0.2955	0.3863	0.5344	0.6825	0.8125	0.8481	0.9594	1.113	1.2656	
30 RPM	B	0.1532	0.2954	0.3862	0.5343	0.6824	0.8124	0.8481	0.9593	1.1129	1.2655
	F	0.1535	0.2956	0.3865	0.5345	0.6826	0.8126	0.8481	0.9596	1.1131	1.2657
60 RPM	B	0.1531	0.2952	0.3861	0.5342	0.6823	0.8123	0.8481	0.9592	1.1129	1.2654
	F	0.1536	0.2958	0.3866	0.5346	0.6827	0.8127	0.8482	0.9597	1.1132	1.2657
100 RPM	B	0.1529	0.2951	0.3859	0.534	0.6821	0.8122	0.8481	0.9591	1.1127	1.2653
	F	0.1538	0.2959	0.3867	0.5348	0.6828	0.8128	0.8482	0.9598	1.1133	1.2659
500 RPM	B	0.1511	0.2933	0.3843	0.5325	0.6808	0.8109	0.8478	0.9578	1.1117	1.2642
	F	0.1557	0.2977	0.3883	0.5363	0.6842	0.8141	0.8485	0.9611	1.1144	1.2669
1000RPM	B	0.1489	0.2912	0.3824	0.5306	0.6791	0.8093	0.8475	0.9561	1.1103	1.2629
	F	0.158	0.2999	0.3904	0.5382	0.6859	0.8158	0.8488	0.9628	1.1157	1.2683

Table 5.10

Torsional & Axial natural frequencies for rotating drillstring

rad/sec	f_1	f_2	f_3	f_4	f_5	f_6	f_7	f_8	f_9	f_{10}
Torsional	1.705	10.1197	19.8168	29.7083	39.699	48.6099	52.2853	61.5118	72.4139	83.8122
	*1.7048	*10.1184	*19.814	*29.7038	*39.693	*48.603	*52.2774	*61.5023	*72.4011	*83.7988
Axial	4.0076	17.2617	32.8832	48.9437	65.028	79.0416	87.6804	102.2349	119.8074	138.3143
	*4.0077	*17.2618	*32.8831	*48.9435	*65.031	*79.0425	*87.6819	*102.2337	*119.8078	*138.3118

* ANSYS Result, B:backward, F:forward

b) Effect of drillpipe length:

In this case, different drillpipe length were considered while keeping drillcollar length constant, which would simulate the drilling operation of adding drillpipe segments. Drillpipe lengths in the range from 300m up to 1000m are considered to study their effect on the natural frequencies. The bending natural frequencies for 200m long drillcollar and 300m long drillpipe were shown for the first three modes in figure 5.8 and tabulated in table 5.13 up to the tenth mode. Increasing the drillpipe length to 600m, shown in figure 5.10 for the first three modes and tabulated in table 5.17, will decrease the drillstring stiffness. As the drillpipe length is increased more to 1000m, shown in figure 5.3 for the first three modes, the drillstring becomes even more flexible. Figure 5.11 compares each mode of the different lengths of drillpipe with their stiffness.

Unlike the first case of different neutral point locations, the change of the drillpipe length influenced the torsional and axial natural frequencies as shown in figures 5.12 and 5.13. The same affect is noticed on torsional and axial frequencies as was noticed on the bending frequencies that is as the length of the drillpipe is increased the drillstring becomes less stiff, as expected .

On the other hand the stabilizers location along a constant length of drillcollar had no significant effect on the bending stiffness. Moreover it did not affect the torsional or axial stiffness as shown for 300m drillcollar length in figure 5.14 for bending stiffness and tables 5.12 and 5.14 for torsional and axial stiffness and for 600m drillcollar length in figure 5.14 for bending stiffness and tables 5.16 and 5.18 for torsional and axial stiffness.

c) Effect of drillpipe/drillcollar length ratio

In this case, different values of the drillpipe/drillcollar length ratio are considered. The length ratio (γ) is varied in the range from 5 to 2. This would correspond to drillpipe length of 1000m and 200m long drillcollar for the first length ratio and 900m/300m for the second length ratio and 800m/400m for the third length ratio. For the first length ratio figure 5.3 shows the first three modes of the bending frequencies. Figures 5.15 and 5.16 show the first three modes of the bending frequencies for the second length ratio and tabulated in tables 5.19 and 5.21. For the third length ratio figures 5.17 and 5.18 shows the first three modes of the bending frequencies and tabulated in tables 5.23 and 5.25. No significant change in the bending natural frequencies in case of changing length ratio as shown in figure 5.19. The number of stabilizers was increased as the drillcollar length increased; however, no significant effect was noticed on the bending natural frequencies.

Torsional and axial frequencies are also not significantly affected by changing the length ratio nor by the number of stabilizers as shown in figures 5.20 and 5.21 and tabulated in tables 5.20, 5.22, 5.24, and 5.26.

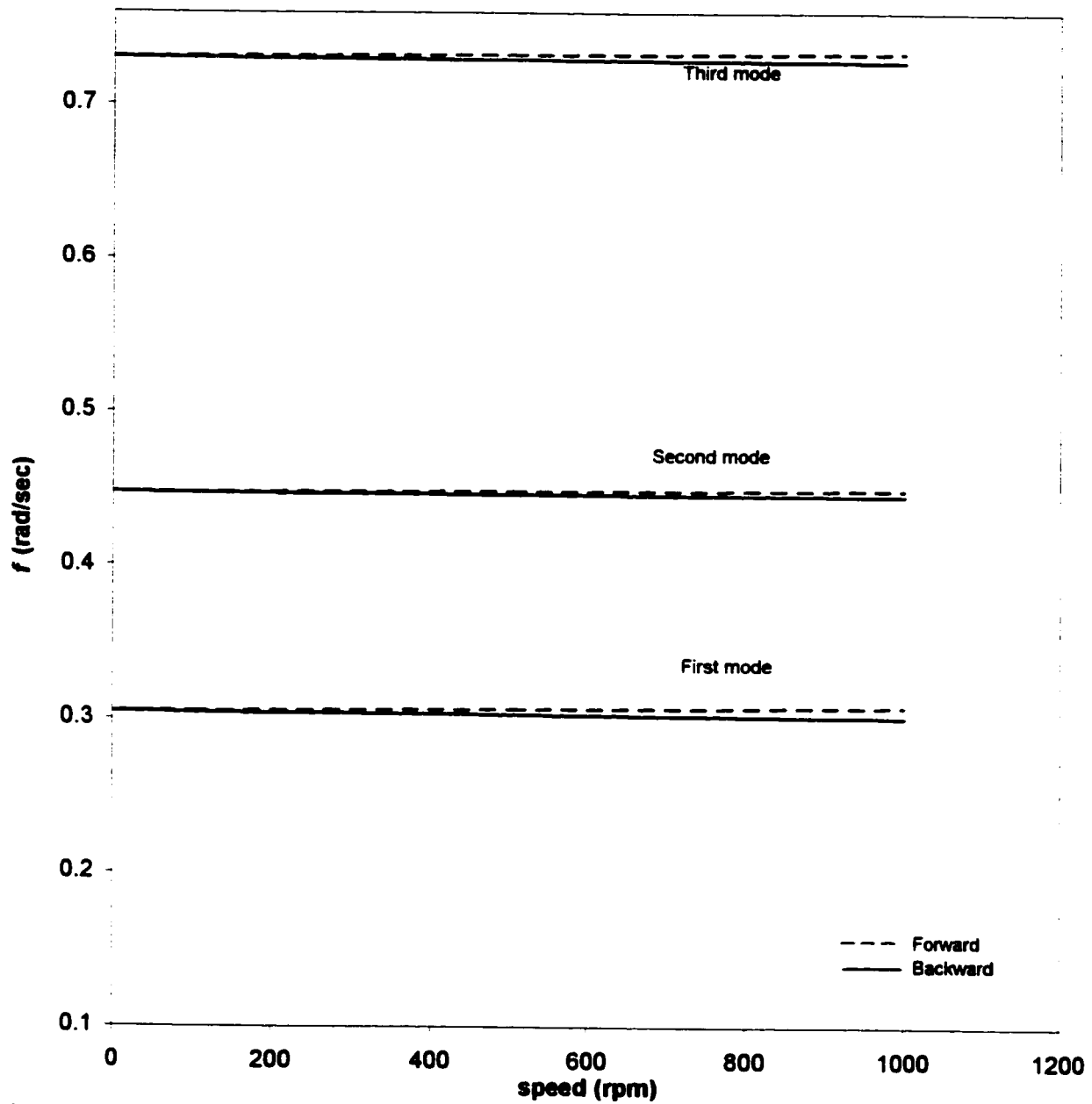


Figure 5.7: Bending frequency for drillcollar 200m long and drillpipe 300m long with one stabilizer at bottom and the other at 100m above bottom

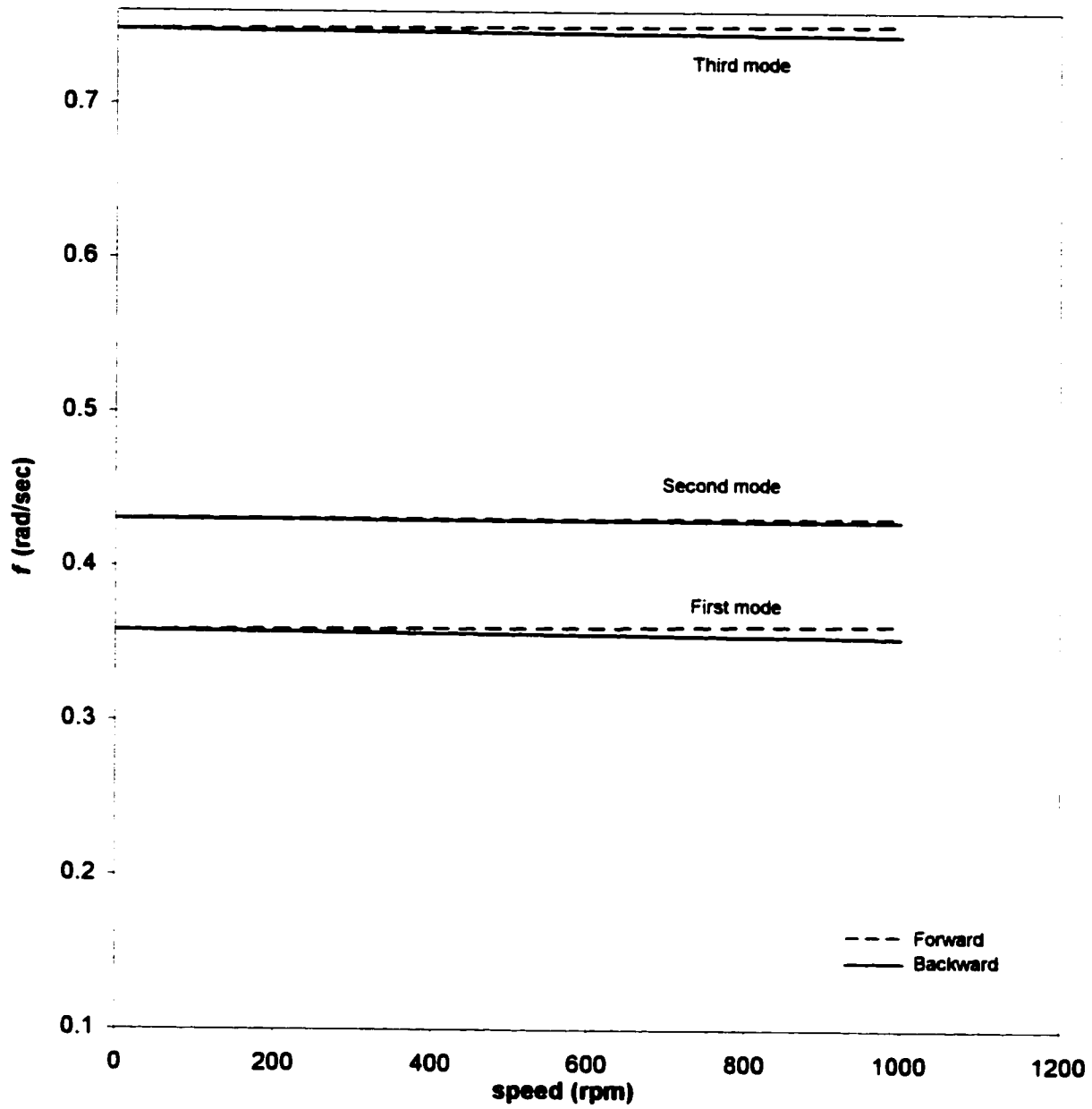


Figure 5.8: Bending frequency for drillcollar 200m long and drillpipe 300m long with one stabilizer at bottom and the other at 200m above bottom

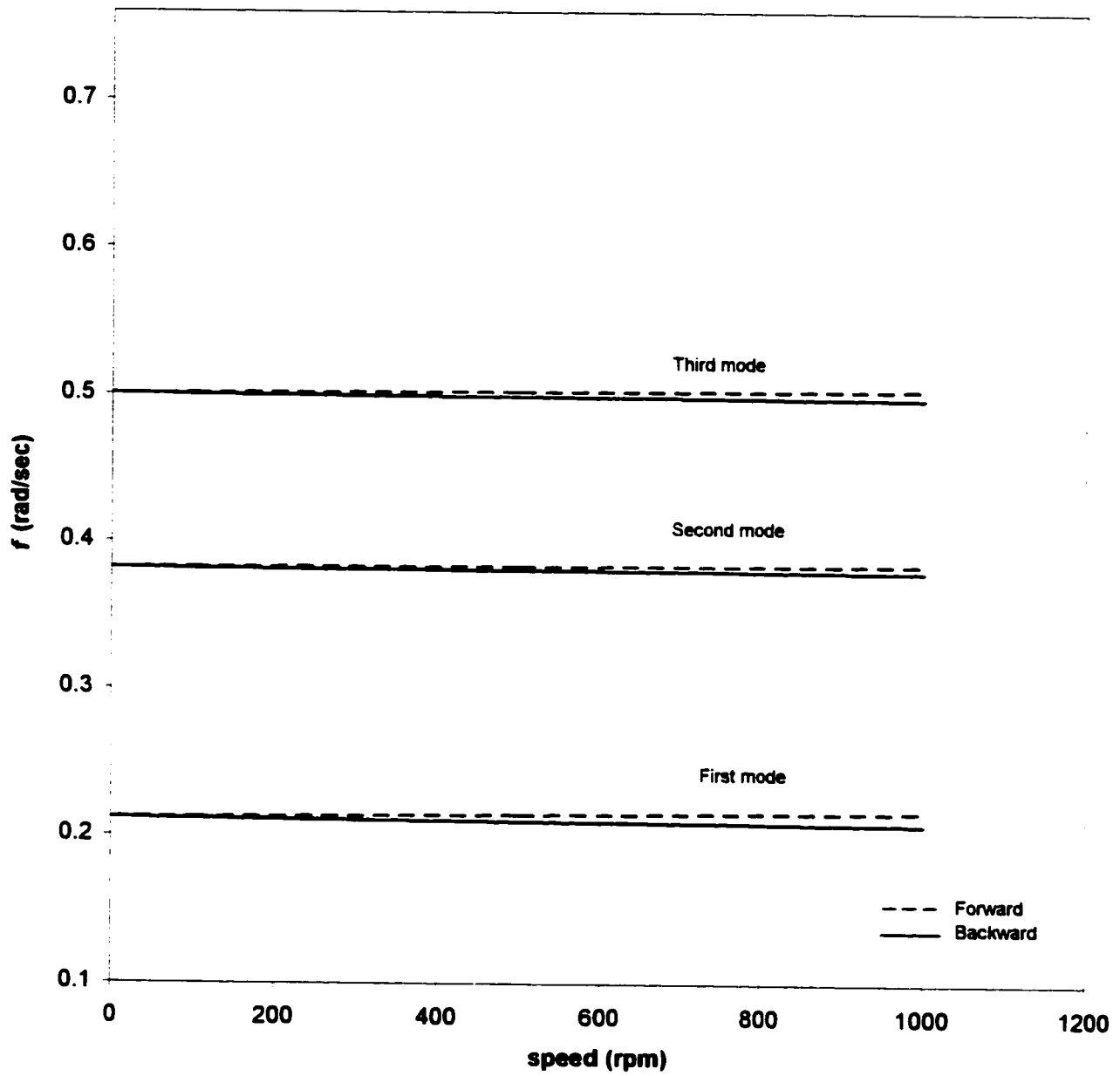


Figure 5.9: Bending frequency for drillcollar 200m long and drillpipe 600m long with one stabilizer at bottom and the other at 100m above bottom

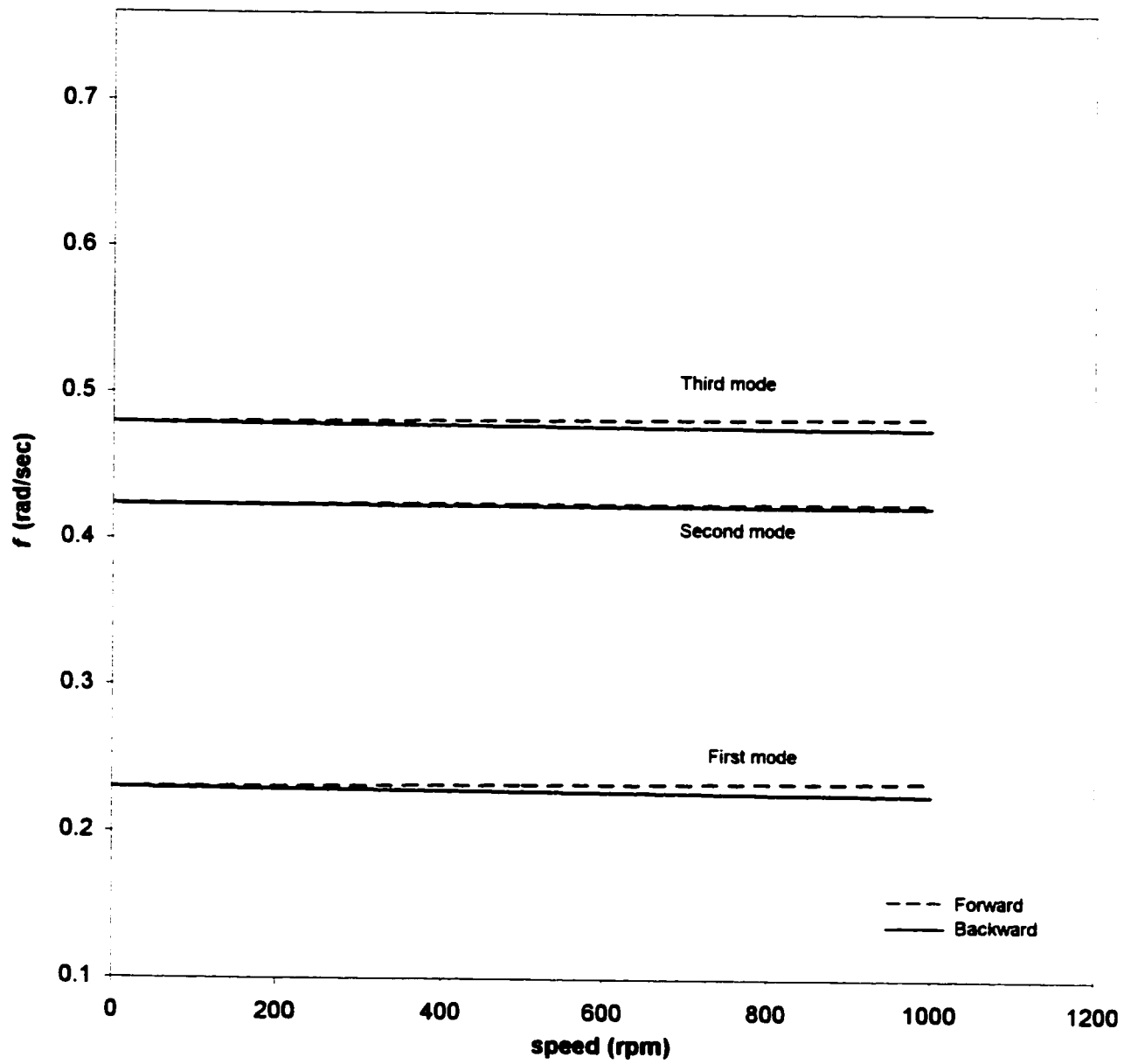


Figure 5.10: Bending frequency for drillcollar 200m long and drillpipe 600m long with one stabilizer at bottom and the other at 200m above bottom

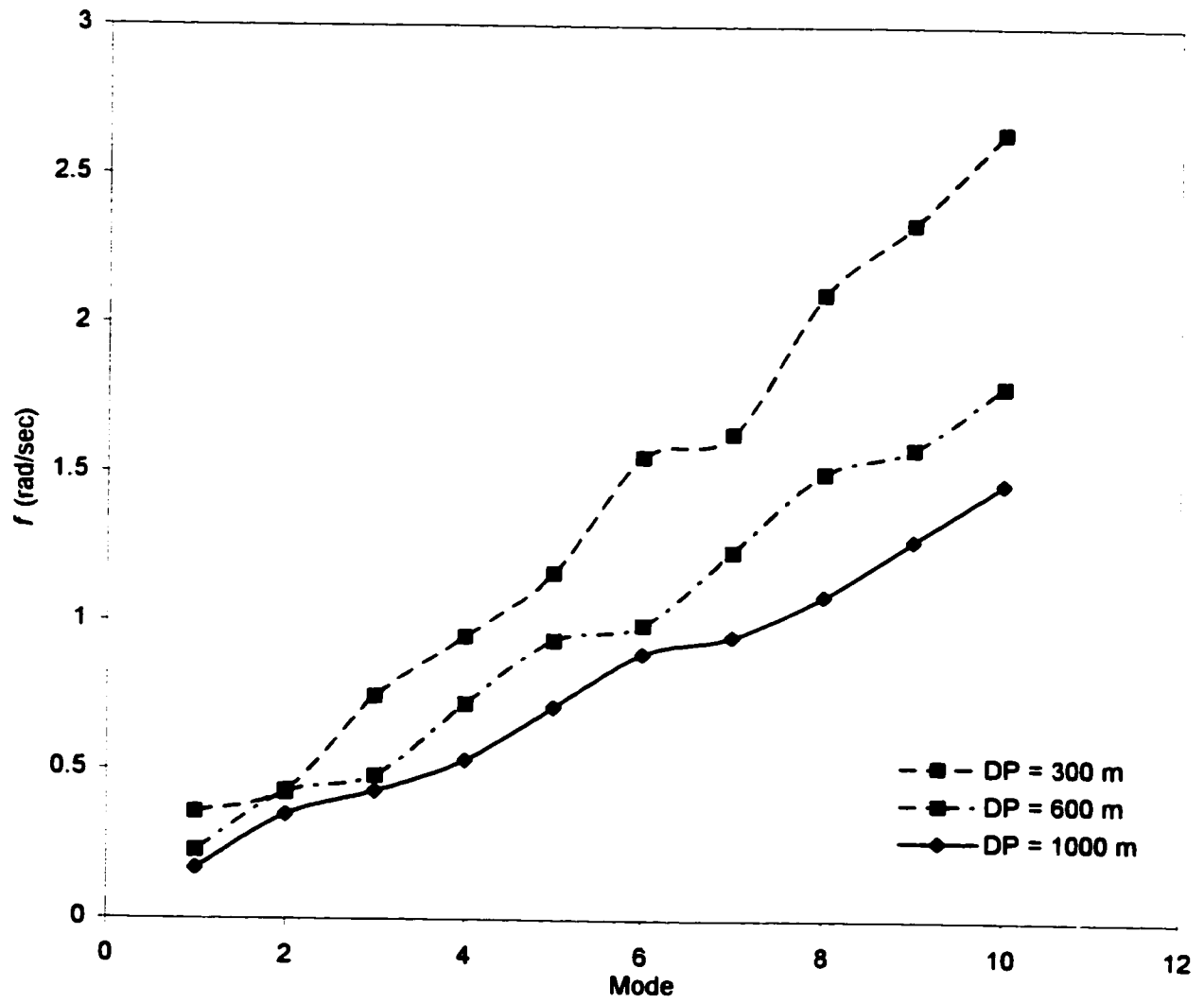


Figure 5.11: Bending frequency for different length of drillpipe

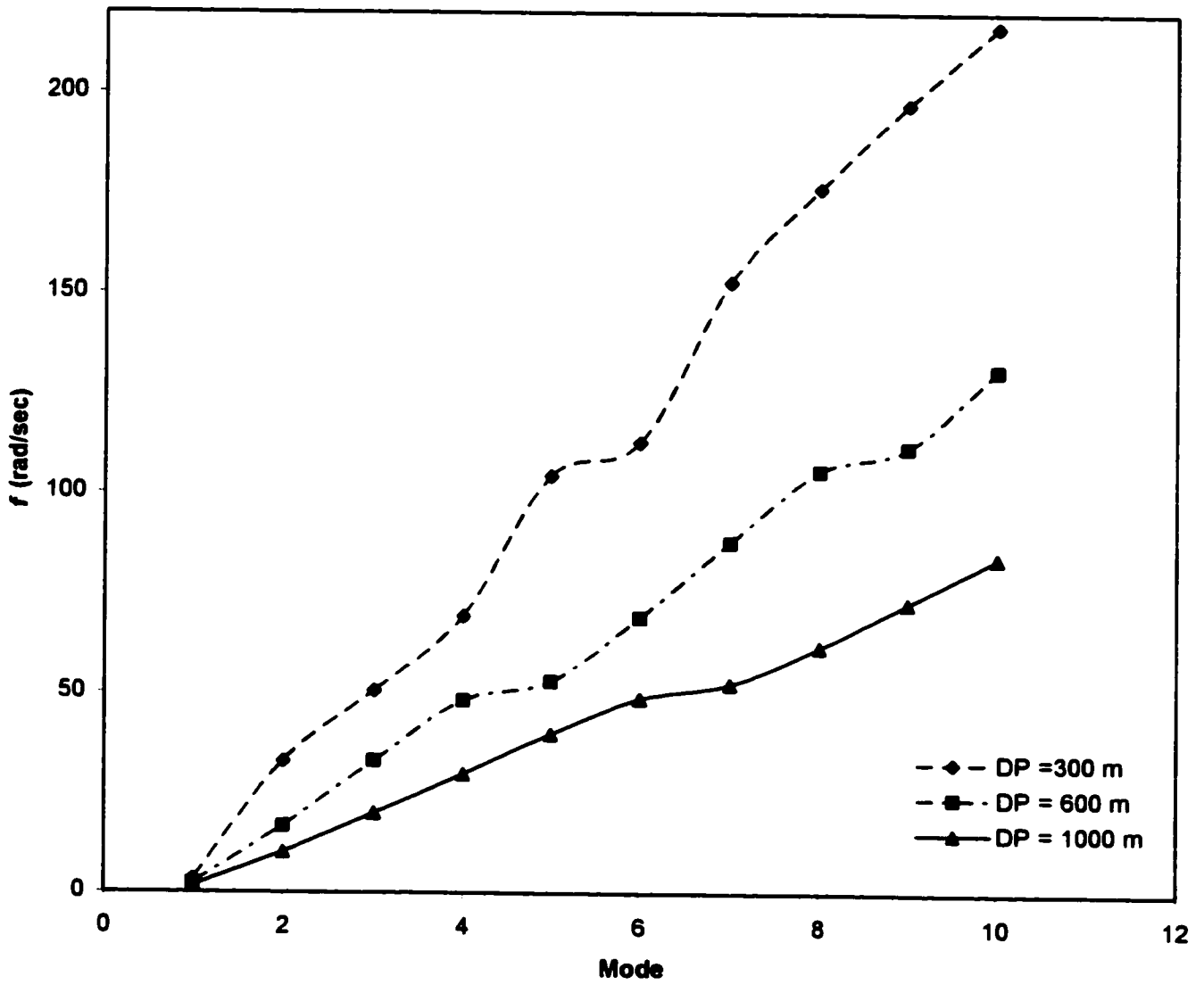


Figure 5.12: Torsional frequency for variable dirllpipe length

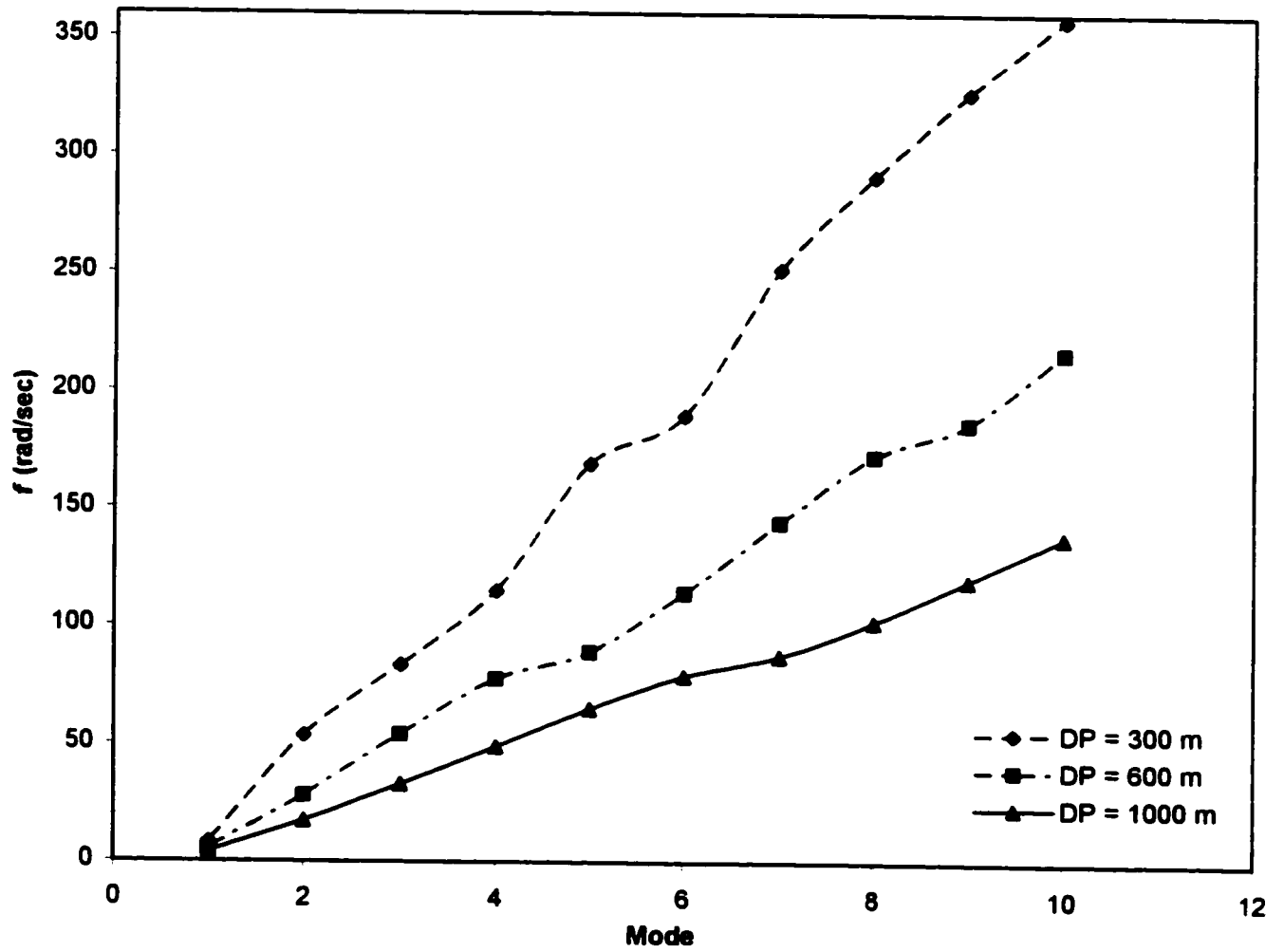


Figure 5.13: Axial frequency for variable dirllpipe length

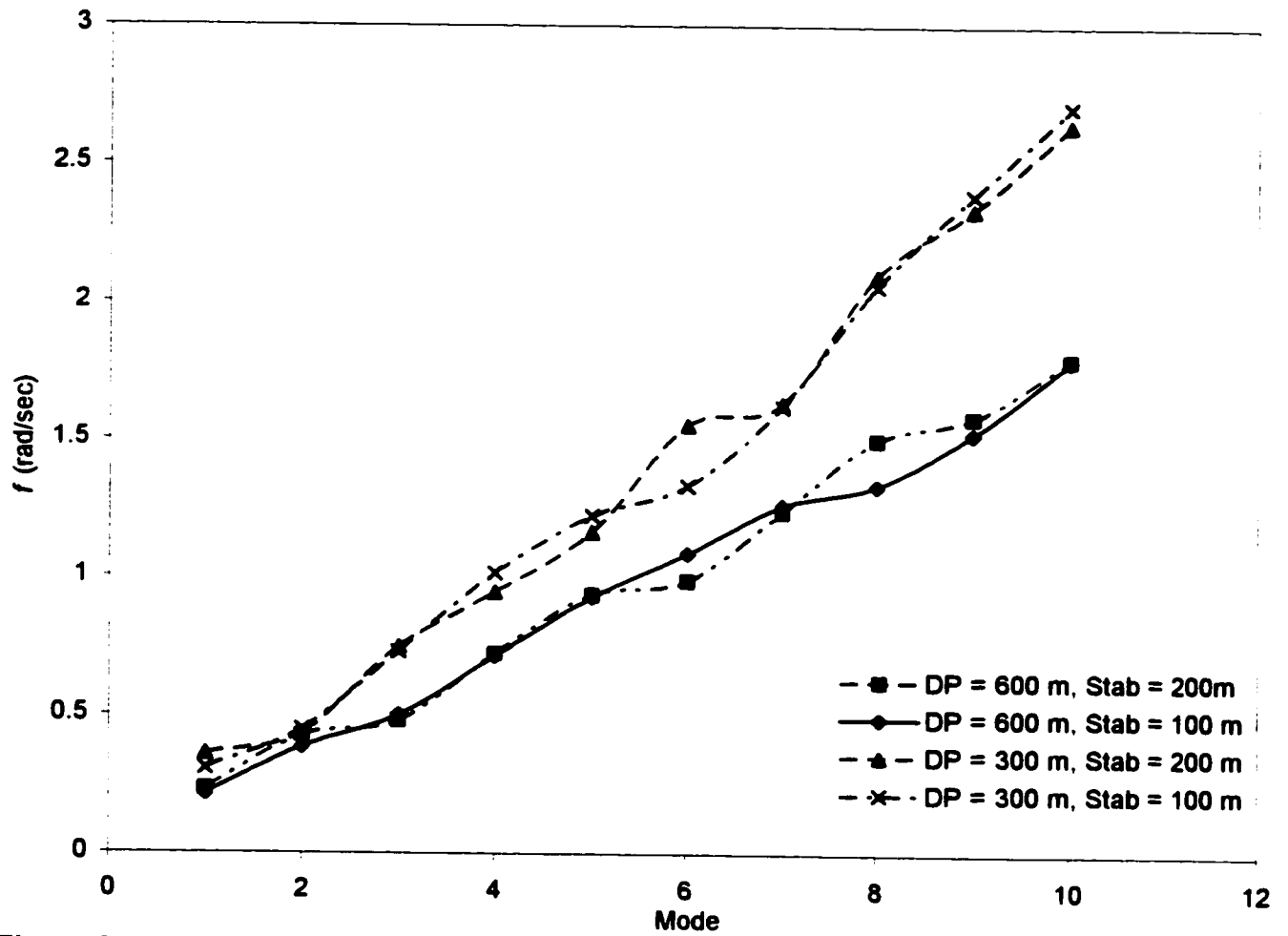


Figure 5.14: Bending frequency for 200m drillcollar, 300m/600m drillpipe and different location of stabilizers

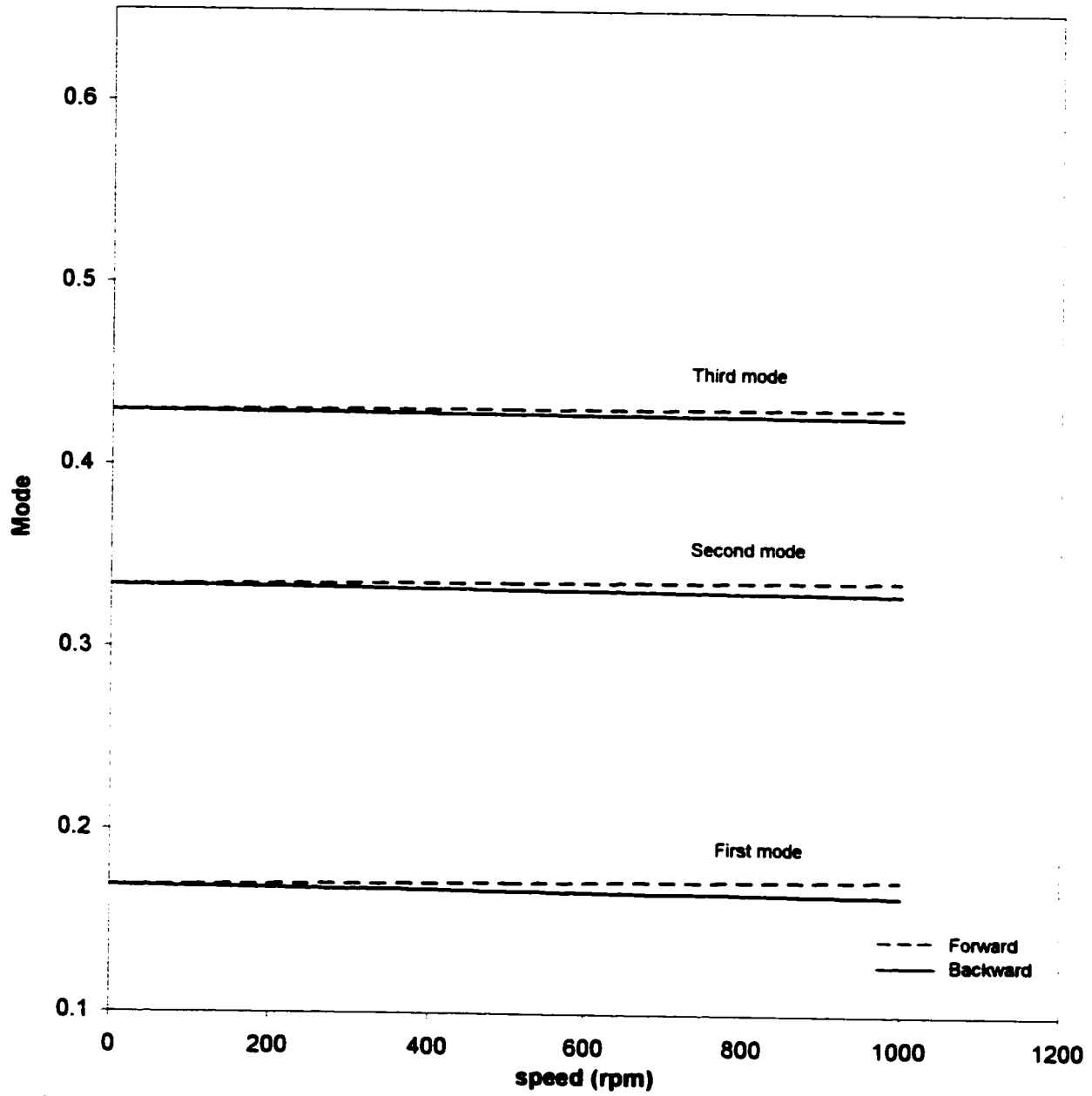


Figure 5.15: Bending frequency for drillcollar 300m long and drillpipe 900m long with one stabilizer at bottom and the other at 200m above bottom

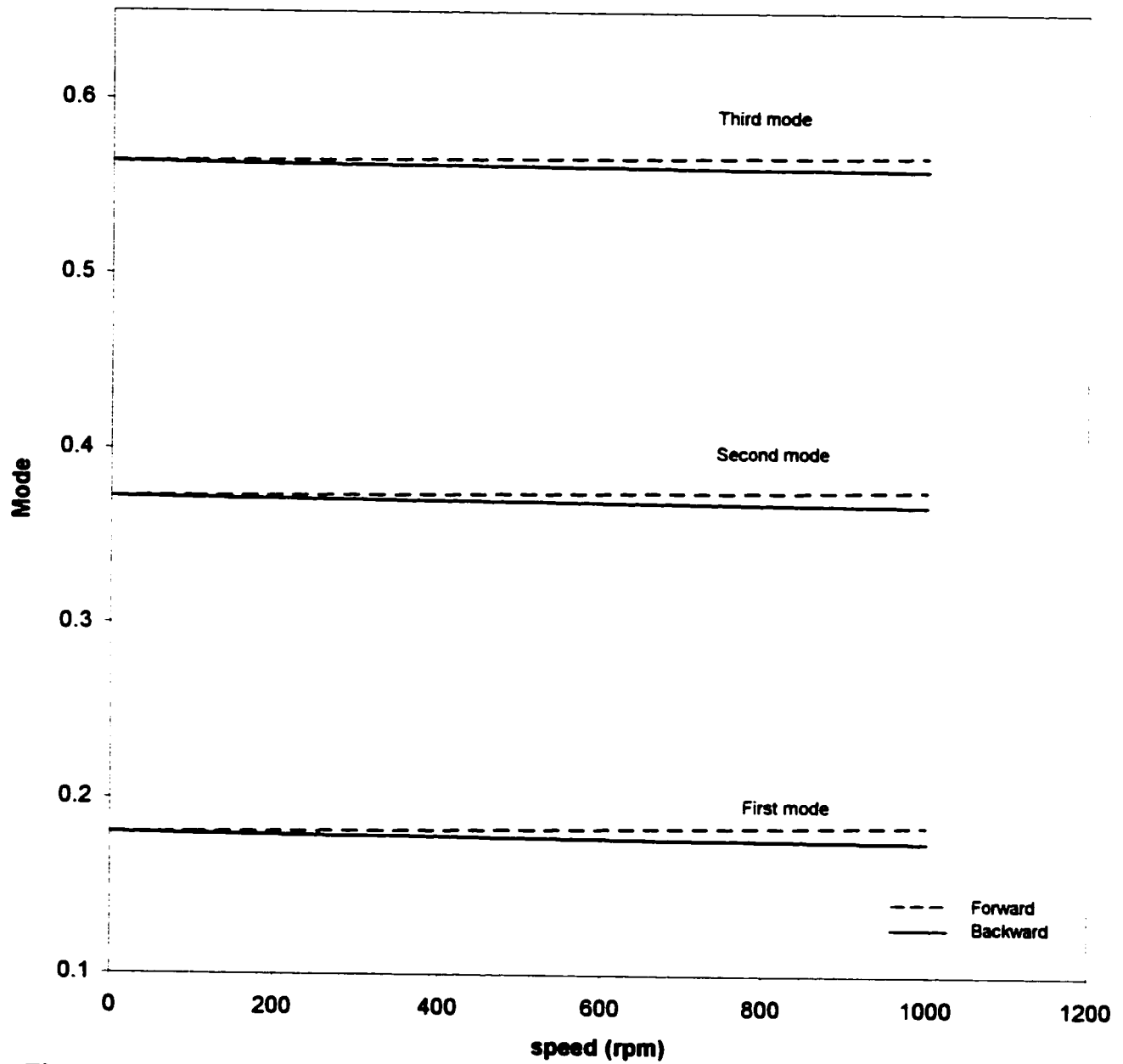


Figure 5.16: Bending frequency for drillcollar 300m long and drillpipe 900m long with one stabilizer at bottom, one at 200m and one at 300m above bottom

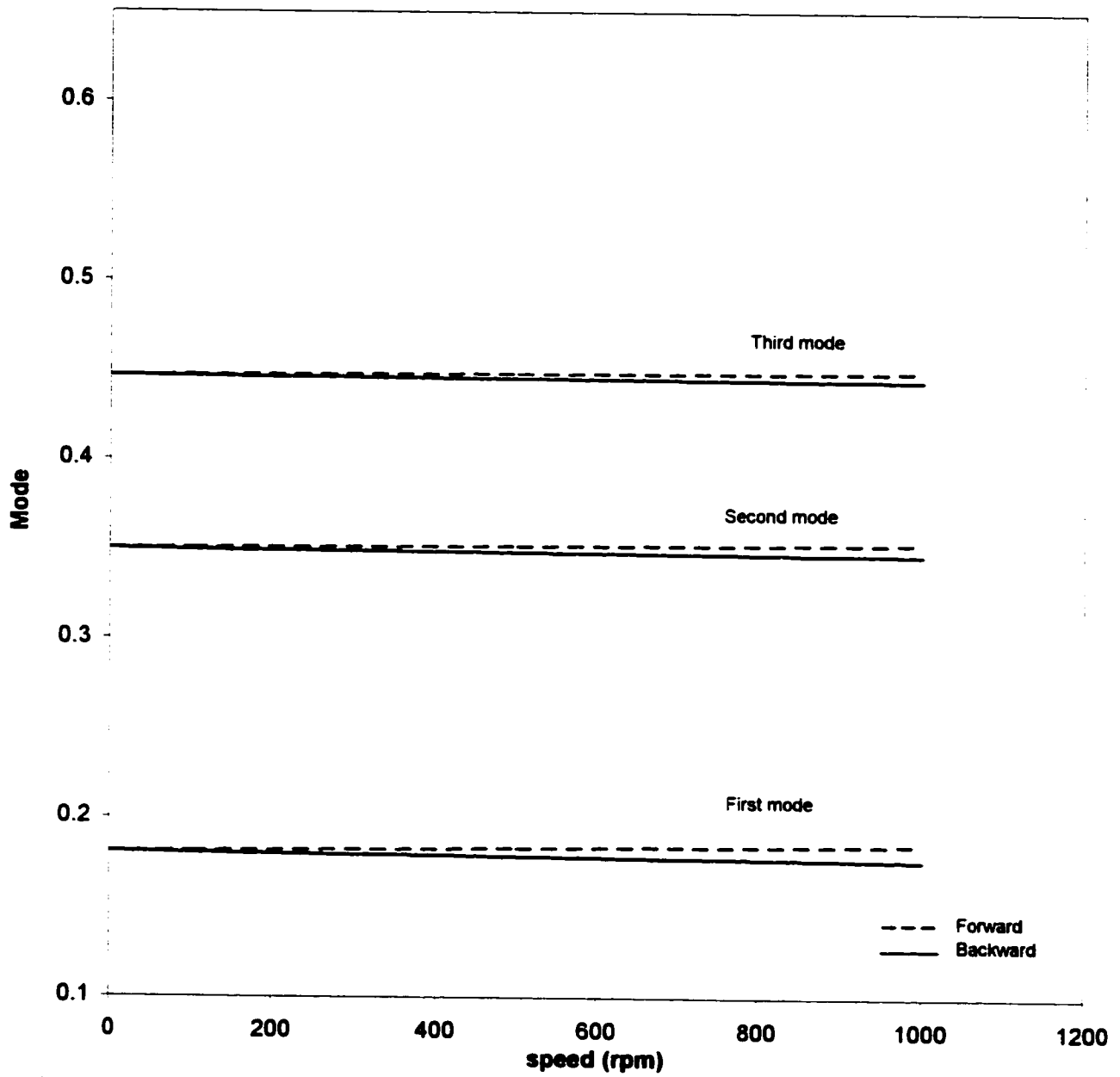


Figure 5.17: Bending frequency for drillcollar 400m long and drillpipe 800m long with one stabilizer at bottom, one at 200m and one at 300m above bottom

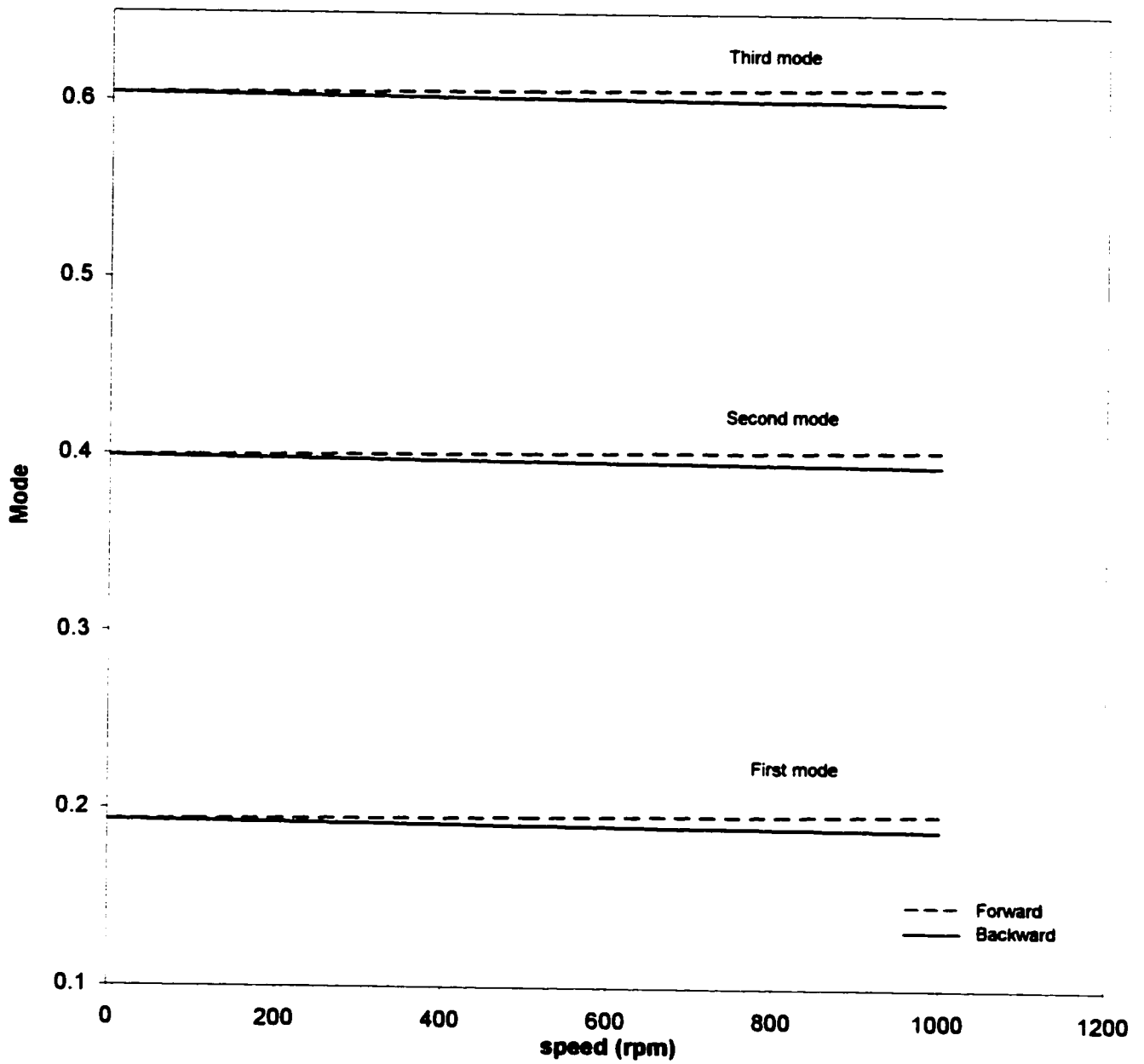


Figure 5.18: Bending frequency for drillcollar 400m long and drillpipe 800m long with one stabilizer at bottom, one at 200m, one at 300m and one at 400m above bottom

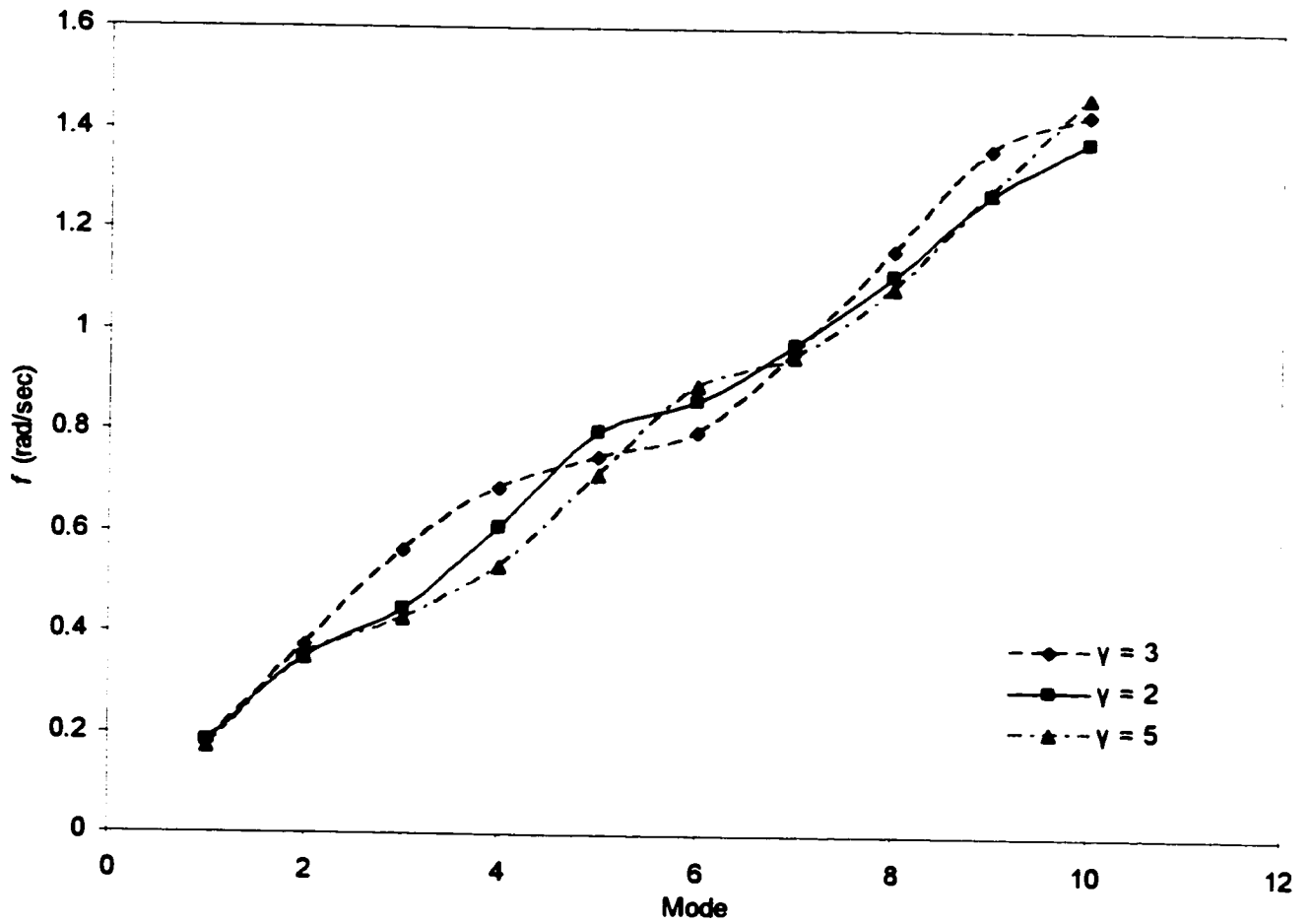


Figure 5.19: Bending frequency for different length of drillpipe/drillcollar

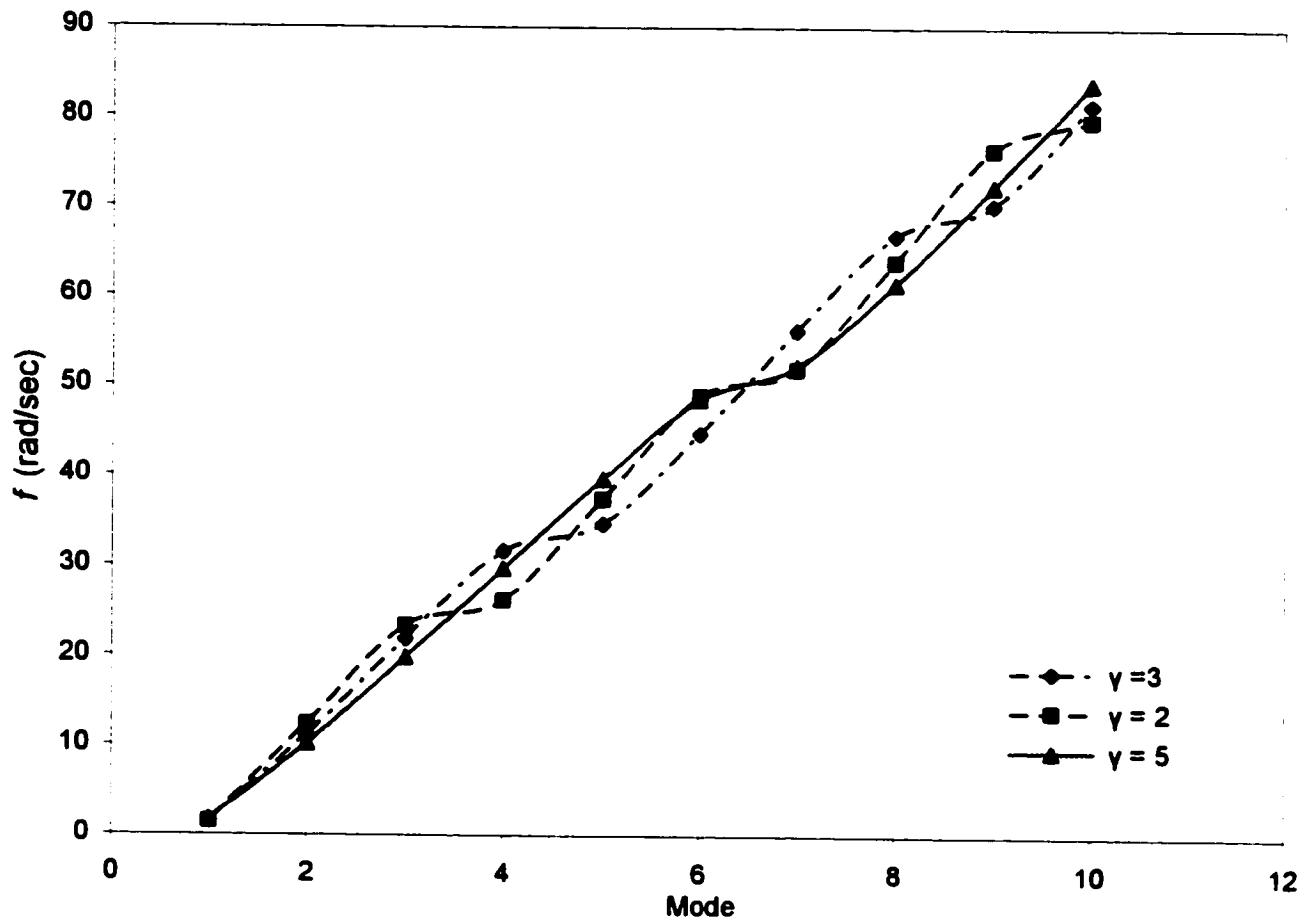


Figure 5.20: Torsional frequency for different length of drillpipe/drillcollar

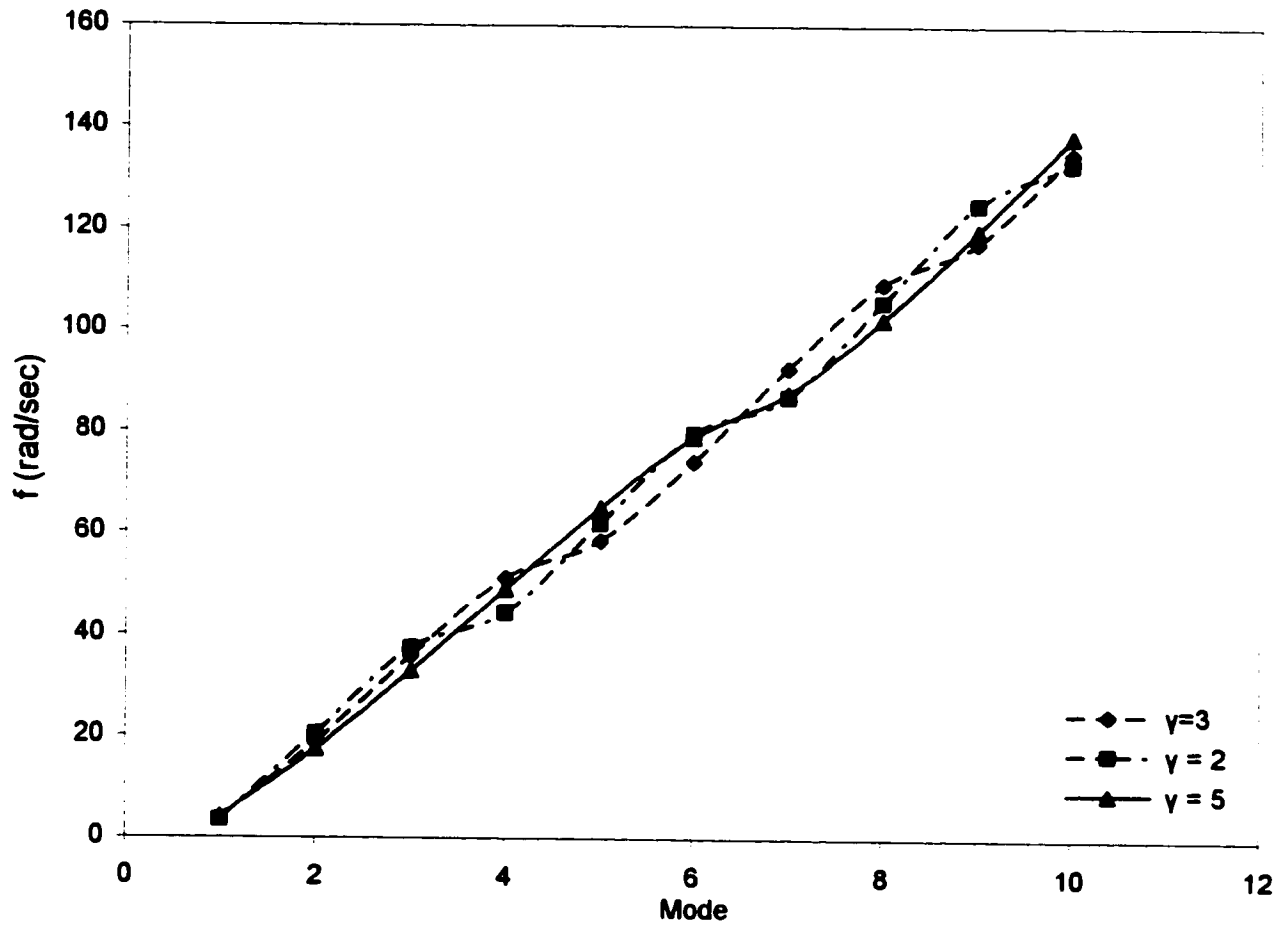


Figure 5.21: Axial frequency for different length of drillpipe/drillcollar

Table 5.11

Bending Natural frequencies for rotating drillstring

Drillcollar length is 200m, Drillpipe length is 300m, two stabilizers one at bottom and one at 100m from bottom

rad/sec	f_1	f_2	f_3	f_4	f_5	f_6	f_7	f_8	f_9	f_{10}
0 RPM	0.3048	0.4472	0.7308	1.0141	1.2224	1.332	1.6212	2.0609	2.3894	2.7087
30 RPM	B 0.3047	0.4471	0.7307	1.014	1.2223	1.332	1.6211	2.0607	2.3893	2.7085
	F 0.305	0.4472	0.7309	1.0141	1.2224	1.332	1.6213	2.0611	2.3895	2.7089
60 RPM	B 0.3046	0.447	0.7306	1.014	1.2223	1.332	1.6211	2.0606	2.3893	2.7083
	F 0.3051	0.4473	0.731	1.0142	1.2225	1.332	1.6214	2.0612	2.3896	2.7091
100 RPM	B 0.3045	0.447	0.7305	1.0139	1.2222	1.3319	1.621	2.0603	2.3891	2.7081
	F 0.3052	0.4473	0.7311	1.0142	1.2225	1.3321	1.6215	2.0614	2.3897	2.7093
500 RPM	B 0.3031	0.4462	0.7294	1.0132	1.2216	1.3317	1.62	2.0581	2.388	2.7056
	F 0.3066	0.4481	0.7323	1.0149	1.2231	1.3323	1.6224	2.0637	2.3908	2.7118
1000RPM	B 0.3013	0.4453	0.7279	1.0123	1.2209	1.3314	1.6188	2.0554	2.3867	2.7025
	F 0.3084	0.449	0.7337	1.0158	1.2239	1.3326	1.6237	2.0664	2.3921	2.715

Table 5.12

Torsional & Axial natural frequencies for rotating drillstring

rad/sec	f_1	f_2	f_3	f_4	f_5	f_6	f_7	f_8	f_9	f_{10}
Torsional	3.2141	32.7667	50.443	69.0121	104.2907	112.64	152.8221	176.217	197.1418	216.6631
	*3.2137	*32.7618	*50.4358	*69.0019	*104.2757	*112.63	*152.8008	*176.1931	*197.1098	*216.6317
Axial	7.8419	53.3964	83.3455	114.8474	169.0825	189.4502	251.4866	291.1585	326.5236	357.57
	*7.8420	*53.3964	*83.3465	*114.8503	*169.0805	*189.4506	*251.4855	*291.1565	*326.5246	*357.5698

* ANSYS Result, B:backward, F:forward

Table 5.13

Bending Natural frequencies for rotating drillstring

Drillcollar length is 200m, Drillpipe length is 300m, two stabilizers one at bottom and one at 200m from bottom

rad/sec	f_1	f_2	f_3	f_4	f_5	f_6	f_7	f_8	f_9	f_{10}
0 RPM	0.358	0.4305	0.7479	0.9466	1.1624	1.5527	1.631	2.0993	2.3361	2.6434
30 RPM	B 0.3579	0.4305	0.7478	0.9466	1.1623	1.5527	1.6309	2.0991	2.3361	2.6432
	F 0.3581	0.4305	0.748	0.9466	1.1625	1.5528	1.631	2.0995	2.3362	2.6436
60 RPM	B 0.3578	0.4305	0.7477	0.9465	1.1623	1.5527	1.6308	2.0989	2.336	2.6431
	F 0.3582	0.4306	0.7481	0.9466	1.1625	1.5528	1.6311	2.0997	2.3362	2.6438
100 RPM	B 0.3576	0.4304	0.7476	0.9465	1.1622	1.5526	1.6308	2.0987	2.336	2.6428
	F 0.3584	0.4306	0.7483	0.9466	1.1626	1.5529	1.6312	2.0999	2.3363	2.644
500 RPM	B 0.356	0.4301	0.7463	0.9463	1.1612	1.552	1.63	2.0962	2.3353	2.6406
	F 0.36	0.4309	0.7496	0.9469	1.1636	1.5535	1.632	2.1023	2.337	2.6463
1000RPM	B 0.354	0.4297	0.7446	0.946	1.16	1.5512	1.629	2.0932	2.3345	2.6378
	F 0.362	0.4313	0.7513	0.9472	1.1648	1.5542	1.633	2.1054	2.3378	2.6492

Table 5.14

Torsional & Axial natural frequencies for rotating drillstring

rad/sec	f_1	f_2	f_3	f_4	f_5	f_6	f_7	f_8	f_9	f_{10}
Torsional	3.2141	32.7667	50.443	69.0121	104.2907	112.64	152.8221	176.217	197.1418	216.6631
	*3.2137	*32.7618	*50.4358	*69.0019	*104.2757	*112.63	*152.8008	*176.1931	*197.1098	*216.6317
Axial	7.8419	53.3964	83.3455	114.8474	169.0825	189.4502	251.4866	291.1585	326.5236	357.57
	*7.8420	*53.3964	*83.3465	*114.8503	*169.0805	*189.4506	*251.4855	*291.1565	*326.5246	*357.5698

* ANSYS Result, B:backward, F:forward

Table 5.15

Bending Natural frequencies for rotating drillstring

Drillcollar length is 200m, Drillpipe length is 600m, two stabilizers one at bottom and one at 100m from bottom

rad/sec	f_1	f_2	f_3	f_4	f_5	f_6	f_7	f_8	f_9	f_{10}
0 RPM	0.2123	0.3821	0.5003	0.7138	0.9289	1.087	1.2623	1.334	1.5235	1.7876
30 RPM	B 0.2121	0.382	0.5002	0.7137	0.9289	1.087	1.2623	1.3339	1.5234	1.7875
	F 0.2124	0.3821	0.5003	0.7139	0.929	1.0871	1.2624	1.334	1.5235	1.7877
60 RPM	B 0.212	0.3819	0.5001	0.7136	0.9288	1.0869	1.2622	1.3339	1.5233	1.7874
	F 0.2125	0.3822	0.5004	0.714	0.9291	1.0871	1.2624	1.334	1.5236	1.7878
100 RPM	B 0.2118	0.3818	0.5	0.7134	0.9287	1.0868	1.2621	1.3339	1.5232	1.7873
	F 0.2127	0.3823	0.5006	0.7141	0.9292	1.0872	1.2625	1.334	1.5237	1.7879
500 RPM	B 0.2101	0.3809	0.4987	0.7121	0.9276	1.0861	1.2613	1.3335	1.5223	1.786
	F 0.2144	0.3832	0.5018	0.7154	0.9303	1.088	1.2633	1.3344	1.5246	1.7892
1000RPM	B 0.208	0.3797	0.4973	0.7104	0.9263	1.0851	1.2604	1.3331	1.5211	1.7844
	F 0.2166	0.3844	0.5033	0.7171	0.9316	1.0889	1.2643	1.3348	1.5258	1.7908

Table 5.16

Torsional & Axial natural frequencies for rotating drillstring

rad/sec	f_1	f_2	f_3	f_4	f_5	f_6	f_7	f_8	f_9	f_{10}
Torsional	2.2445	16.6328	32.9562	48.0319	52.8702	68.8033	87.6104	105.5361	111.3672	130.6612
	*2.2442	*16.6303	*32.9515	*48.0249	*52.8623	*68.7946	*87.6002	*105.520	*111.351	*130.640
Axial	5.3945	27.8771	54.0477	77.5594	89.1877	114.1282	144.2813	172.209	186.2224	216.4275
	*5.3945	*27.8772	*54.0480	*77.5596	*89.1898	*114.1278	*144.2818	*172.2095	*186.2210	*216.4306

* ANSYS Result, B:backward, F:forward

Table 5.17

Bending Natural frequencies for rotating drillstring

Drillcollar length is 200m, Drillpipe length is 600m, two stabilizers one at bottom and one at 200m from bottom

rad/sec	f_1	f_2	f_3	f_4	f_5	f_6	f_7	f_8	f_9	f_{10}
0 RPM	0.2303	0.4236	0.4795	0.723	0.9362	0.9883	1.2384	1.4994	1.5822	1.7927
30 RPM	B 0.2302	0.4235	0.4794	0.7229	0.9362	0.9882	1.2383	1.4993	1.5821	1.7926
	F 0.2304	0.4236	0.4796	0.7231	0.9362	0.9883	1.2384	1.4995	1.5822	1.7928
60 RPM	B 0.23	0.4235	0.4793	0.7228	0.9361	0.9881	1.2382	1.4993	1.5821	1.7925
	F 0.2306	0.4236	0.4797	0.7232	0.9363	0.9884	1.2385	1.4996	1.5822	1.7929
100 RPM	B 0.2299	0.4235	0.4791	0.7226	0.9361	0.988	1.2381	1.4992	1.5821	1.7924
	F 0.2308	0.4237	0.4799	0.7233	0.9363	0.9885	1.2386	1.4997	1.5823	1.793
500 RPM	B 0.2281	0.4231	0.4776	0.7211	0.9357	0.9869	1.237	1.4981	1.5817	1.7911
	F 0.2326	0.424	0.4815	0.7248	0.9367	0.9896	1.2397	1.5007	1.5826	1.7943
1000RPM	B 0.2259	0.4227	0.4756	0.7193	0.9351	0.9856	1.2356	1.4968	1.5813	1.7895
	F 0.2348	0.4244	0.4835	0.7266	0.9372	0.9909	1.2411	1.502	1.5831	1.7959

Table 5.18

Torsional & Axial natural frequencies for rotating drillstring

rad/sec	f_1	f_2	f_3	f_4	f_5	f_6	f_7	f_8	f_9	f_{10}
Torsional	2.2445	16.6328	32.9562	48.0319	52.8702	68.8033	87.6104	105.5361	111.3672	130.6612
	*2.2442	*16.6303	*32.9515	*48.0249	*52.8623	*68.7946	*87.6002	*105.520	*111.351	*130.640
Axial	5.3945	27.8771	54.0477	77.5594	89.1877	114.1282	144.2813	172.209	186.2224	216.4275
	*5.3945	*27.8772	*54.0480	*77.5596	*89.1898	*114.1278	*144.2818	*172.2095	*186.2210	*216.4306

* ANSYS Result, B:backward, F:forward

Table 5.19

Bending Natural frequencies for rotating drillstring

Drillcollar length is 300m, Drillpipe length is 900m, two stabilizers, one at bottom and one at 200m from bottom

rad/sec	f_1	f_2	f_3	f_4	f_5	f_6	f_7	f_8	f_9	f_{10}
0 RPM	0.1694	0.3341	0.4298	0.5711	0.6981	0.7508	0.9236	1.065	1.2017	1.3775
30 RPM	B 0.1692	0.334	0.4297	0.571	0.6981	0.7507	0.9235	1.0649	1.2016	1.3775
	F 0.1695	0.3342	0.4299	0.5712	0.6981	0.7509	0.9237	1.0651	1.2017	1.3776
60 RPM	B 0.1691	0.3339	0.4296	0.5709	0.698	0.7506	0.9234	1.0649	1.2015	1.3774
	F 0.1696	0.3343	0.4299	0.5713	0.6981	0.751	0.9238	1.0651	1.2018	1.3777
100 RPM	B 0.1689	0.3338	0.4295	0.5707	0.698	0.7505	0.9233	1.0648	1.2014	1.3773
	F 0.1698	0.3345	0.43	0.5715	0.6982	0.7512	0.9239	1.0652	1.2019	1.3778
500 RPM	B 0.1672	0.3323	0.4286	0.5693	0.6977	0.7491	0.9221	1.0639	1.2005	1.3763
	F 0.1716	0.3359	0.431	0.5729	0.6984	0.7525	0.9251	1.0662	1.2029	1.3788
1000RPM	B 0.165	0.3306	0.4275	0.5675	0.6974	0.7474	0.9206	1.0627	1.1992	1.375
	F 0.1739	0.3376	0.4321	0.5747	0.6988	0.7542	0.9266	1.0673	1.2041	1.38

Table 5.20

Torsional & Axial natural frequencies for rotating drillstring

rad/sec	f_1	f_2	f_3	f_4	f_5	f_6	f_7	f_8	f_9	f_{10}
Torsional	1.4963	11.071	21.834	31.611	34.707	44.737	56.239	66.884	70.291	81.438
	*1.4961	*11.0891	*21.8310	*31.6063	*34.7014	*44.7306	*56.2307	*66.8719	*70.2774	*81.4238
Axial	3.5961	18.554	35.811	51.072	58.512	74.195	92.636	109.24	117.43	134.87
	*3.5961	*18.5536	*35.8104	*51.0722	*58.5121	*74.1981	*92.6393	*109.2395	*117.4265	*134.8686

* ANSYS Result, B:backward, F:forward

Table 5.21

Bending Natural frequencies for rotating drillstring. Drillcollar length is 300m, Drillpipe length is 900m, three stabilizers, one at bottom, one at 200m and one at 300m above bottom.

rad/sec	f_1	f_2	f_3	f_4	f_5	f_6	f_7	f_8	f_9	f_{10}
0 RPM	0.1805	0.3723	0.5637	0.688	0.7492	0.7991	0.9608	1.1596	1.3631	1.4325
30 RPM	B 0.1803	0.3722	0.5636	0.688	0.7491	0.799	0.9607	1.1595	1.363	1.4325
	F 0.1806	0.3725	0.5638	0.688	0.7493	0.7991	0.9609	1.1597	1.3632	1.4325
60 RPM	B 0.1802	0.3721	0.5634	0.688	0.749	0.799	0.9606	1.1594	1.3629	1.4325
	F 0.1807	0.3726	0.5639	0.6881	0.7494	0.7992	0.961	1.1598	1.3633	1.4325
100 RPM	B 0.18	0.3719	0.5633	0.688	0.7489	0.7989	0.9604	1.1593	1.3628	1.4325
	F 0.1809	0.3728	0.5641	0.6881	0.7495	0.7992	0.9611	1.1599	1.3634	1.4325
500 RPM	B 0.1782	0.3702	0.5617	0.6877	0.7477	0.7984	0.9591	1.158	1.3616	1.4323
	F 0.1828	0.3745	0.5657	0.6883	0.7506	0.7998	0.9625	1.1611	1.3645	1.4327
1000RPM	B 0.176	0.368	0.5597	0.6874	0.7462	0.7977	0.9574	1.1565	1.3602	1.4321
	F 0.1851	0.3767	0.5677	0.6886	0.7521	0.8006	0.9642	1.1627	1.366	1.4329

Table 5.22

Torsional & Axial natural frequencies for rotating drillstring

rad/sec	f_1	f_2	f_3	f_4	f_5	f_6	f_7	f_8	f_9	f_{10}
Torsional	1.4963	11.071	21.834	31.611	34.707	44.737	56.239	66.884	70.291	81.438
	*1.4961	*11.0891	*21.8310	*31.6063	*34.7014	*44.7306	*56.2307	*66.8719	*70.2774	*81.4238
Axial	3.5961	18.554	35.811	51.072	58.512	74.195	92.636	109.24	117.43	134.87
	*3.5961	*18.5536	*35.8104	*51.0722	*58.5121	*74.1981	*92.6393	*109.2395	*117.4265	*134.8686

* ANSYS Result, B:backward, F:forward

Table 5.23

Bending Natural frequencies for rotating drillstring. Drillcollar length is 400m, Drillpipe length is 800m, three stabilizers one at bottom, one at 200m and one at 300m above bottom.

rad/sec	f_1	f_2	f_3	f_4	f_5	f_6	f_7	f_8	f_9	f_{10}
0 RPM	0.1809	0.35	0.4464	0.6087	0.799	0.8637	0.9746	1.1094	1.2724	1.3804
30 RPM	B 0.1807	0.3499	0.4463	0.6086	0.7989	0.8637	0.9745	1.1093	1.2723	1.3804
	F 0.181	0.35	0.4464	0.6088	0.7991	0.8638	0.9746	1.1094	1.2724	1.3804
60 RPM	B 0.1806	0.3498	0.4462	0.6085	0.7988	0.8637	0.9744	1.1093	1.2722	1.3804
	F 0.1811	0.3501	0.4465	0.6089	0.7992	0.8638	0.9747	1.1095	1.2725	1.3805
100 RPM	B 0.1804	0.3496	0.4461	0.6083	0.7986	0.8637	0.9743	1.1092	1.2721	1.3803
	F 0.1813	0.3503	0.4466	0.609	0.7993	0.8638	0.9748	1.1096	1.2726	1.3805
500 RPM	B 0.1787	0.3484	0.4451	0.6069	0.7973	0.8634	0.9732	1.1083	1.2712	1.38
	F 0.1831	0.3516	0.4476	0.6105	0.8006	0.864	0.9759	1.1105	1.2736	1.3808
1000RPM	B 0.1765	0.3467	0.4439	0.6051	0.7957	0.8631	0.9719	1.1072	1.27	1.3797
	F 0.1854	0.3531	0.4489	0.6123	0.8023	0.8643	0.9772	1.1115	1.2748	1.3812

Table 5.24

Torsional & Axial natural frequencies for rotating drillstring

rad/sec	f_1	f_2	f_3	f_4	f_5	f_6	f_7	f_8	f_9	f_{10}
Torsional	1.3867	12.313	23.332	26.159	37.414	48.952	51.941	63.952	76.434	79.692
	*1.3864	*12.3106	*23.3288	*26.1550	*37.4082	*48.9441	*51.9330	*63.9440	*76.4224	*79.6771
Axial	3.3681	20.344	37.456	44.323	61.818	79.726	86.987	105.67	125.03	132.95
	*3.3682	*20.3437	*37.4560	*44.3222	*61.8177	*79.7273	*86.9844	*105.664	*125.035	*132.946

* ANSYS Result, B:backward, F:forward

Table 5.25

Bending Natural frequencies for rotating drillstring. Drillcollar length is 400m, Drillpipe length is 800m, four stabilizers one at bottom, one at 200m, one at 300m, and one at 400m above bottom.

rad/sec	f_1	f_2	f_3	f_4	f_5	f_6	f_7	f_8	f_9	f_{10}
0 RPM	0.1936	0.3991	0.6041	0.7646	0.8272	0.8639	1.0317	1.2477	1.3666	1.4706
30 RPM	B 0.1935	0.399	0.604	0.7646	0.8271	0.8639	1.0316	1.2477	1.3666	1.3867
	F 0.1938	0.3993	0.6042	0.7647	0.8273	0.864	1.0318	1.2478	1.3666	1.4705
60 RPM	B 0.1934	0.3989	0.6039	0.7646	0.827	0.8639	1.0315	1.2476	1.3666	1.3867
	F 0.1939	0.3994	0.6043	0.7647	0.8274	0.864	1.0319	1.2479	1.3666	1.4704
100 RPM	B 0.1932	0.3987	0.6037	0.7645	0.8269	0.8639	1.0314	1.2474	1.3666	1.3867
	F 0.1941	0.3996	0.6045	0.7647	0.8275	0.864	1.0321	1.248	1.3667	1.4703
500 RPM	B 0.1914	0.397	0.6021	0.7641	0.8256	0.8636	1.0301	1.2463	1.3664	1.3867
	F 0.1959	0.4013	0.6061	0.7652	0.8288	0.8642	1.0334	1.2492	1.3668	1.4692
1000RPM	B 0.1892	0.3949	0.6002	0.7635	0.824	0.8633	1.0285	1.2448	1.3661	1.3867
	F 0.1982	0.4035	0.608	0.7657	0.8304	0.8645	1.035	1.2507	1.3671	1.4678

Table 5.26

Torsional & Axial natural frequencies for rotating drillstring

rad/sec	f_1	f_2	f_3	f_4	f_5	f_6	f_7	f_8	f_9	f_{10}
Torsional	1.3867	12.313	23.332	26.159	37.414	48.952	51.941	63.952	76.434	79.692
	*1.3864	*12.3106	*23.3288	*26.1550	*37.4082	*48.9441	*51.9330	*63.9440	*76.4224	*79.6771
Axial	3.3681	20.344	37.456	44.323	61.818	79.726	86.987	105.67	125.03	132.95
	*3.3682	*20.3437	*37.4560	*44.3222	*61.8177	*79.7273	*86.9844	*105.664	*125.035	*132.946

* ANSYS Result, B:backward, F:forward

5.2 Modeling Accuracy

The number of elements used to represent the drillstring system plays an important role in establishing the accuracy and required computation time in the developed model. A study is conducted with different number of elements in order to establish a measure of accuracy for a particular number of finite elements used in the system model. The only notable differences occur with the models that have elements less than 20 elements for the drillstring system and no changes are apparent beyond the model discretized into 24 elements, based on that a full drillstring system with 24 elements are selected for the study. Figures 5.22-5.24 show good convergence of frequency parameter values with the increase number of elements for both rotating and non-rotating drillstring.

The behavior of the frequency parameter with the increase in the speed rate is studied and shown in figures 5.25 and 5.26. The backward frequency decreases while the forward frequency increases, as the speed is increases. The difference between the backward and forward frequencies becomes larger at higher modes.

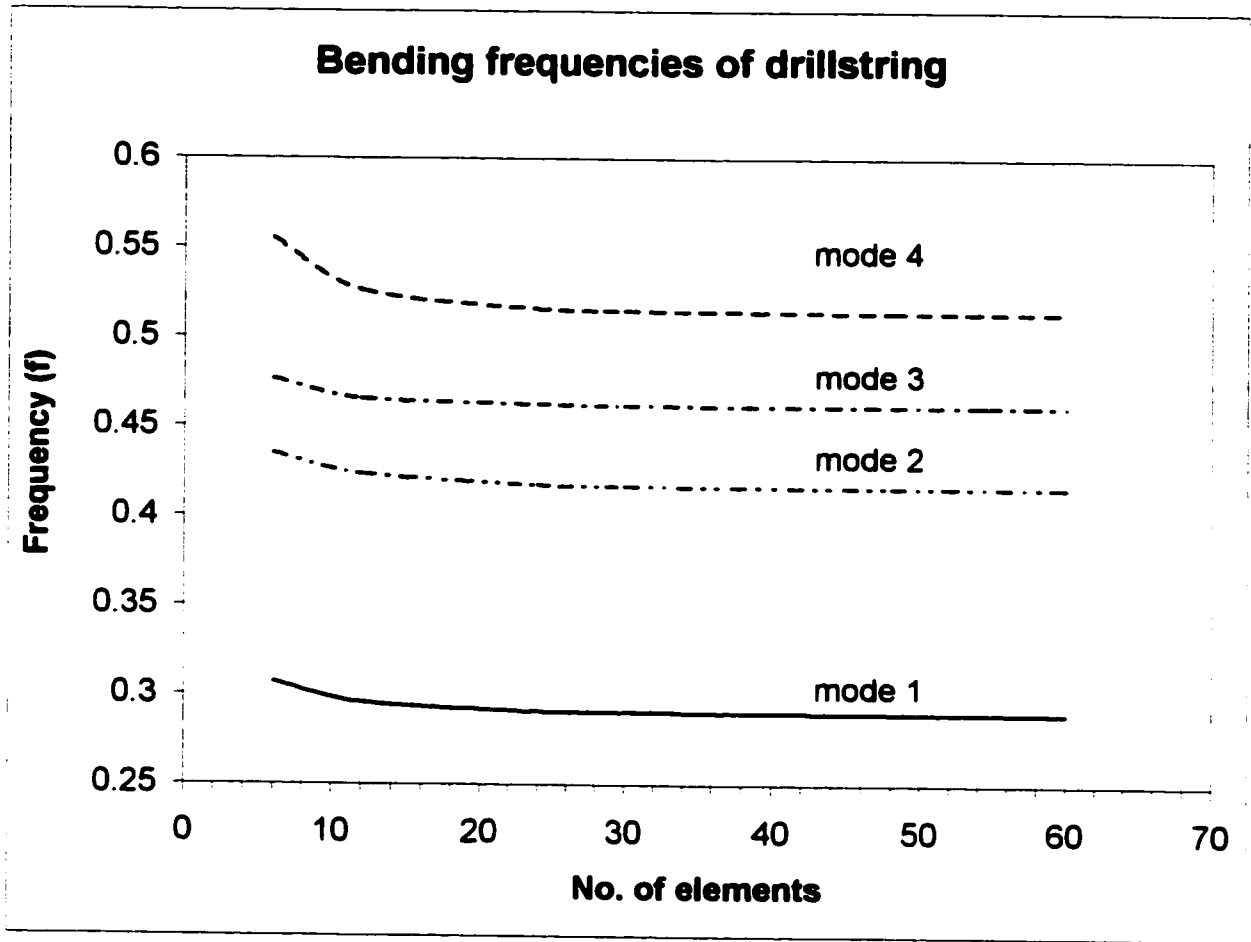


Figure 5.22: No. of elements Vs. frequency for non-rotating drillstring

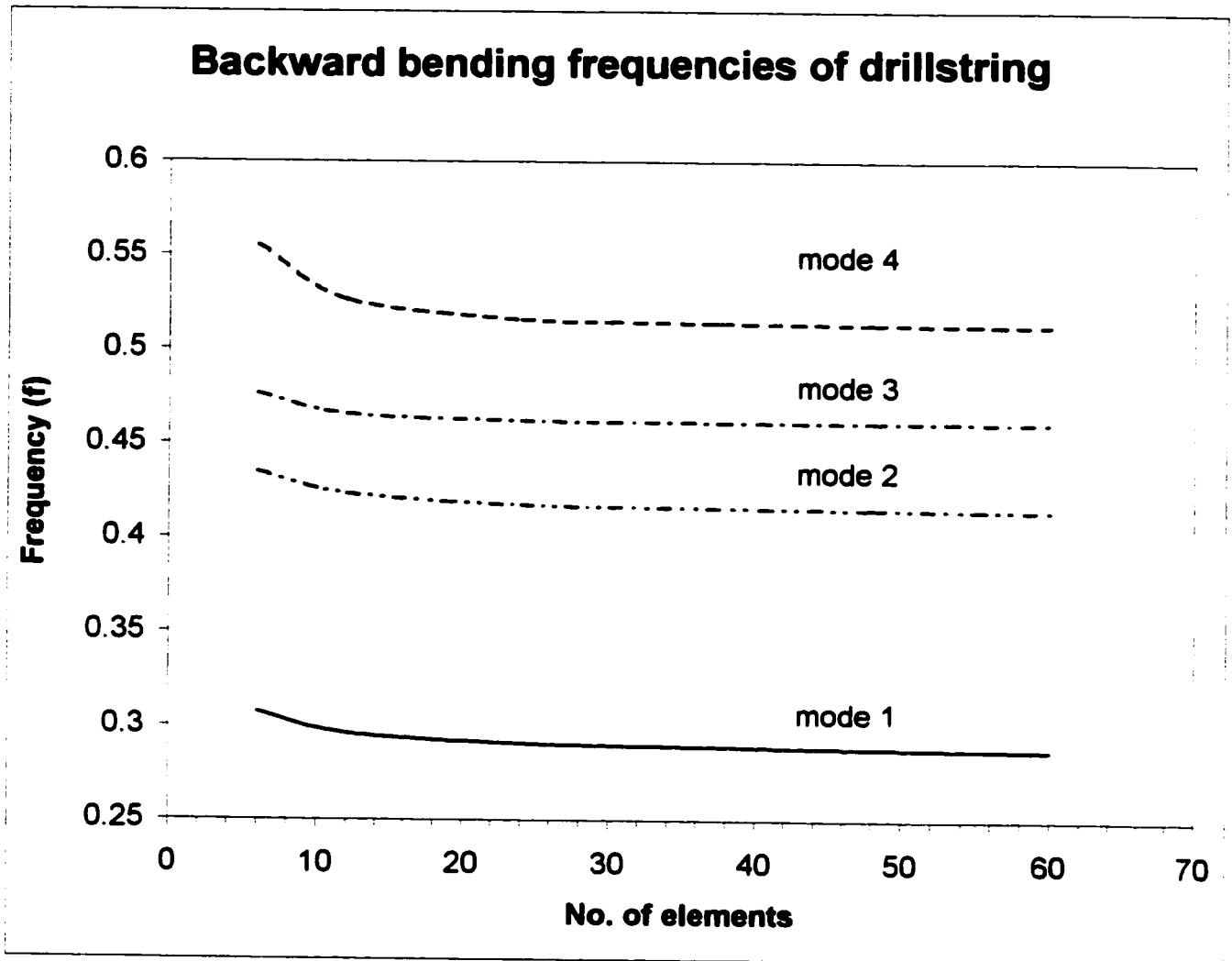


Figure 5.23: No. of elements Vs. frequency for backward bending freq.

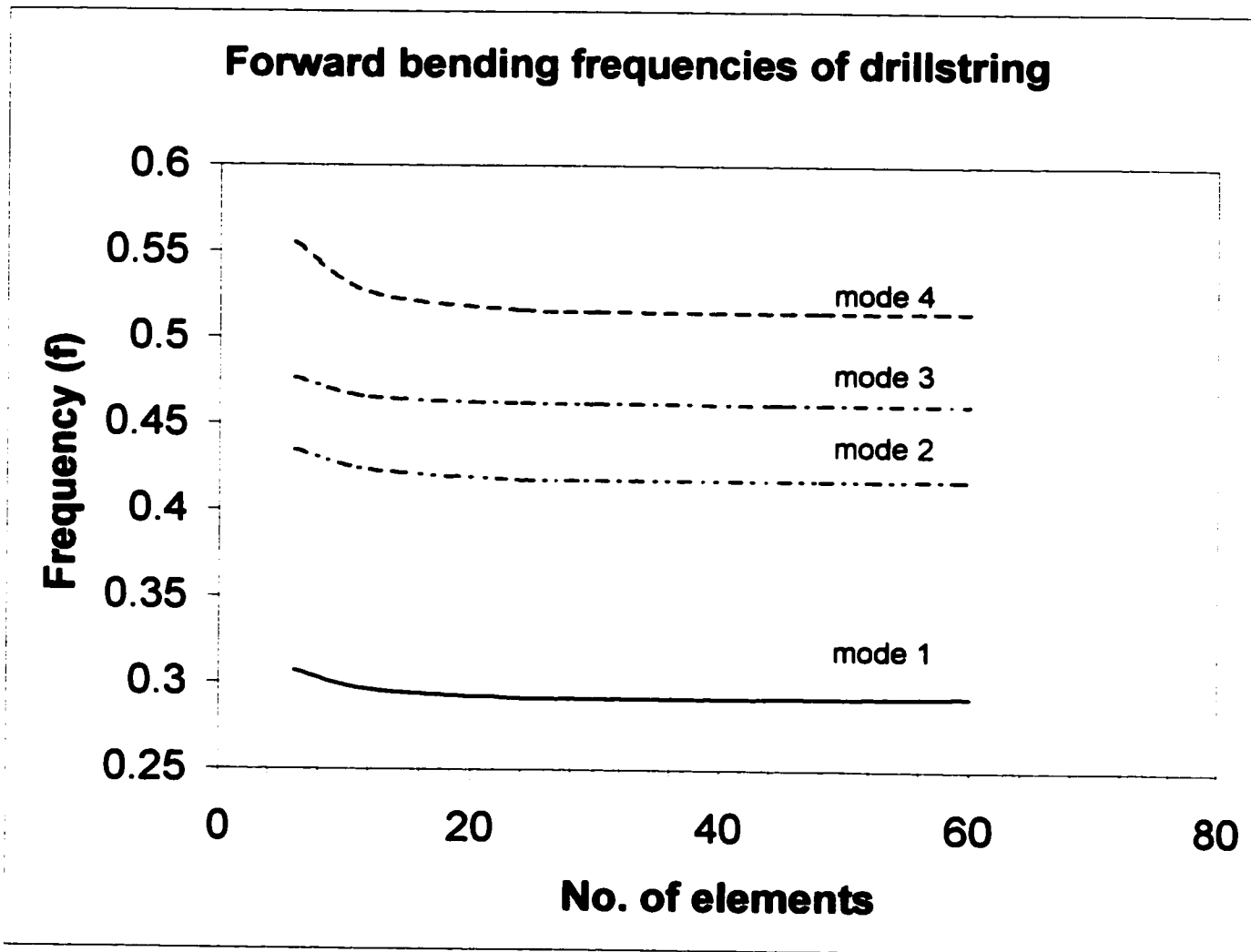


Figure 5.24: No. of elements Vs. frequency for forward bending freq.

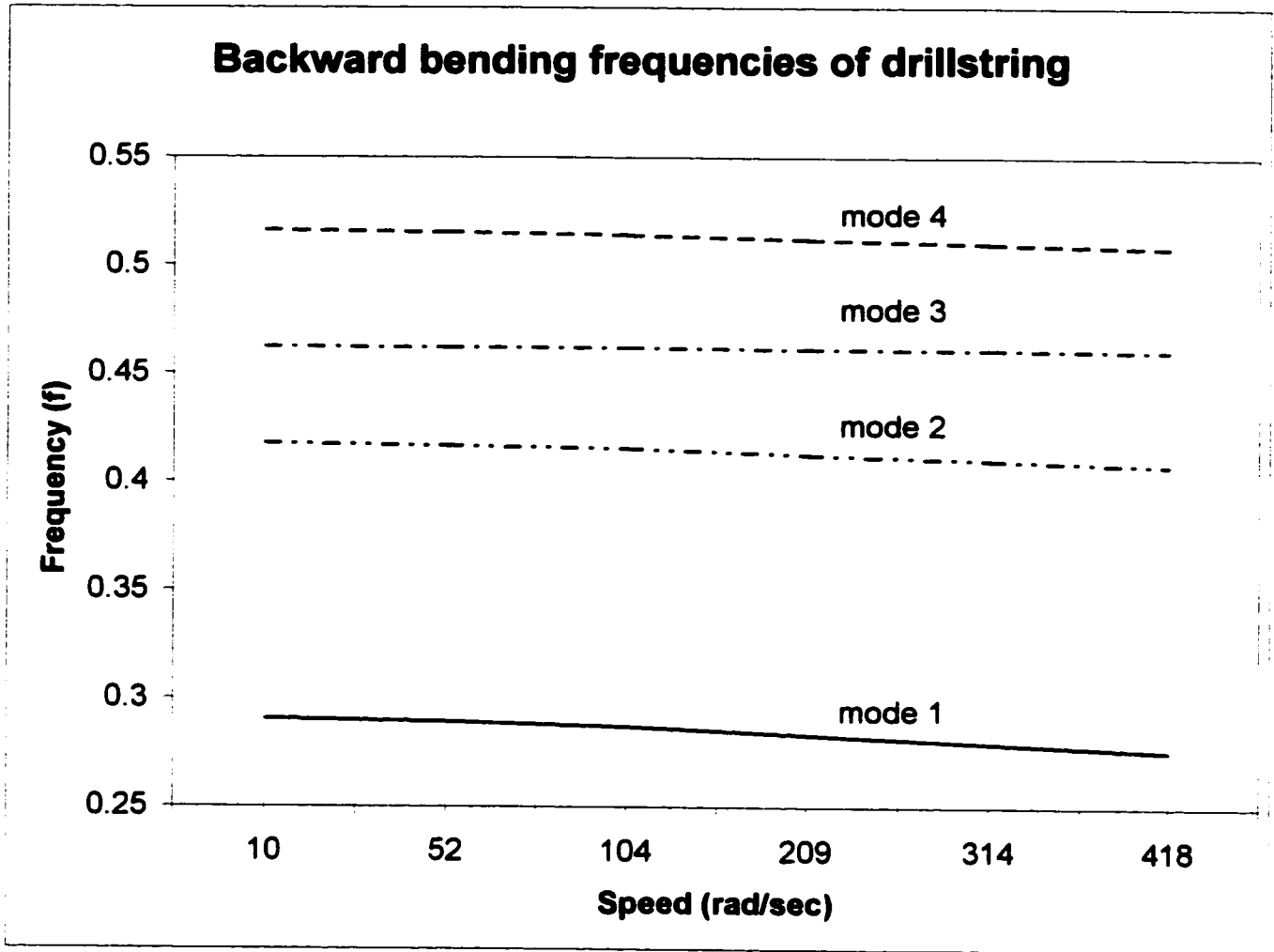


Figure 5.25: Speed Vs. frequency for backward bending frequency

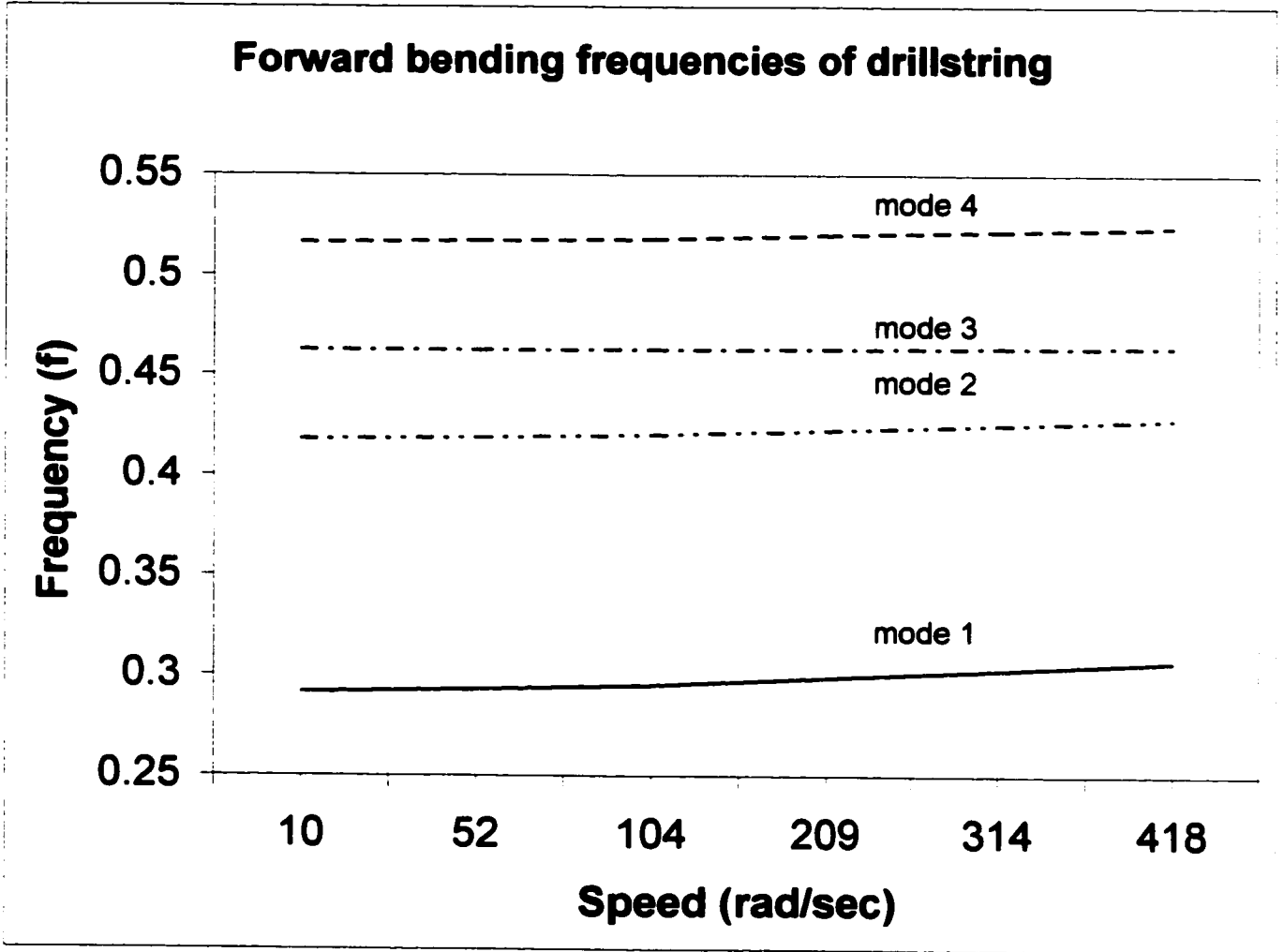


Figure 5.26: Speed Vs. frequency for forward bending frequency

5.3 Transient Response Analysis

The drillstring transient response is obtained by three methods; response to initial displacement, response to initial velocity and response to applied impulsive force.

5.3.1 Response to Initial Displacement

The transient response of the rotating the drillstring due to initial displacement is calculated. The initial displacement field calculated is shown in table 5.26. It is noted, however, that the existing boundary conditions imply zero lateral displacements at the first node, neutral point, and the bit (last node), as shown in figure 2.1. Applying a force at approximately midway of drillpipe and calculating the displacement from the following static deflection equation, we obtained the initial nodal displacements

$$\{y\} = [K]^{-1} \{F\} \quad (5.1)$$

where : $\{y\}$ is the lateral displacement of all nodes

$[K]$ is the global stiffness matrix

$\{F\}$ is the applied force

Because the drillcollar section is short and due to drillcollar thickness compared to drillpipe section, the initial displacement in the drillcollar section is very small and can be neglected.

Figures 5.27-5.29 show the drillstring dynamic response at different nodes for both full-order and reduced-order solutions at rotation speed of 10.47 rad/sec (100 rpm), wherein the reduced-order curve is shown as dashed line while the full-order curve is shown as solid line. All nodes start with the specified deflection in table 5.26 and continue to vary for the rest of the simulation time.

Table 5.27
Nodal lateral initial displacement of drillstring

Node No.	Initial displacement (m)
1	0
2	0.0051
3	0.0109
4	0.0172
5	0.0238
6	0.0309
7	0.0385
8	0.0466
9	0.0554
10	0.0649
11	0.0754
12	0.0868
13	0.0987
14	0.0957
15	0.0912
16	0.0858
17	0.0791
18	0.0705
19	0.0583
20	0.0374
21	0
22	0
23	0
24	0
25	0

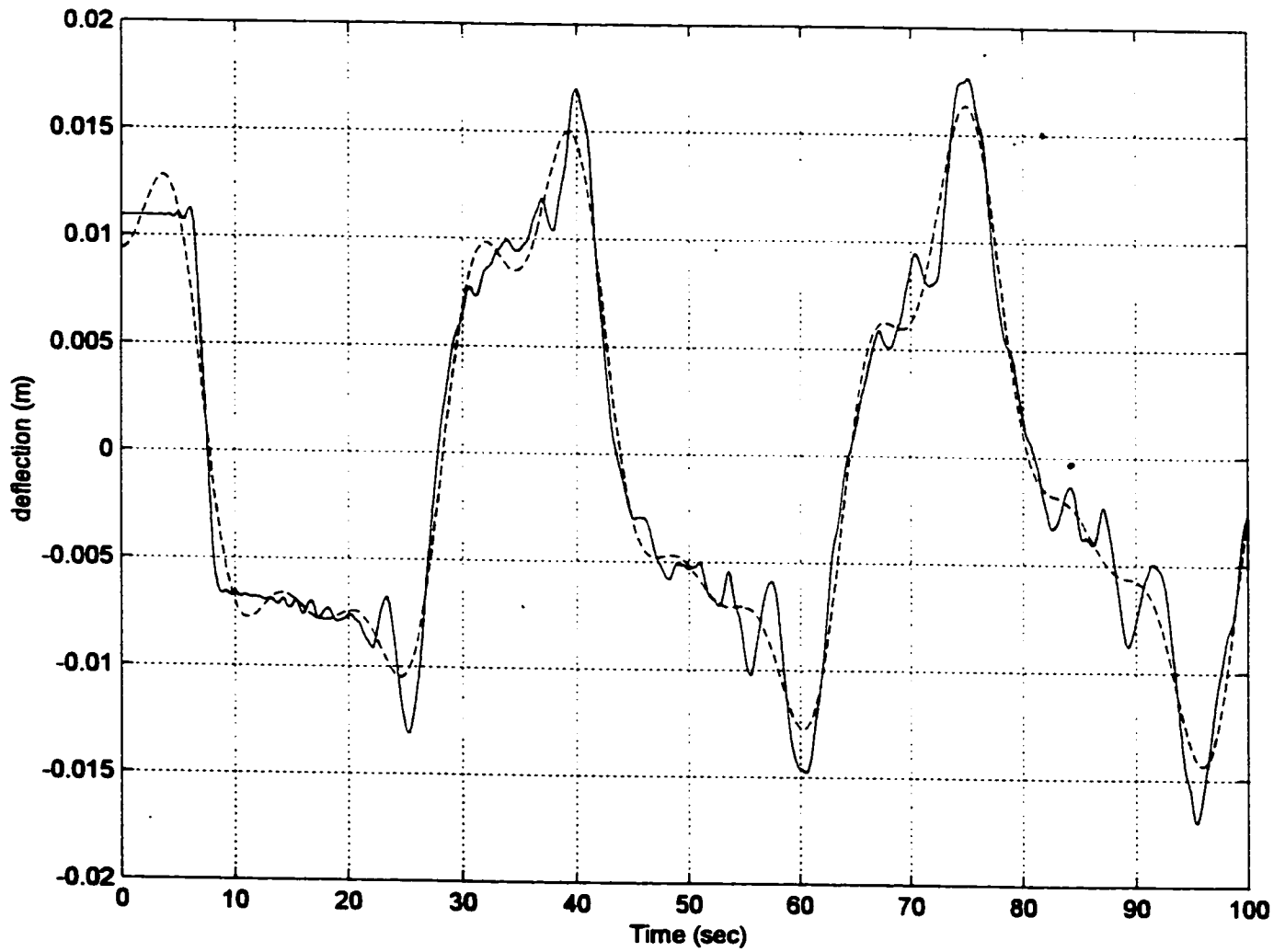
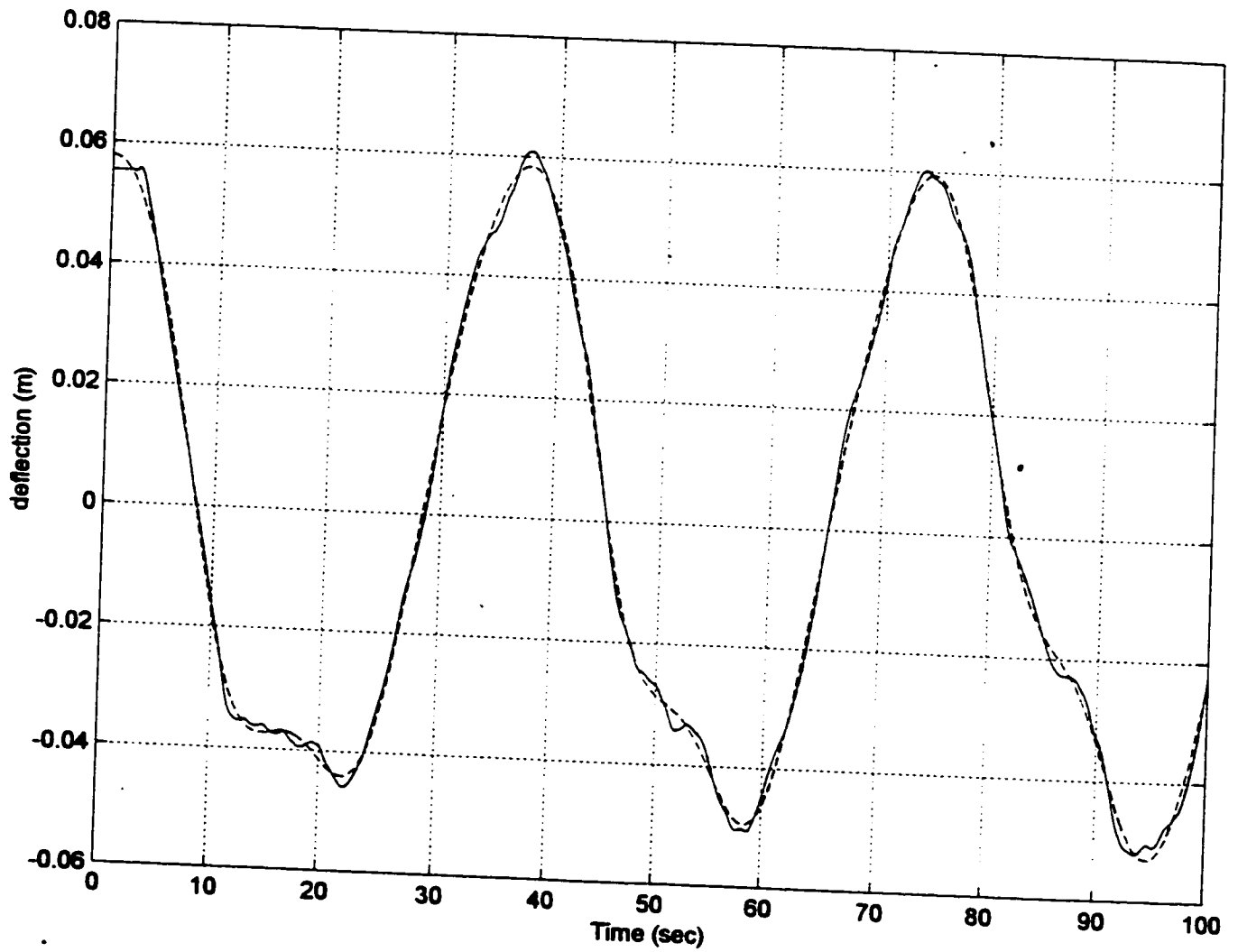


Figure 5.27: Transient response of node 3 due to initial displacement
 (— Full-order, - - - Reduced-order)



14833

Figure 5.28: Transient response of node 9 due to initial displacement
 (— Full-order, ---- Reduced-order)

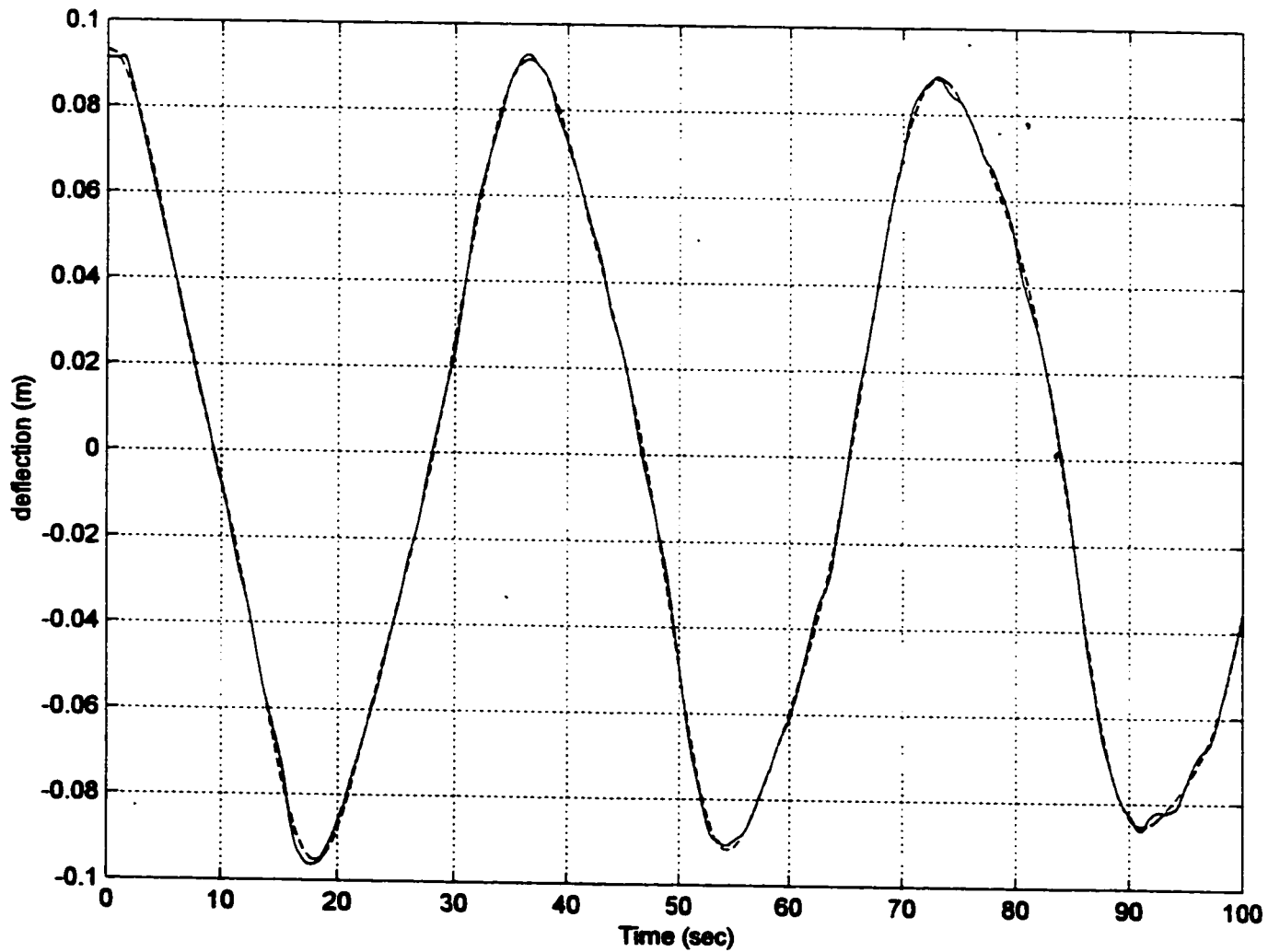


Figure 5.29: Transient response of node 15 due to initial displacement
 (— Full-order, ---- Reduced-order)

The dynamic responses of the same nodes are shown in figures 5.30-5.32 with different rotation speed 104.7 rad/sec (1000 rpm). It can be noticed from the figures that there is a close match between the full-order and reduced-order modules.

5.3.2 Response to Initial Velocity

The transient response for the rotating drillstring due to initial velocity is also calculated. Initial velocity application is essentially equivalent to an impulsive force application. The initial velocity application can be applied at any node along the drillstring. The transient dynamic responses for nodes 3, 9, and 15 are shown in figures 5.33-5.35. When velocity is applied as initial condition, it will excite the higher modes as shown in figures 5.33-5.35. Modal reduction is used in order to compare the reduced-order model (dashed line) with the full-order model (solid line). Two sets of results for the reduced-order model were presented; the first set is for a reduced-order model in terms of the first 5 modes, shown in figures 5.33-5.35, while figures 5.36-5.38 shows the response obtained from a reduced-order model of 10 modes. The more modes included in the reduction scheme the closer the reduced-order solution is to the full-order solution. It is noted that, in this case, including other modes higher than the 10th mode would only result in negligible improvement in the calculated solution.

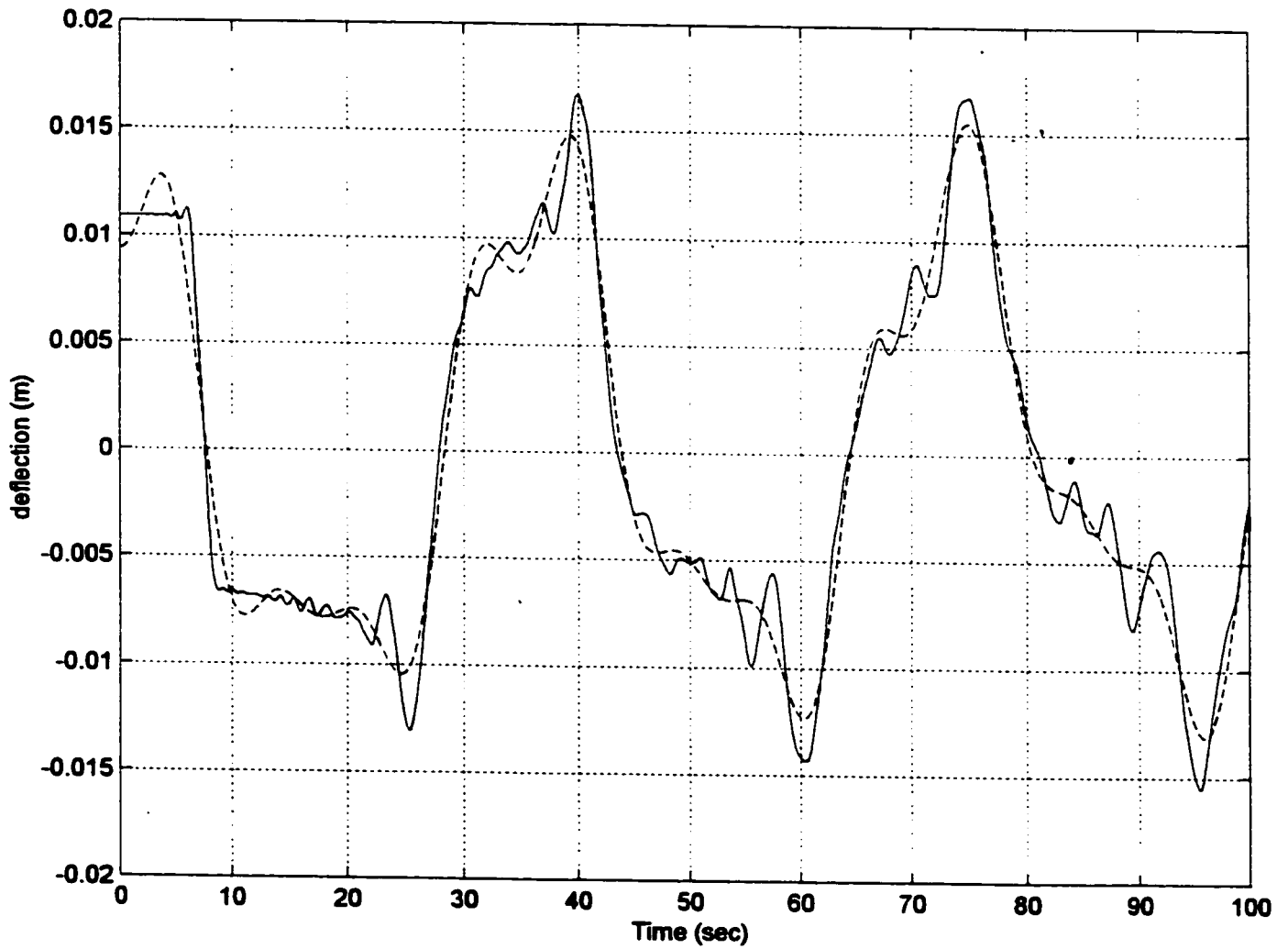


Figure 5.30: Transient response of node 3 due to initial displacement
 (— Full-order, ---- Reduced-order)

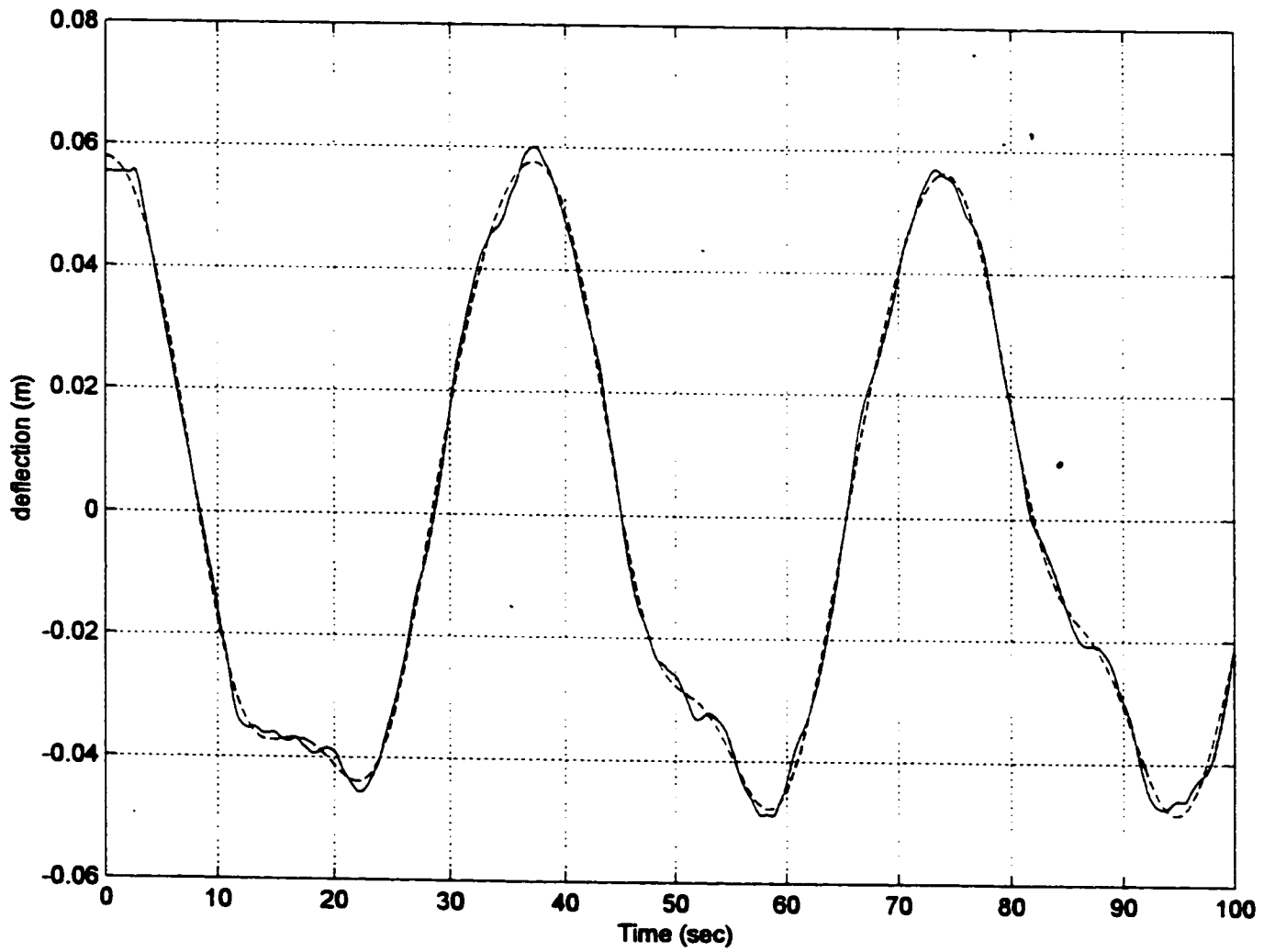


Figure 5.31: Transient response of node 9 due to initial displacement
(— Full-order, ---- Reduced-order)

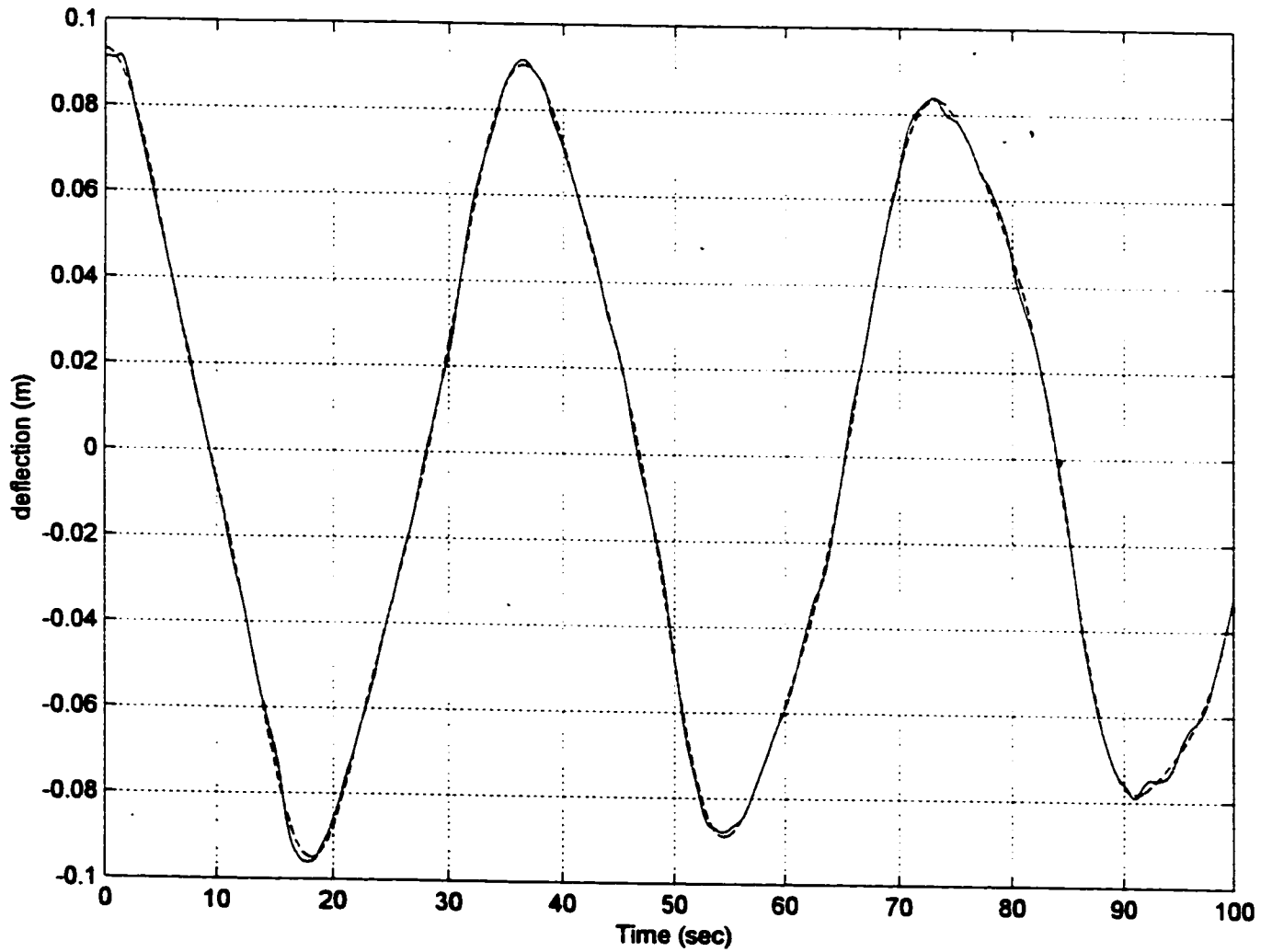


Figure 5.32: Transient response of node 15 due to initial displacement
 (— Full-order, ---- Reduced-order)

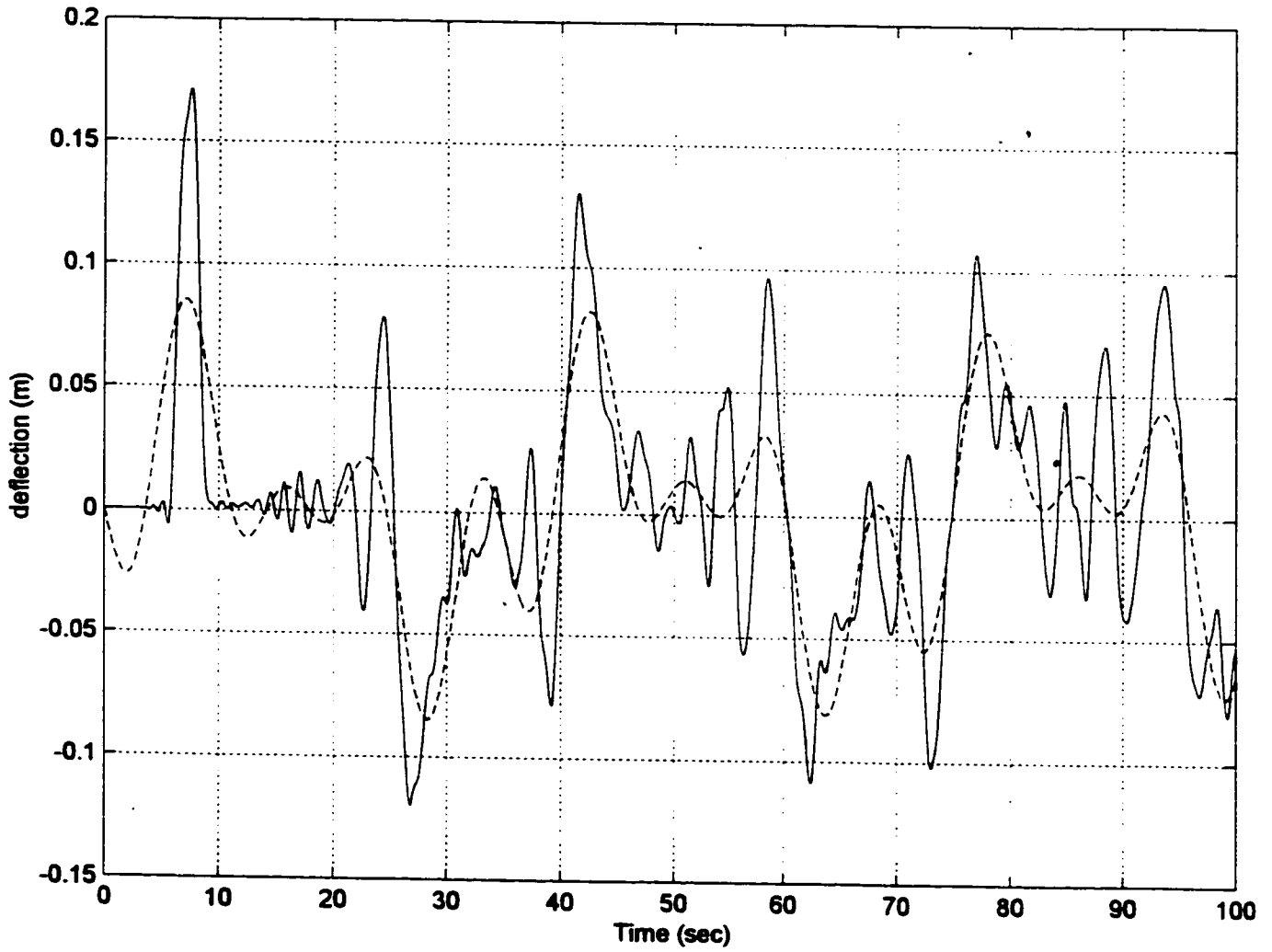


Figure 5.33: Transient response of node 3 due to initial velocity
 (— Full order, - - - - Reduced order)

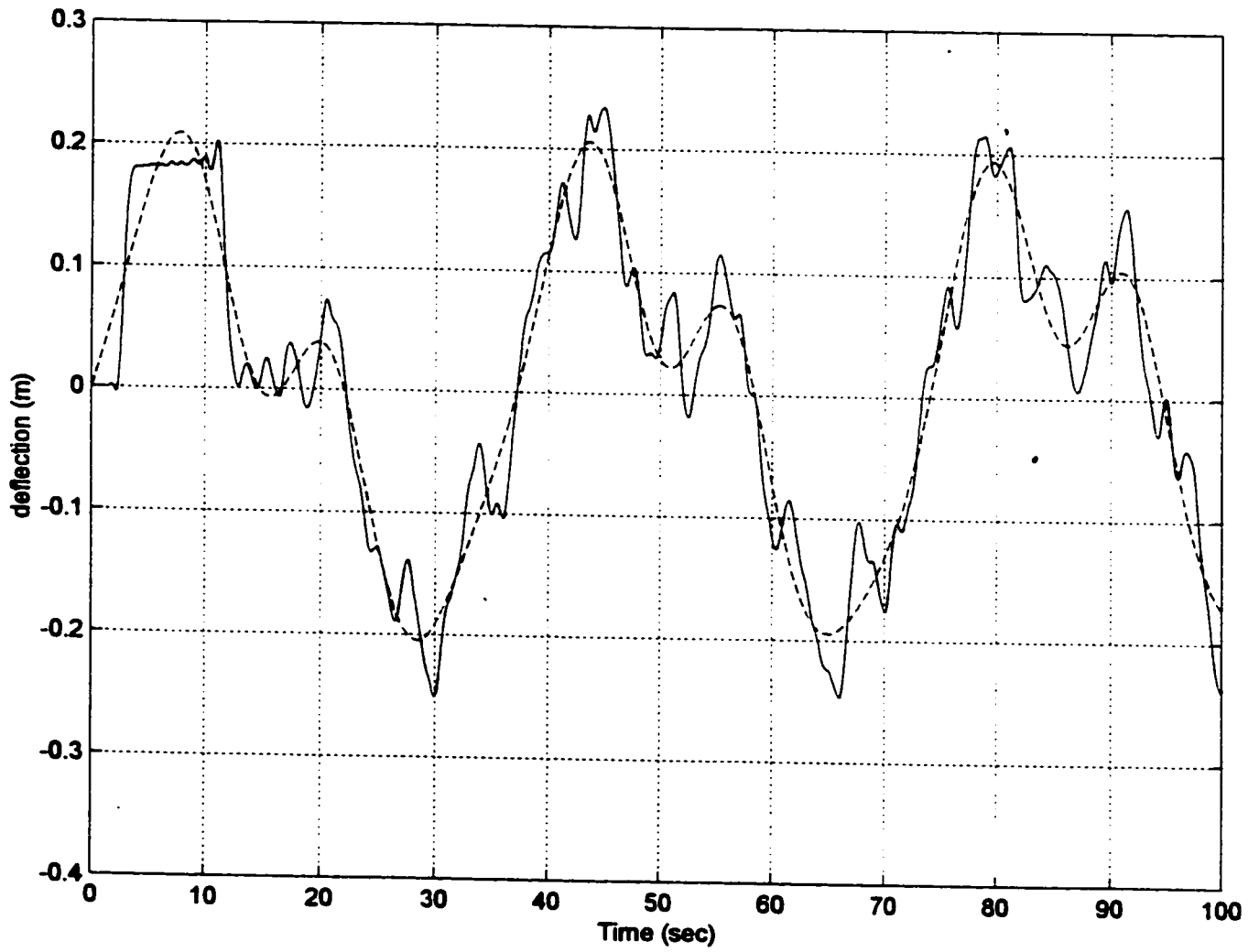


Figure 5.34: Transient response of node 9 due to initial velocity
 (— Full order, - - - Reduced order)

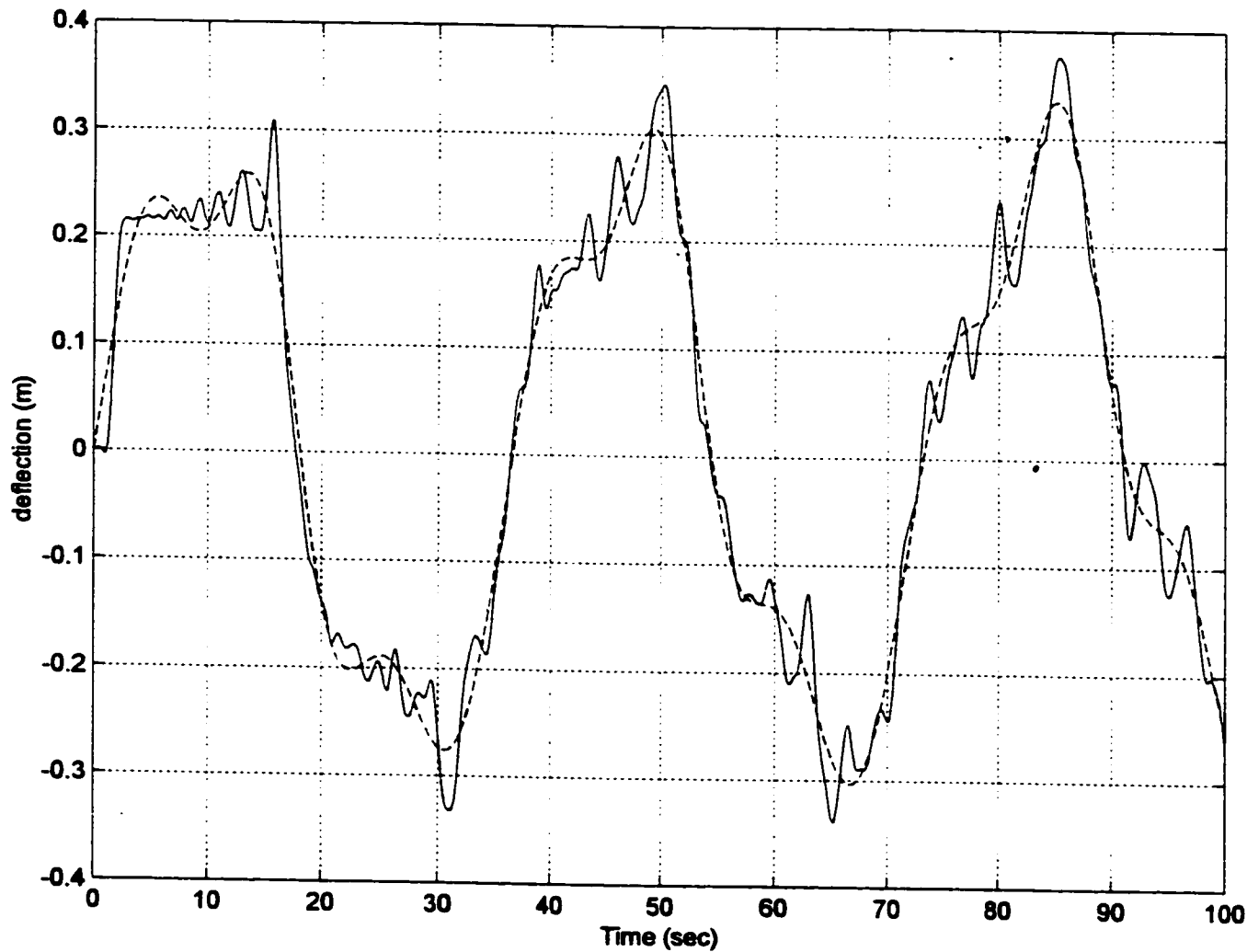


Figure 5.35: Transient response of node 15 due to initial velocity
 (— Full order, ---- Reduced order)

14833

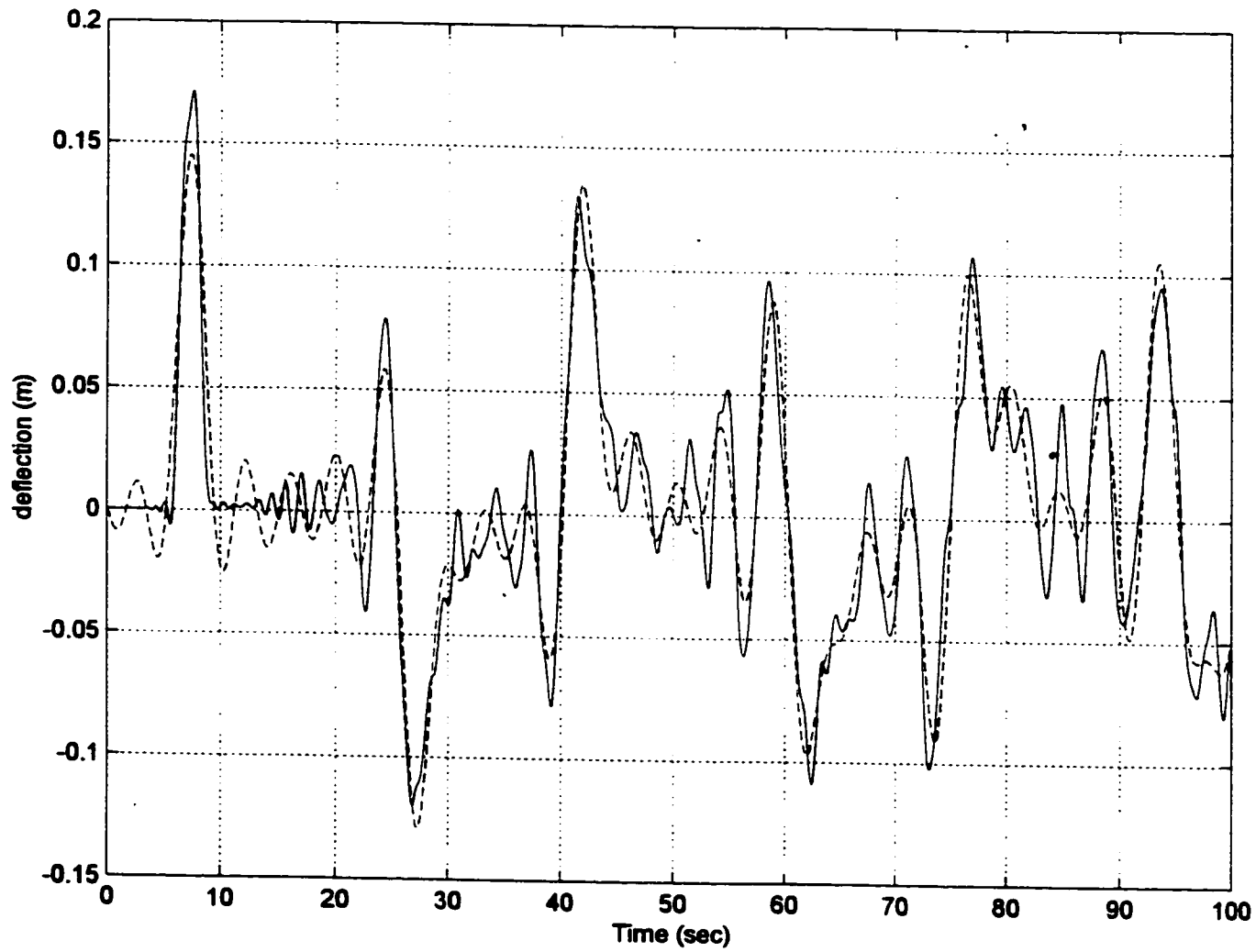


Figure 5.36: Transient response of node 3 due to initial velocity
 (— Full order, ---- Reduced order)

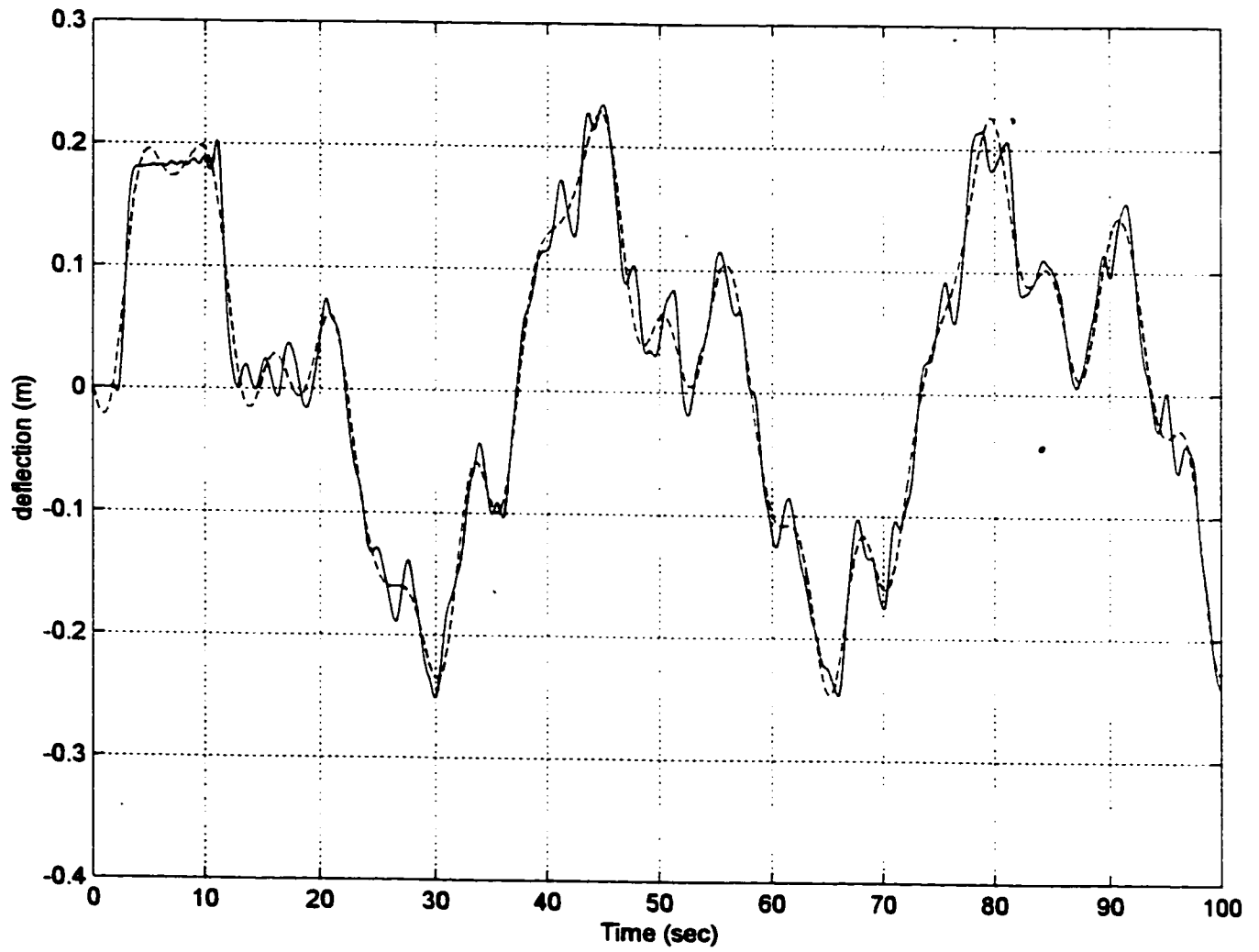


Figure 5.37: Transient response of node 9 due to initial velocity
 (— Full order, ---- Reduced order)

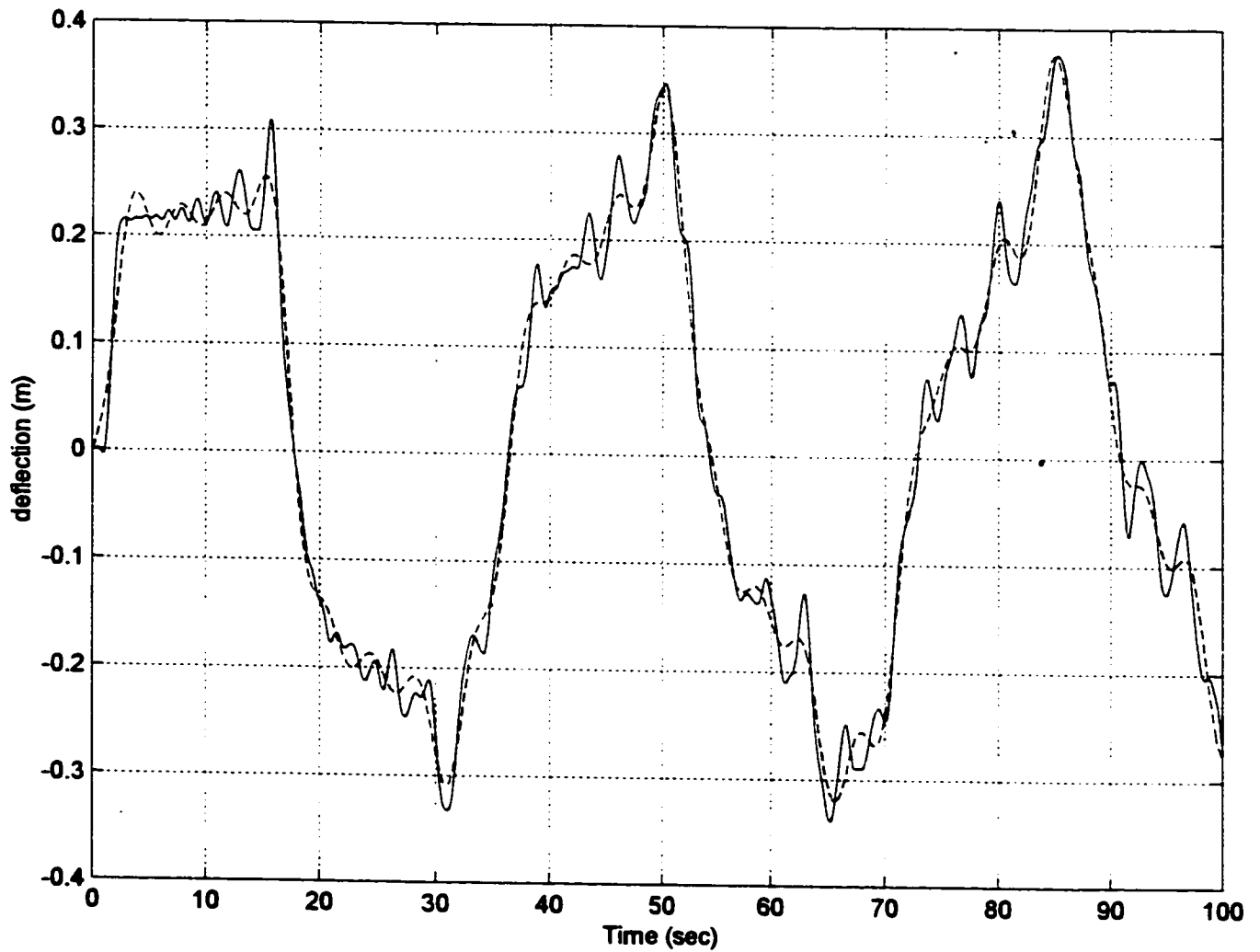


Figure 5.38: Transient response of node 15 due to initial velocity
 (— Full order, ---- Reduced order)

5.3.3 Response to Impulsive Force

The drillstring model developed is capable of applying an impulsive force at any node to simulate the impact between drillstring and borehole wall. An impulsive force is used at node 12 to excite the drillstring. The transient dynamic responses for nodes 3, 9, and 15 are shown in figures 5.39-5.41. When an impulsive force is applied, it will excite the higher modes as shown in figures 5.39-5.41. Modal reduction is used in order to compare the reduced-order model (dashed line) with the full-order model (solid line). Two sets of results for the reduced-order model were presented; the first set is for a reduced-order model in terms of the first 5 modes, shown in figures 5.39-5.41, while figures 5.42-5.44 shows the response obtained from a reduced-order model of 10 modes. The same observation is noticed in this case as the response to initial velocity condition, that is the more modes included in the reduction scheme the closer the reduced-order result are to the full-order solution. It is noted that, in this case, including other modes higher than the 10th mode would only result in negligible improvement in the calculated solution.

Impulsive force can also be applied axially to simulate the axial force from the bit. Figures 5.44-5.46 show the axial transient responses of nodes 3, 9, and 15. The figures show both the full-order solution as well as the reduced-order solution. Modal reduction is used in order to compare the reduced-order model (dashed line) with the full-order model (solid line). Unlike the previous cases, where the first 5 or 10 modes are selected to obtain the reduced-order solution, in this case the axial modes are to be included, which is not necessarily in the first few modes. An excellent agreement between the reduced-order and full-order solutions is observed.

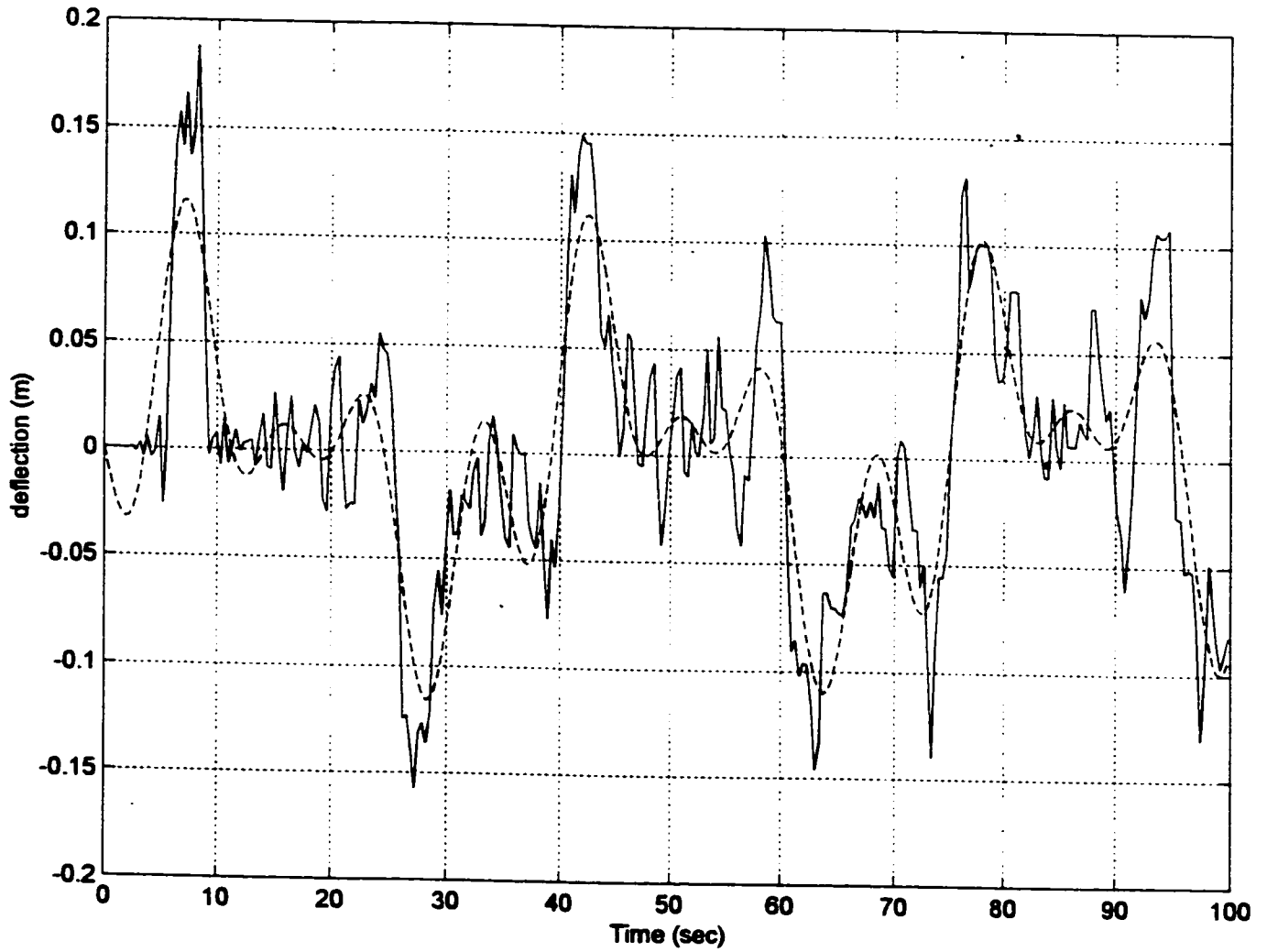


Figure 5.39: Transient response of node 3 due to impulsive force
 (— Full order, ---- Reduced order)

14833

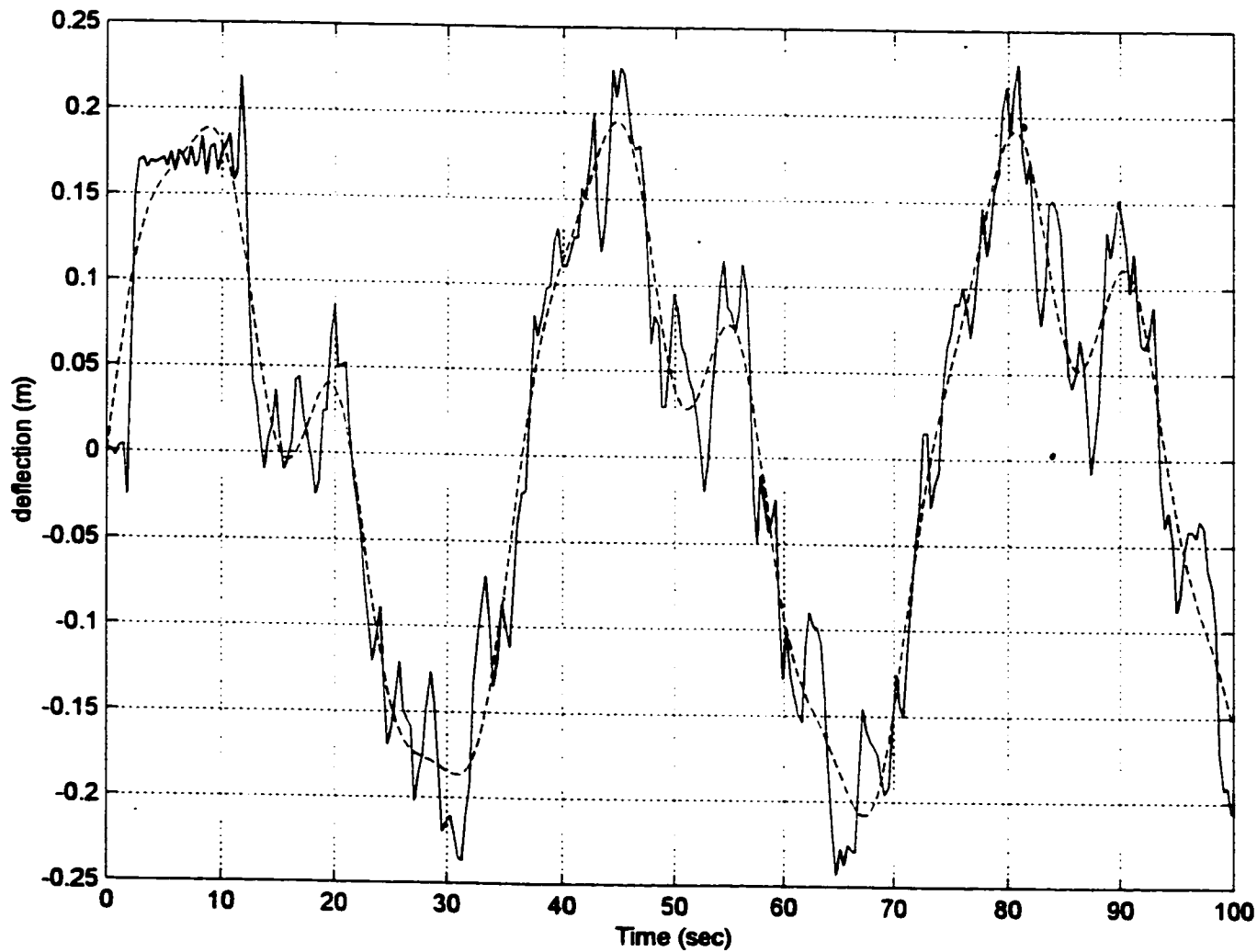


Figure 5.40: Transient response of node 9 due to impulsive force
 (— Full order, ---- Reduced order)

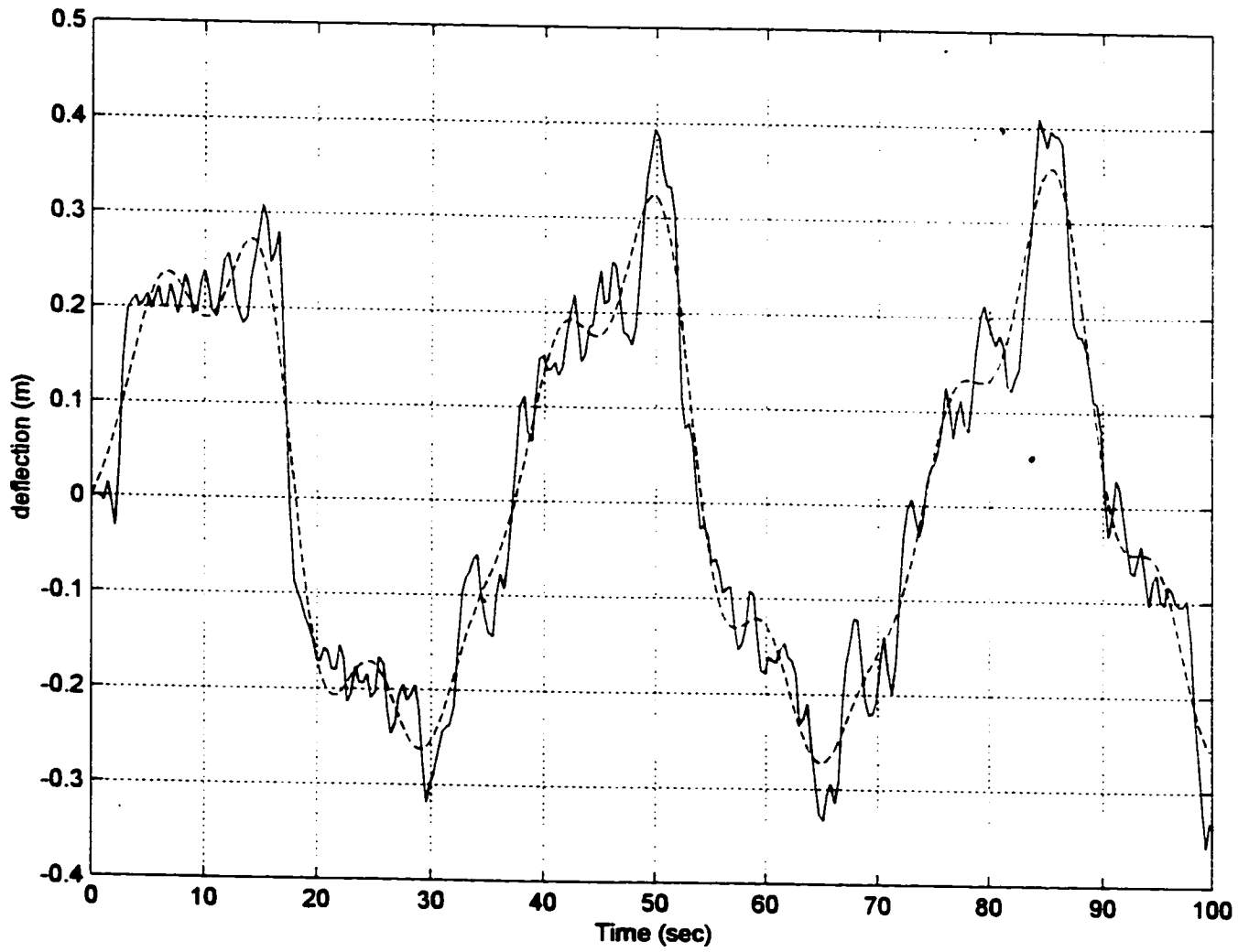


Figure 5.41: Transient response of node 15 due to impulsive force
(— Full order, ---- Reduced order)

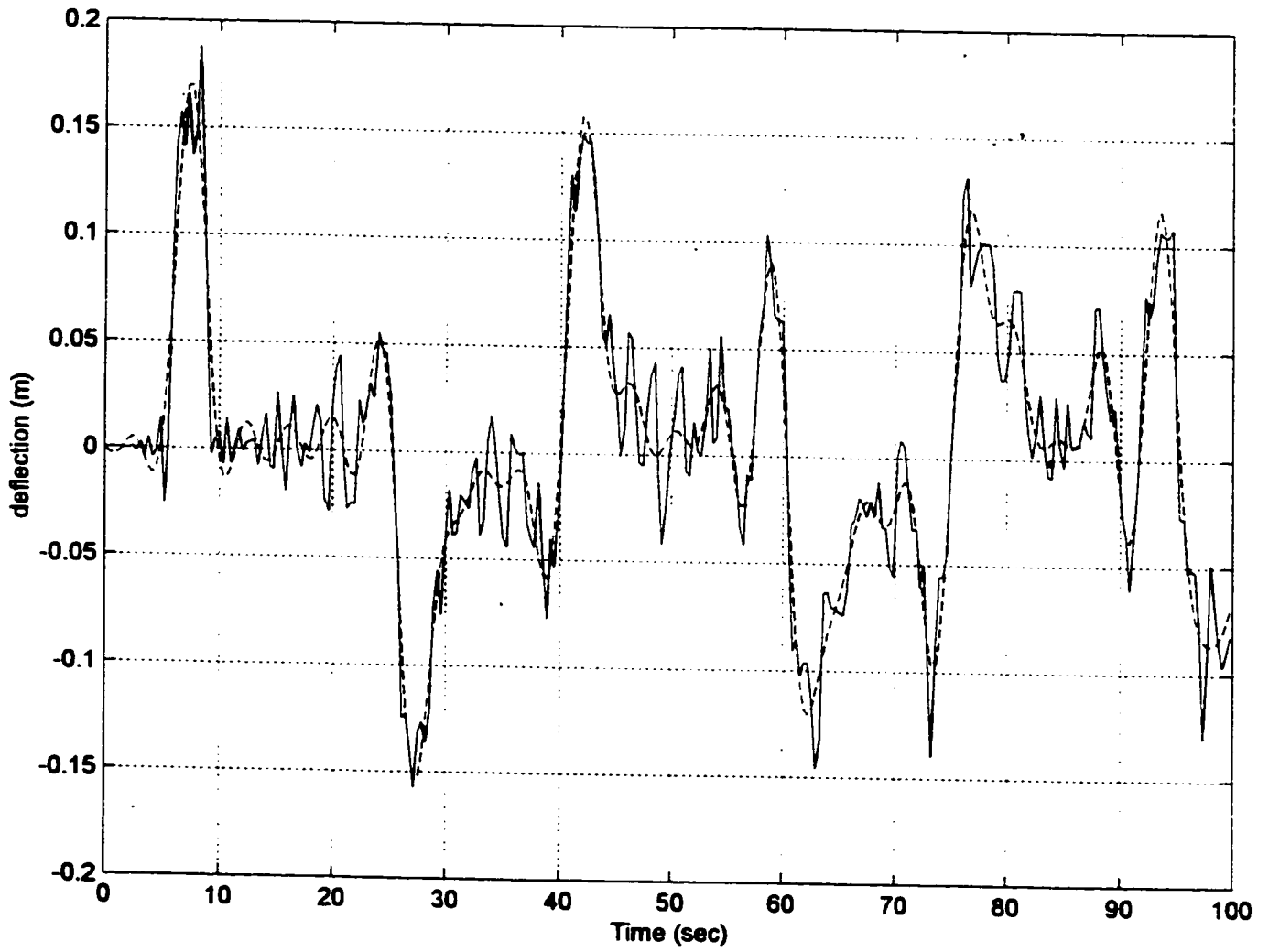
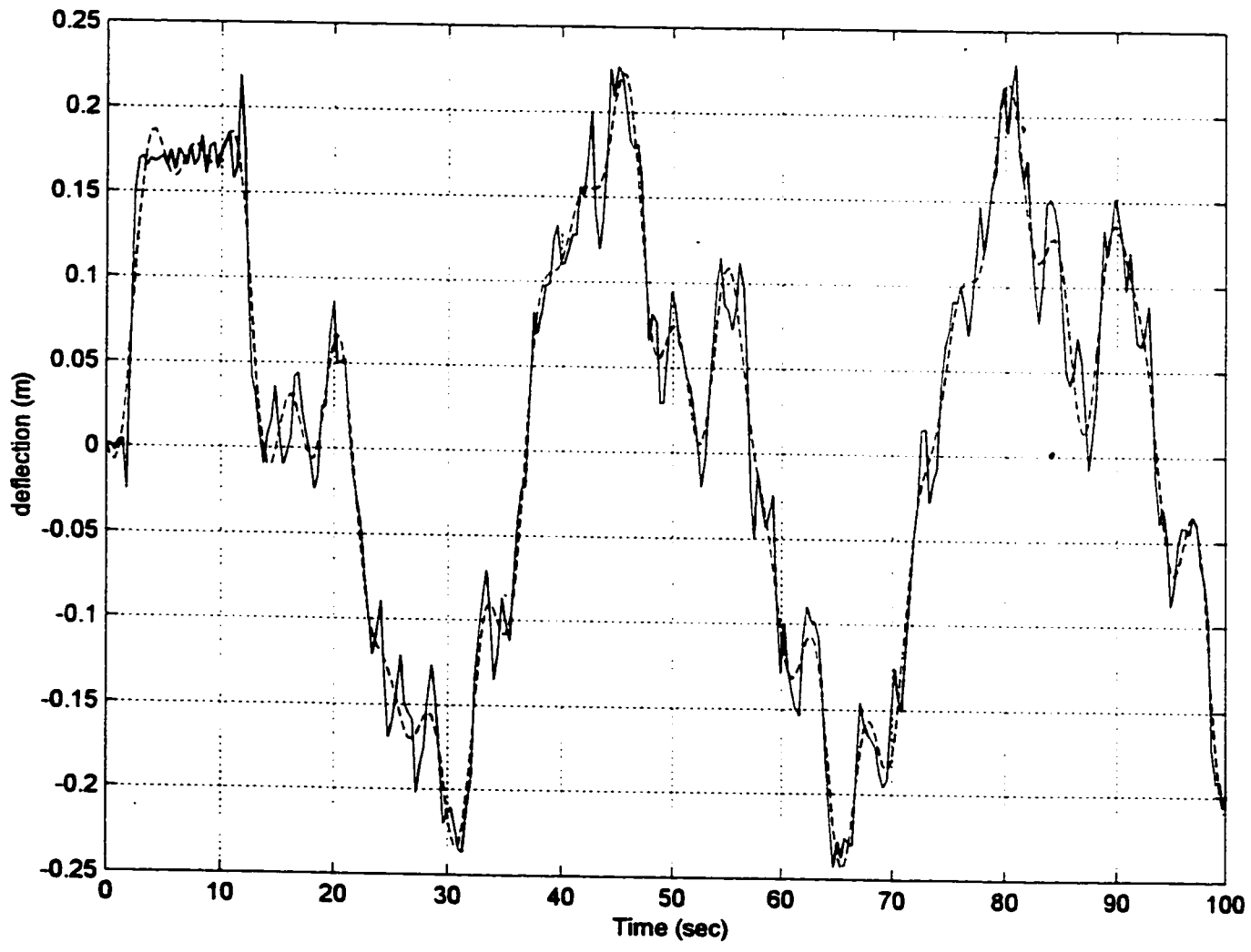


Figure 5.42: Transient response of node 3 due to impulsive force
(— Full order, ---- Reduced order)



14833

Figure 5.43: Transient response of node 9 due to impulsive force
 (— Full order, ---- Reduced order)

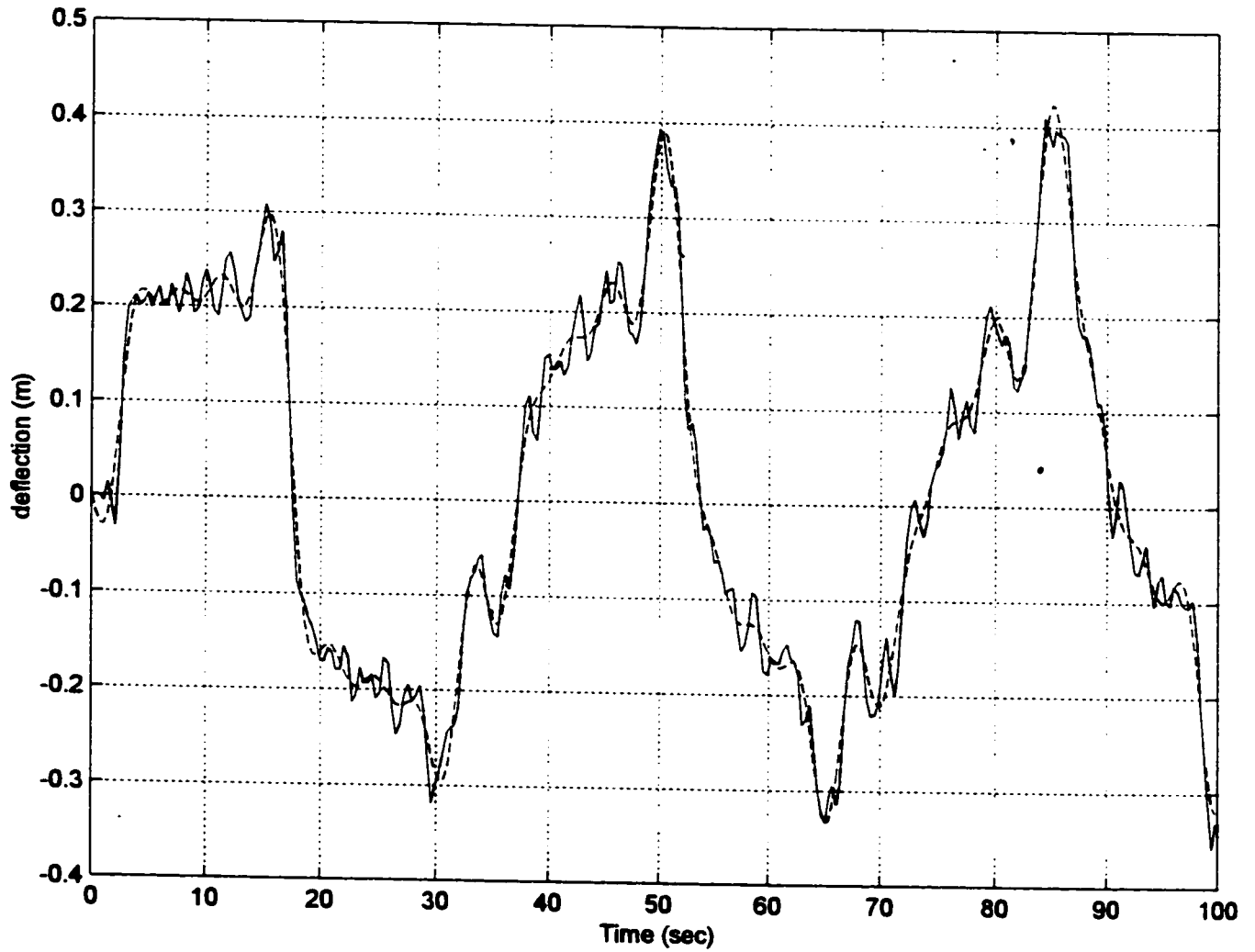


Figure 5.44: Transient response of node 15 due to impulsive force
 (— Full order, ---- Reduced order)

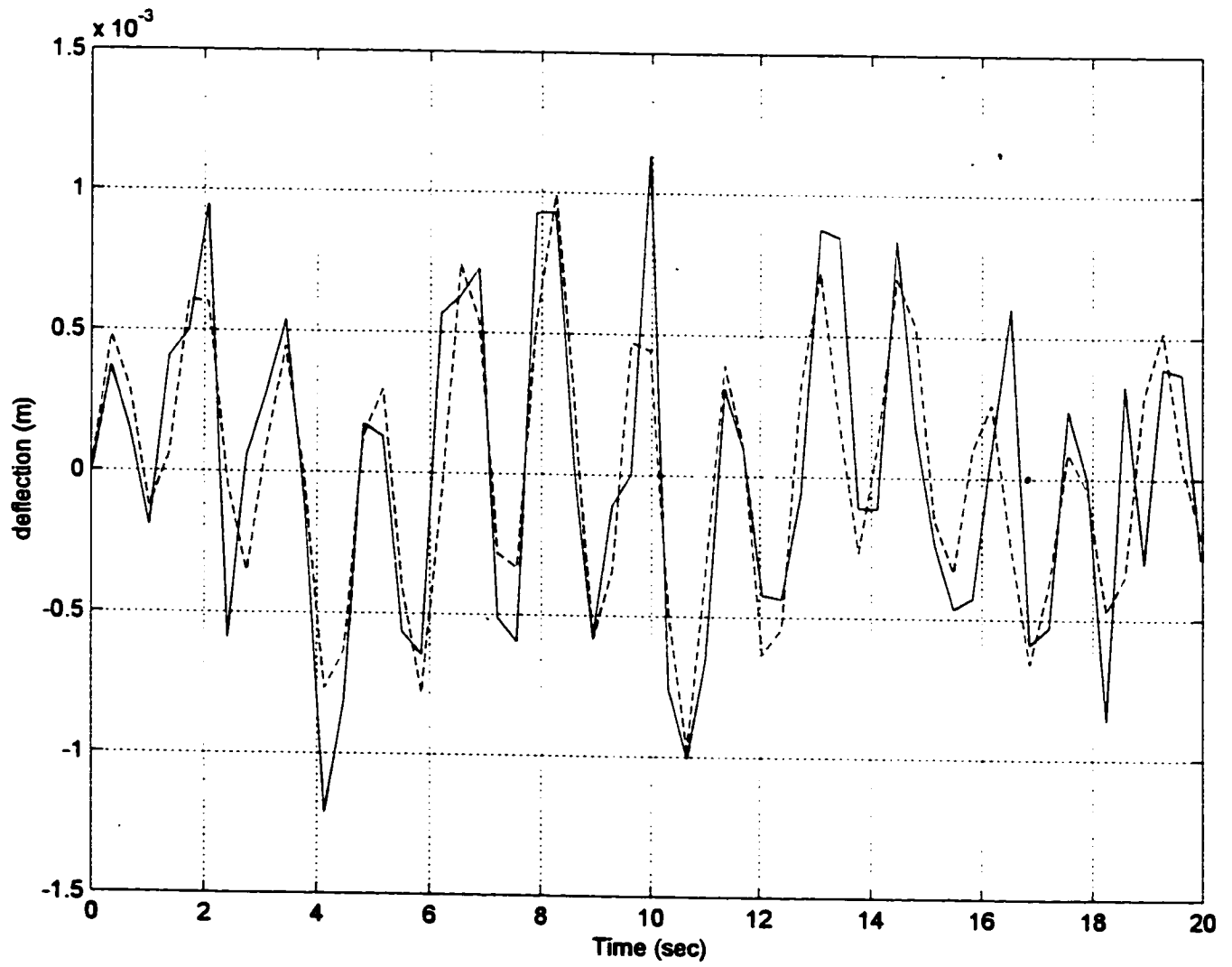


Figure 5.45: Axial transient response of node 3 due to impulsive force
 (— Full order, ---- Reduced order)

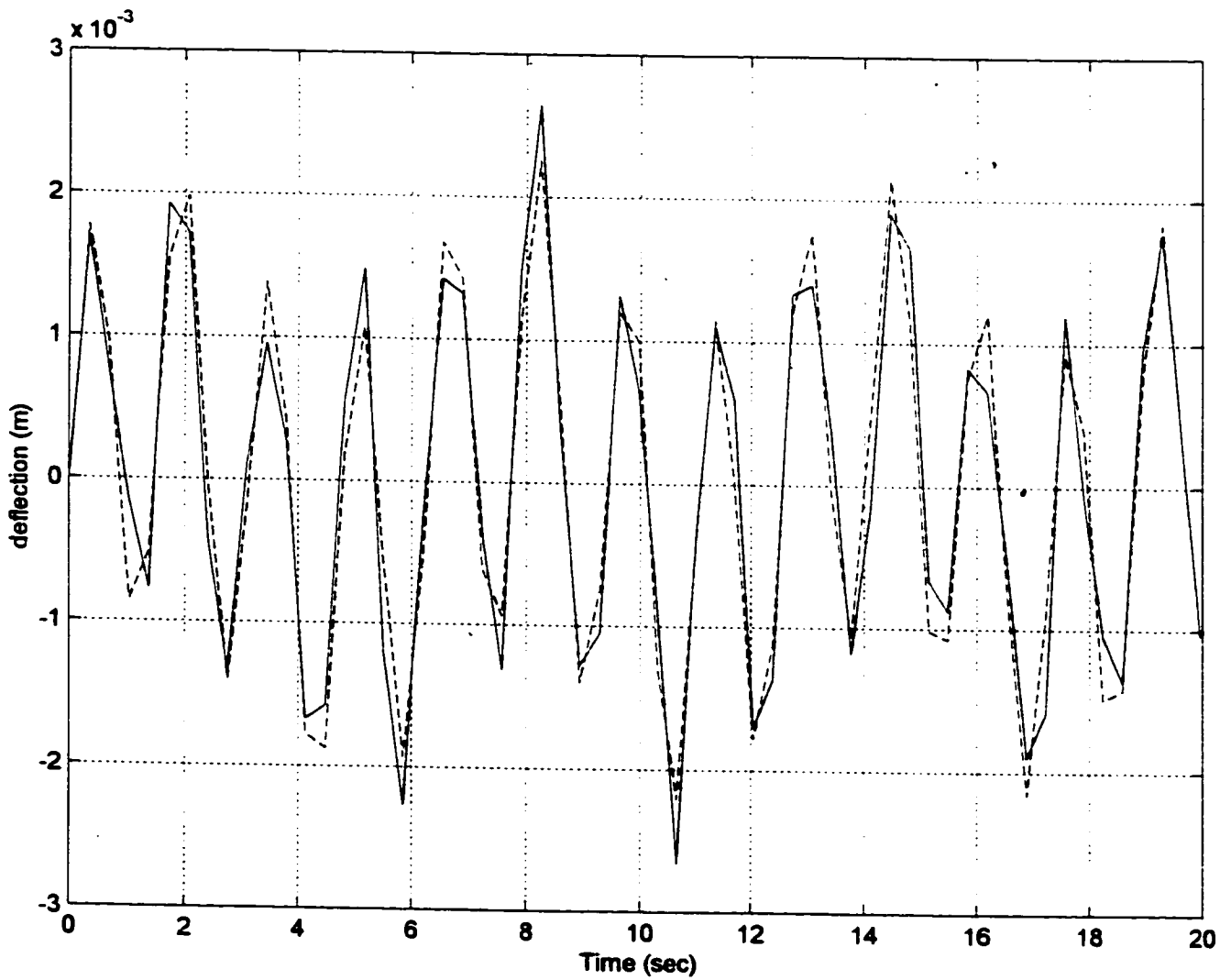


Figure 5.46: Axial transient response of node 9 due to impulsive force
 (— Full order, ---- Reduced order)

14833

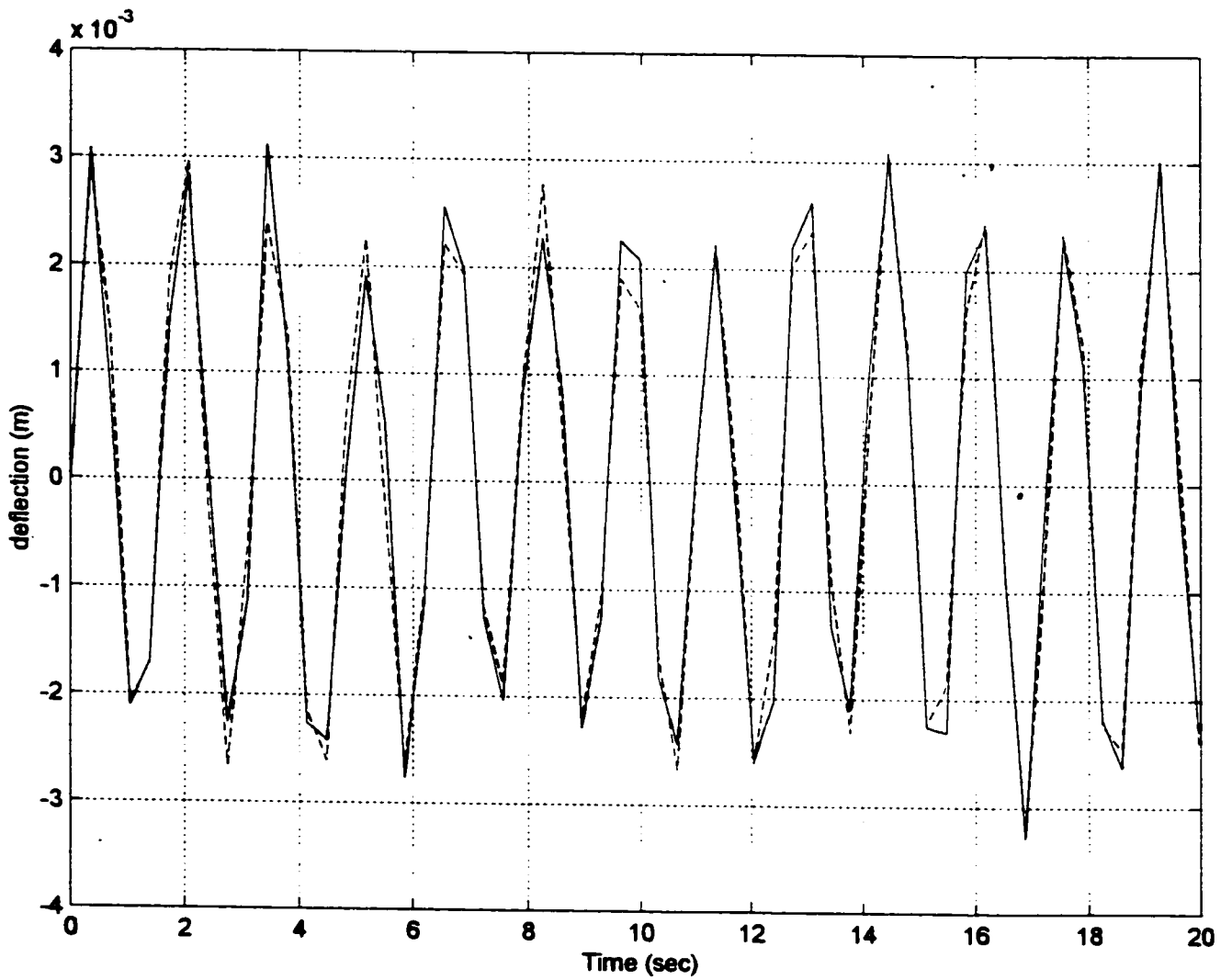


Figure 5.47: Axial transient response of node 15 due to impulsive force
 (— Full order, ---- Reduced order)

CONCLUSIONS

A dynamic model is developed for studying bending, torsional and axial vibration of rotating drillstring using the finite element formulation. The equation of motion of the drillstring is derived using Lagrangian formulation that account for the rotation of the drillstring as well as the stiffening effect due to the gravitational force field. The consistent finite element approach is employed, and explicit expressions of the finite element matrices are derived. The formulation addresses a general drillstring geometry, wherein elements of different lengths and material properties are permitted by the model.

A dynamic analysis computer program is developed using MATLAB[®] code. The program numerically generate and assemble the FEM matrices, construct the equations of motion, solve for the eigenvalues, perform modal transformations, and integrate the equations of motion to obtain time-histories of the drillstring response.

The developed drillstring dynamic analysis and simulation scheme has the following important features:

- a) Generality, which is manifested by the versatility of the FEM in handling large-scale complex structural configurations.
- b) Efficiency, which is achieved by great saving in computational time as implied by using reduced-order model instead of the full-order model of the equations.
- c) The computational scheme is programmed on MATLAB[®] code, thus availing the utilization of the powerful numerical tools associated with this versatile software.

Dynamic simulations are performed, and numerical results are obtained and presented to serve two purposes; (a) to demonstrate the applicability and reliability of the developed dynamic analysis scheme, and (b) to gain more insight into the dynamic behavior of the drillstring system.

The presented numerical results show that backward bending natural frequencies decreases while the forward bending natural frequency increases with increasing drillstring rotation speed. The modal reduction scheme is also shown to obtain very accurate solutions as compared to the full-order model. In addition, the versatility of the developed dynamic model is utilized in studying the dynamic behavior of the drillstring when different values of the location of the neutral point, and when different drillpipe/drillcollar length ratios are considered.

RECOMMENDATIONS FOR FUTURE WORK

Although this investigation lays down the foundation for a general FEM dynamic model of a rotating drillstring, several extensions to this work are foreseen to arrive at a comprehensive dynamic model. The following are some issues for future research work:

1. **Modeling the drilling fluids and the associated inertia and damping effects.**
2. **Including the effect of the dynamic coupling between axial and flexural deformations.**
3. **Modeling of the dynamics of contact impact between the drillstring and the borehole, which is known to give rise to impulsive excitations.**
4. **Modeling of inclined or horizontal drillstring, which will have different forces associated with it.**

APPENDIX (A)

In this appendix, a test case is studied for static and dynamic analysis using the developed computer program and the results are compared with exact solution and with results obtained from ANSYS model. Consider a cantilever Euler-Bernoulli circular beam as in figure (A-1). The beam is 10 m long, 0.1 m in diameter and modeled by ten finite elements. The beam modulus of elasticity and shear modulus are $2.1 \times 10^{11} \text{ N/m}^2$ and 7.69×10^{10} , respectively. A force (p) of 1 N is applied at the free end.

Analytical static deflection solution

$$\sum M_o = px \quad (\text{A-1})$$

$$EI \frac{d^2 y}{dx^2} = px \quad (\text{A-2})$$

Integrating equation (A-2)

$$EI \frac{dy}{dx} = \frac{px^2}{2} + c_1 \quad (\text{A-3})$$

Integrating equation (A-3)

$$EIy = \frac{px^3}{6} + c_1x + c_2 \quad (\text{A-4})$$

Boundary conditions

$$@ x=L \quad y=0,$$

$$x=L \quad dy/dx=0$$

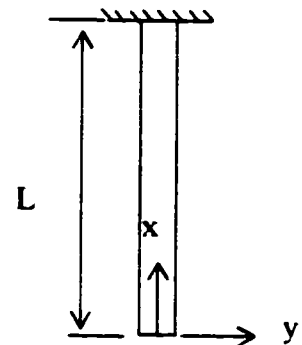


Figure (A-1)

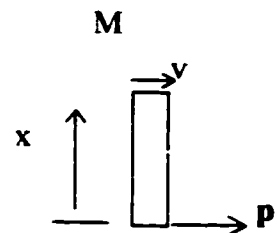


Figure (A-2)

Applying boundary conditions on equations (A-3) and (A-4), the following displacement equation is obtained

$$y = \frac{1}{EI} \left(\frac{px^3}{6} - \frac{pL^2x}{2} + \frac{pL^3}{3} \right) \quad (A-5)$$

The deflection, equation (A-5), for the data given above was calculated and compared with the results obtained through the finite element solution and with a ready made program, ANSYS, the results are shown in table A-1. The three method used are in good agreement, the maximum difference does not exceed 0.1%. The bending natural frequencies, shown in table A-2, were calculated using the developed FEM and compared to the exact solution equation (A-6) and with results from ANSYS; the results are in very good agreement. Likewise, the torsional and axial natural frequencies, shown in table A-3, were calculated using the developed FEM and compared to the exact solution equations (A-7) and (A-8) and with the results from ANSYS; the results are in very good agreement

$$\omega_n = k_n^2 \sqrt{\frac{EI}{\rho A}} \quad (A-6)$$

where $k_n = 1.875, 4.694, 7.855, 10.996, (2n-1)\pi/2$

$$\omega_n = \frac{n\pi}{2l} \sqrt{\frac{G}{\rho}} \quad (A-7)$$

where $n = 1, 3, 5, 7, \dots$

$$\omega_n = \frac{n\pi}{2l} \sqrt{\frac{E}{\rho}} \quad (A-8)$$

where $n = 1, 3, 5, 7, \dots$

Table A-1
Lateral deflections of the test case

x (m)	y(m) Exact	y(m) ANSYS	y(m) Develped FEM
0	0.323345E-03	0.32340E-03	0.323362E-03
1	0.275005E-03	0.27505E-03	0.275020E-03
2	0.227635E-03	0.22767E-03	0.227647E-03
3	0.182205E-03	0.18224E-03	0.182215E-03
4	0.139685E-03	0.13971E-03	0.139693E-03
5	0.101045E-03	0.10107E-03	0.101051E-03
6	0.672558E-04	0.67273E-04	0.672594E-04
7	0.392864E-04	0.39298E-04	0.392885E-04
8	0.181073E-04	0.18115E-04	0.181083E-04
9	0.468851E-05	0.46921E-05	0.468876E-05
10	0	0	0

Table A-2

Natural bending frequencies of the test case

		f_1 (rad/sec)	f_2 (rad/sec)	f_3 (rad/sec)	f_4 (rad/sec)
Non-rotating Shaft	Exact	4.5458	28.491	79.782	156.34
	ANSYS	4.5459	28.474	79.677	156.06
	Developed FEM	4.5463	28.4897	79.7785	156.4111
	Developed FEM (Compression)	4.7127	28.6382	79.9317	156.5722
	Developed FEM (Tension)	4.8605	28.8949	80.0996	156.6978
Rotating Shaft (30 RPM)	Developed FEM (B) (Compression) (F)	4.3093	28.2609	79.5727	156.2362
	Developed FEM (B) (Tension) (F)	4.6231	28.6660	79.8938	156.5229
Rotating Shaft (100 RPM)	Developed FEM (B) (Compression) (F)	3.8065	27.7343	79.0945	155.8287
		5.4300	29.2657	80.4685	156.9957
	Developed FEM (B) (Tension) (F)	4.1161	28.1392	79.4156	156.1155
		5.7395	29.6709	80.7896	157.2824

Table A-3

Torsion/Axial natural frequencies of the test case

		f_1 (rad/sec)	f_2 (rad/sec)	f_3 (rad/sec)	f_4 (rad/sec)
Torsional	Developed FEM	492	1489	2522	3617
	ANSYS	492	1489	2522	3616.3
	Exact	491.6	1475	2458	3442
Axial	Developed FEM	813	2460	4167	5976
	ANSYS	813	2460	4167	5976
	Exact	812.4	2437.3	4062.2	5687

References

1. Bourgoyne, A. T., Chenevert, M. E., Millheim, K. K. and Young, F. S., **Applied Drilling Engineering**, Society of Petroleum Engineers. Richardson, TX 1986.
2. Besaisow, A. A. and Payne, M. L., **A Study of Excitation Mechanisms and Resonances Inducing BHA vibrations**, Society of Petroleum Engineers, October 1986.
3. Fischer, F. J., **Analysis of Drillstrings in Curved Boreholes**, Society of Petroleum Engineers, October 1974.
4. Walker, B. H. and Friedman, M. B., **Three Dimensional Force and Deflection Analysis of a Variable Cross-section Drillstring**, Transactions of the ASME, Journal of Pressure Vessel Technology, May 1977, pp. 363-373.
5. Millheim, K. and Jordan, S., **Bottom-Hole Assembly Analysis Using the Finite-Element Method**, Society of Petroleum Engineers, February 1978.
6. Chandra, U., **Basic Concepts in BHA Analysis for Directional Drilling**, Society of Petroleum Engineers, October 1986.
7. Vandiver, J. K., Nicholson, J. W. and Shyu, R. J., **Case Studies of the Bending Vibration and Whirling Motion of Drill Collars**, Society of Petroleum Engineers, **Drilling Engineering**, vol. 5, 1990, pp. 282-290.
8. Jansen, J. D., **Whirl and Chaotic Motion of Stabilized Drill Collars**, Society of Petroleum Engineers, **Drilling Engineering**, vol. 7, 1992, pp. 107-114.

9. Brett, J. F., The Genesis of Torsional Drillstring Vibration, Society of Petroleum Engineers, *Drilling Engineering*, vol. 7, 1992, pp. 168-174.
10. Richard, T. and Detounay, E., Stick-slip vibrations of PDC bits, *Pacific Rocks 2000*, Girard, Liebman, Breeds & Doe (eds).
11. Halsey, G. W., Killingstad, A., Aarrestad, T.V. and Lysne, D., Drillstring torsional vibrations: Comparison between theory and experiment on a full-scale research drilling rig, Society of Petroleum Engineers, 1986.
12. Close, D. A., Owens, S. C. and MacPherson, J. D., Measurement of BHA Vibration Using MWD, Society of Petroleum Engineers, March 1988.
13. Clayer, F., Vandiver, J. K., and Lee, H. Y., The Effect of Surface and Downhole Boundary Conditions on the Vibration of Drillstrings, Society of Petroleum Engineers, September 1990, .
14. Axisa, F. and Antunnes, J., Flexural Vibrations of Rotors Immersed in Dense Fluids, third international symposium on transport phenomena and dynamics of rotating machinery, Honolulu, Hawaii, April 1990.
15. Dunayevsky, V. A., Abbassian, F., and Judzis, A., Dynamic Stability of Drillstrings Under Fluctuating Weight on Bit, Society of Petroleum Engineers *Drilling & Completion* vol. 8, June 1993, pp. 84-92.
16. Yigit, A. S. and Christoforou, A. P., Coupled Axial and Transverse Vibrations of Oilwell Drillstrings, *Journal of Sound and Vibration*, vol. 195, no. 4, 1996, pp. 617-627.

17. Christoforou, A. P. and Yigit, A. S., Dynamic Modeling of Rotating Drillstrings with Borehole Interactions, *Journal of Sound and Vibration*, vol. 206, no. 9, 1997, pp. 243-260.
18. Berlioz, A., Hogopian, J. D., Dufour, R. and Draoui, Dynamic behavior of a drillstring: Experimental investigation of lateral instabilities, *Transaction of the American Society of Mechanical Engineers, Journal of Vibration and Acoustics*, vol. 118, 1996, pp. 292-298.
19. Dykstra, M. W., Chen, D. C., Warren, T. M. and Azar, J. J., Drillstring Component Mass Imbalance: A Major Source of Downhole Vibrations, *Society of Petroleum Engineers, Drilling & completion*, December 1996.
20. Abbassian, F. and Dunayevsky, V. A., Application of Stability Approach to Torsional and Lateral Bit Dynamics, *Society of Petroleum Engineers Drilling & Completion*, June 1998, pp. 99-107.
21. Heisig, G. and Neubert, M., Lateral Drillstring Vibrations in Extended-Reach Wells, *Society of Petroleum Engineers*, February 2000.
22. Challamel, N., Sellami, H., Chenevez, E. and Gossuin, L., A Stick-slip Analysis Based on Rock/Bit Interaction: Theoretical and Experimental Contribution, *Society of Petroleum Engineers*, February 2000.
23. Dareing, D. W., Drill Collar Length is a Major Factor in Vibration Control, *Society of Petroleum Engineers*, September 1982.
24. Meirovitch, L., *Analytical Methods in Vibrations*, Macmillan, New York, 1967.
25. Przemieniecki, J. S., *Theory of Matrix Structural Analysis*, McGraw-Hill Co, NY, 1968.

26. Chen, Wai-Fah, Theory of Beam-Columns, McGraw-Hill, Inc., 1976.
27. Blevins, R. D., Formulas for Natural Frequency and Mode Shape, Van Nostrand Reinhold Company, New York, 1979.
28. Rao, S. S., Mechanical Vibration, Addison Wesley, 1986.
29. Khulief, Y. A., Vibration Frequencies of a Rotating Tapered Beam with End Mass, Journal of Sound and Vibration, vol. 134, 1989, pp. 87-97.
30. Mohiuddin, M. A., Coupled Bending Torsional vibration of Rotating Shafts Using Finite Element, Master Thesis, KFUPM, Department of Mechanical Engineering, 1992.
31. Logan, D. L., A First Course in the Finite Element Method, Pws publishing company, 1993.
32. Kwon, Y. W. and Bang, H., The Finite Element Method Using Matlab, CRC Press, 1997.
33. Bazoune, A. and Khulief, Y. A., A Finite Beam Element for Vibration Analysis of Rotating Tapered Timoshenko Beams, Journal of Sound and Vibration, vol. 156, 1992, pp. 141-164.
34. Khulief, Y. A. and Mohiuddin, M. A., On the dynamic analysis of rotors using modal reduction, Journal of Finite Elements in Analysis and Design, vol. 26, 1997, pp. 41-55.
35. Karanam, U. M. and Misra, B., Principles of Rock Drilling, A.A. Balkema, 1998.
36. Mohiuddin, M. A. and Khulief, Y. A., Coupled Bending Torsional Vibration of Rotors Using Finite Element, Journal of Sound and Vibration, vol. 223 no. 2, 1999, pp. 297-316.

37. Bazoune, A., Khulief, Y. A., Stephen, N. G and Mohiuddin, M. A., Dynamic response of spinning tapered Timoshenko beams using modal reduction, *Journal of Finite Elements in Analysis and Design*, vol. 37, 2001, pp. 199-219.